Order Number 9215826

Ultrasonic reflection mode imaging of the acoustic nonlinearity parameter

Houshmand, Hooman, Ph.D.

University of Illinois at Urbana-Champaign, 1992

U·M·I
300 N. Zeeb Rd.
Ann Arbor, MI 48106

ULTRASONIC REFLECTION MODE IMAGING OF THE ACOUSTIC NONLINEARITY PARAMETER

BY

HOOMAN HOUSHMAND

B.S., University of Illinois, 1983
M.S., University of Illinois, 1985

THESIS

Submitted in partial fulfillment of the requirements
for the degree of Doctor of Philosophy in Electrical Engineering
in the Graduate College of the
University of Illinois at Urbana-Champaign, 1992

Urbana, Illinois

UNIVERSITY OF ILLINOIS AT URBANA-CHAMPAIGN

THE GRADUATE COLLEGE

NOVEMBER 1991

WE HEREBY RECOMMEND THAT THE THESIS BY

HOOMAN HOUSHMAND

ENTITLED ULTRASONIC REFLECTION MODE IMAGING OF THE ACOUSTIC NONLINEARITY PARAMETER

BE ACCEPTED IN PARTIAL FULFILLMENT OF THE REQUIREMENTS FOR THE DEGREE OF DOCTOR OF PHILOSOPHY

Charles Cain
Director of Thesis Research

N. Narayana Rao
Head of Department

Committee on Final Examination†

Leon A. Frizzell
Chairperson

Charles Cain

William D. O'Brien, Jr.

Shyh-Wei Lee

† Required for doctor's degree but not for master's.

O-517

TABLE OF CONTENTS

CHAPTER 1

INTRODUCTION

The counterpropagation method has been proposed for imaging the nonlinear parameter B/A (defined in Equations (1.4) and (1.5)). This method is based on the nonlinear interaction of counterpropagating pump and probe waves. However, in previous formulations, the pump reflections from the interfaces in the medium were not taken into account. These reflections copropagate with the probe and modulate it nonlinearly. The copropagating pump reflections cause more nonlinear interaction with the probe than the counterpropagating interactions; this will be shown using mathematical, simulation, and experimental techniques. The mathematical formulation of the nonlinear interaction of these pump reflections with the probe (called the copropagation reflection model) shows that this nonlinear interaction has the potential to form a basis for a nonlinear imaging system.

This chapter reviews the fundamental wave equations, explains the relationship of the nonlinearity parameter to pathological conditions, simulates nonlinear wave propagation, discusses nonlinear interaction of sound waves, and summarizes existing nonlinear ultrasonic imaging systems. Finally, the scope and purpose of the underlying research are presented leading to to a new simulation program and a new analytical model.

1.1 The Nonlinear Wave and State Equations

The nonlinear distortion of ultrasound pulses is analytically modeled in this section following the derivations by Beyer (1974). For a planar ultrasound wave, the propagation displacement along the direction of propagation y is related to the propagation velocity as

$$dy/dt = c \ , \tag{1.1}$$

where t is time. As will be shown later the velocity of propagation is not a constant, and the different components of the wave travel at different velocities.

The effective wave velocity, for a mechanical wave traveling in a moving medium, is the vector sum of the velocity of propagation when the medium is stationary and the velocity of the moving medium. The mechanical or acoustic wave is the result of the propagation of the medium particle oscillation energy. For a longitudinal, planar acoustic wave, the particle oscillation is either in the same direction or in the opposite direction of the wave propagation. In the positive half-cycle of the particle oscillation, the particle velocities are in the same direction as the propagation velocity, c; for the negative half-cycle, the particles move in the opposite direction to the wave propagation. Taking the particle velocity as u, the effective propagation velocity is

$$dy/dt = c + u \ . \tag{1.2}$$

The nonlinearity of the wave propagation is also affected by the dependence of the propagation velocity, c, on the particle velocity, u. The relationship between the particle velocity and propagation velocity is derived from the state equation. The state equation describes a relationship between the pressure, p, and the density, ρ, of a medium. A common way to describe the state equation is to expand the pressure in a Taylor's series about the ambient density as

$$p = p_o + (\delta p / \delta \rho)_{s,\rho = \rho_o} (\rho - \rho_o) + (1/2!) (\delta^2 p / \delta \rho^2)_{s,\rho = \rho_o} (\rho - \rho_o)^2 + (1/3!) (\delta^3 p / \delta \rho^3)_{s,\rho = \rho_o} (\rho - \rho_o)^3 + \ldots \ , \tag{1.3}$$

where p_o and ρ_o are the ambient pressure and ambient density of the medium, respectively, and s denotes the isentropic process. Defining the coefficients of the Taylor series A, B, C, ... as

$$A = \rho_o \left(\delta p / \delta \rho \right)_{s,\rho = \rho_o} = \rho_o c_o^2 \tag{1.4}$$

$$B = \rho_o^2 \left(\delta^2 p / \delta \rho^2 \right)_{s,\rho = \rho_o} \tag{1.5}$$

$$C = \rho_o^3 \left(\delta^3 p / \delta \rho^3 \right)_{s,\rho = \rho_o} \tag{1.6}$$

gives

$$p = p_o + A \left((\rho-\rho_o)/\rho_o\right) + \left(B / 2! \right) \left((\rho-\rho_o)/\rho_o\right)^2 + \left(C/ 3! \right) \left((\rho-\rho_o)/\rho_o\right)^3 + \ldots \; . \tag{1.7}$$

The acoustic nonlinearity parameter (B/A) is used to approximate the propagation velocity, c, to the second order as

$$\begin{aligned} c^2 &= (\delta p/\delta \rho)_s \\ &= A/\rho_o + B \left(\rho - \rho_o\right) / \rho_o^2 \\ &= c_o^2 \left(1 + (B/A) \left(\rho - \rho_o\right) / \rho_o\right) \; . \end{aligned} \tag{1.8}$$

Velocity is not a constant; it depends on B/A and the condensation $((\rho-\rho_o)/\rho_o)$ which is related to the amplitude of the acoustic wave. The derivation by Blackstock (1972) showed that

$$c = c_o + (B/2A)\, u \; . \tag{1.9}$$

Combining Equations (1.9) and (1.2) results in

$$\begin{aligned} dy/dt &= c + u \\ &= c_o + ((B/2A) + 1)\, u \; . \end{aligned} \tag{1.10}$$

Propagation velocity (dy/dt) is a function of the particle velocity, u (which could have positive and negative values) as seen in Equation (1.10). The different parts of the wave have different particle oscillation amplitudes and propagate at different velocities. This amplitude-dependent propagation speed leads to a distortion of the waveform with its propagation. The nonlinear waveform distortion produces the secondary effect of harmonic generation and results in the transfer of ultrasound energy to higher harmonics.

1.1.1 Formulation of the wave equation in Lagrangian coordinates

The generation of harmonics is analytically modeled in this section. A fluid particle at rest at point *a*, under the action of a harmonic wave, will undergo oscillations. The instantaneous position of this particle will be labeled y.

$$y = a + \zeta \ . \tag{1.11}$$

The displacement of the particle originally at *a* is ζ. The quantity *a* defines the point along the y-axis of the Lagrangian coordinate system and along with t, are known as the Lagrangian coordinates.

The particle velocity in these coordinates, $u^L(a,t)$, is described as

$$u^L(a,t) = \frac{\delta y}{\delta t} = \frac{\delta \zeta}{\delta t} \ , \tag{1.12}$$

and the Lagrangian acceleration as

$$\frac{\delta u^L}{\delta t} = \frac{\delta^2 \zeta}{\delta t^2} \ . \tag{1.13}$$

Consider a small element of fluid with volume dadxdz initially at rest. Apply a plane wave traveling in the y-direction: the particle originally at rest at a will be displaced a distance ζ, while that ordinarily at rest at $a+da$ will be displaced a distance $\zeta+d\zeta$. Since these new boundaries of the Lagrangian fluid element could be written as x^L and x^L+dx^L, the displaced and distorted volume dV could also be written as dxdydz. If the density of the fluid at rest is represented by ρ_o and that of the displaced fluid by ρ^L, then

$$\rho^L dy^L dxdz = \rho_o dadxdz \quad , \tag{1.14}$$

since the total mass in the fluid box must be the same in the two cases, and thus

$$\rho^L = \rho_o \frac{da}{dy^L} \quad . \tag{1.15}$$

Since $y^L = a + \zeta$, Equation (1.15) becomes

$$\rho^L = \rho_o \left(1+\frac{\delta\zeta}{\delta a}\right)^{-1} \quad . \tag{1.16}$$

If the pressure at any instant at the left side of the volume element is p^L, while the pressure on the right is $p^L + (\delta p^L/\delta y^L)\, \delta y^L$, then the net force to the right on the fluid in the volume element dV is $-(\delta p^L/\delta y^L)\, \delta y^L\, dx\, dz$, and the equation of motion becomes

$$-\frac{\delta p^L}{\delta y^L} dy^L dxdz = (\rho_o dadxdz)\, \ddot{\zeta} \tag{1.17}$$

or

$$-\frac{\delta p^L}{\delta y^L}\frac{\delta y^L}{\delta a} = -\frac{\delta p^L}{\delta a} = \rho_o \ddot{\zeta} \quad . \tag{1.18}$$

The sound speed c is now defined as

$$c^2 = \frac{\delta p^L}{\delta \rho^L} \quad , \tag{1.19}$$

where the derivative is taken under adiabatic conditions. Using Equation (1.16), arrive at

$$-\frac{\delta p^L}{\delta a} = -\frac{\delta p^L}{\delta \rho^L}\frac{\delta \rho^L}{\delta a} = \frac{c^2 \rho_o}{(1+\frac{\partial \zeta}{\partial a})^2}\frac{\partial^2 \zeta}{\partial a^2} \quad . \tag{1.20}$$

Using Equation (1.18), Equation (1.20) becomes

$$\frac{\partial^2 \zeta}{\partial t^2} = \frac{c^2}{(1+\frac{\partial \zeta}{\partial a})^2}\frac{\partial^2 \zeta}{\partial a^2} \quad , \tag{1.21}$$

which is the equation of motion for an acoustic wave in one dimension.

For the special case of an ideal gas (which later will be related to liquids), the adiabatic relation can be written as

$$p = p_o (\frac{\rho}{\rho_o})^\gamma \quad , \tag{1.22}$$

where γ is the ratio of the specific heats. Then, Equation (1.19) becomes

$$c^2 = \frac{\partial p^L}{\partial \rho^L} = \frac{\gamma p_o}{\rho_o}\left(\frac{\rho}{\rho_o}\right)^{\gamma-1} = \frac{\gamma p_o}{\rho_o}\frac{1}{\left(1+\frac{\delta\zeta}{\delta a}\right)^{\gamma-1}} \quad . \tag{1.23}$$

Substituting this expression in Equation (1.21) leads to

$$\frac{\partial^2\zeta}{\partial t^2} = \frac{c_o^2}{\left(1+\frac{\partial\zeta}{\partial a}\right)^{\gamma+1}}\frac{\partial^2\zeta}{\partial a^2} \quad . \tag{1.24}$$

This is the nondissipative wave equation in one dimension in Lagrangian coordinates.

With liquids, the following approach is used to arrive at the wave equation. The Taylor expansion of the pressure in terms of the density for the isentropic case is utilized (Equation (1.3). An expression for c^2 in a liquid medium is now derived in terms of the parameters A, B, and C. This expression is

$$c^2 = c_o^2\left[\,1 + \left(\frac{B}{A}\right)s + \left(\frac{C}{2A}\right)s^2 + \ldots\,\right] \quad . \tag{1.25}$$

It is more convenient to establish the relation between the parameter γ in Equation (1.22) with the ratio B/A. If Equation (1.22) is expanded in powers of the condensation *s*, then

$$p = p_o(1+s)^\gamma = p_o\left[\,1 + \gamma s + \frac{\gamma(\gamma-1)}{2}s^2 + \ldots\right] \quad . \tag{1.26}$$

Comparing this expansion with Equation (1.3) term by term, it is established that $B/A = \gamma - 1$ for the ideal gas. The nondissipative wave equation in one dimension becomes

$$\frac{\partial^2\zeta}{\partial t^2} = \frac{c_0^2}{(1+\frac{\partial\zeta}{\partial a})^{2+\frac{B}{A}}} \frac{\partial^2\zeta}{\partial a^2} \quad . \tag{1.27}$$

1.1.2 Solution of the wave equation

Equation (1.27) is a nonlinear differential equation; it describes the nonlinear propagation of an acoustic wave in a nondissipative medium. Plane wave solutions to this differential equation are given by Fubini, Fay, and Blackstock. The Fubini solution (Beyer, 1974) is valid for the weak nonlinearity region ($\sigma<1$, σ is distance normalized to the discontinuity distance which is the distance at which the slope of the wave goes to infinity). Blackstock's solution (1966) is valid for the region $1<\sigma<3.5$, the weak shock region. The nonlinearities encountered in most biomedical applications of ultrasound are in the weak nonlinearity region or in the weak shock region. Fay's solution (Beyer, 1974) describes a fully developed shock wave (saw-tooth or N-wave) and is valid for the region $\sigma>3.5$. These solutions are given in terms of Fourier series expansions. The physical significance of these solutions is easy to interpret such as the harmonic generation resulting from the nonlinear distortion and the production of shock waves.

The solution to another nonlinear differential equation approximating Equation (1.27) is given by Burger. The nonlinear differential equation describing the equation of motion can be transformed to a Burger's equation format. An exact solution, taking into account viscosity, is available for Burger's equation . However, this solution is not easy to interpret physically. Each of these solutions is discussed in more detail later.

1.1.2.1 Fubini solution

Equation (1.27) was solved by Earnshaw. Assume a boundary condition on the particle velocity at the origin, y = 0, to be

$$u(0,t) = u_o \sin \omega t \ , \tag{1.28}$$

where u_o is the magnitude of the particle velocity at the $y = 0$, ω is the angular frequency and t denotes time. Earnshaw's implicit solution can be expressed as

$$u(y,t) = u_o \sin[\omega t - \frac{\omega y}{c_o}(1 + \frac{B}{2A}\frac{u}{c_o})^{-\frac{2A}{B}-1}] \ , \tag{1.29}$$

where c_o is the infinitesimal speed, B/A is the nonlinearity parameter, and u/c_o is the Mach number. For a low Mach number, Equation (1.29) can be written using a binomial expansion of the term in the inner parentheses as

$$u(y,t) = u_o \sin[\omega t - \frac{\omega y}{c_o}(1 - (1+\frac{B}{2A})\frac{u}{c_o})] \ . \tag{1.30}$$

From the argument of Equation (1.30), it is seen that the phase of the planar wave is modulated by its own amplitude, the particle velocity u(y,t). The Fubini solution was obtained by expanding Equation (1.30) in a Fourier series as

$$\frac{u}{u_o} = 2 \sum_{n=1}^{\infty} \frac{J_n(\frac{ny}{L})}{\frac{ny}{L}} \sin n(\omega t - ky) \ , \tag{1.31}$$

where J_n is the nth-order Bessel function of the first kind. The effect of nonlinear distortion is readily seen as harmonic generation.

1.1.2.2 Burger's equation

If the viscosity of a dissipating medium is taken into account, the equations governing the wave propagation can be expressed by the Navier-Stokes equation (Kinsler et al., 1982) as

$$\rho_o \frac{\partial^2 \zeta}{\partial t^2} = - \frac{\partial p}{\partial y} + (\frac{4}{3}\eta + \eta_B) \frac{\partial^3 \zeta}{\partial y^2 \delta t} \quad , \tag{1.32}$$

where η and η_B are the shear and bulk viscosities, respectively. The quadratic equation of state is (Kinsler et al., 1982)

$$\frac{\partial p}{\partial y} = -A \frac{\partial^2 \zeta}{\partial y^2} + 2A(1 + \frac{B}{2A}) \frac{\partial \zeta}{\partial y} \frac{\partial^2 \zeta}{\partial y^2} \quad . \tag{1.33}$$

This equation substituted in Equation (1.32) gives

$$\rho_o \frac{\partial^2 \zeta}{\partial t^2} = A \frac{\partial^2 \zeta}{\partial y^2} - 2A(1 + \frac{B}{2A}) \frac{\partial \zeta}{\partial y} \frac{\partial^2 \zeta}{\partial y^2} + (\frac{4}{3}\eta + \eta_B) \frac{\partial^3 \zeta}{\partial y^2 \delta t} \quad . \tag{1.34}$$

Equation (1.34) can be written in the Burger's equation format with the coordinate transformation, $x = y - c_o t$ and $\tau = t$, and by neglecting terms higher than the second order, as

$$c_o^3 \frac{\partial u}{\partial x} - (1 + \frac{B}{2A}) c_o u \frac{\partial u}{\partial \tau} = \frac{c_o^3 \alpha}{\omega^2} \frac{\partial^2 u}{\partial \tau^2} \quad , \tag{1.35}$$

where α is the absorption coefficient. Equation (1.35) has an exact solution for the particle velocity as

$$\frac{u}{u_o} = \frac{\sum_{n=1}^{\infty} (-1)^{n+1}\, n\, I_n(\frac{\Gamma}{2})\, e^{-n^2\alpha y} \sin n(\omega t - ky)}{I_o(\frac{\Gamma}{2}) + 2\sum_{n=1}^{\infty} (-1)^n\, I_n(\frac{\Gamma}{2}) e^{-n^2\alpha y} \cos n(\omega t - ky)} \quad , \tag{1.36}$$

where I_n is the Bessel function of order n of the first kind of the imaginary argument. This function is given as

$$I_n(y) = (i)^{-n} J_n(iy) \quad , \tag{1.37}$$

and $\Gamma = (1+B/2A)\,(u_o/c_o\alpha)\,(2\pi/\lambda)$. The Burger's solution stated in Equation (1.36) takes into account viscosity and is valid for all ranges of σ, but it requires numerical evaluation before physical interpretations can be extracted from it.

1.1.3 Diffraction theory

The above solutions do not take diffraction into account. The acoustic beam could possibly diffract as it propagates away from the source. The starting point for almost all of the work on diffraction theory in nonlinear acoustics is the derivation of an ad hoc approximation of the equation of motion as pointed out in a survey by Kuznetsov (Beyer, 1974). Heaps (1962) started with the Euler equation of motion and derived a set of equations involving the acoustic pressures of different frequency components. Westervelt (1963) and Tjøtta and Tjøtta (1981) used the Lighthill's exact equations (Beyer, 1974) for fluid motion in calculating the diffraction pattern of the scattered wave in parametric acoustic arrays. The analytical methodology constructs a set of equations governing motion in a fluid medium. A differential equation is derived from the equations of motion taking into account different absorption mechanisms and the nonlinearity of the medium. A set of equations governing different frequency components is derived assuming time

harmonic motion and a Fourier series representation of the acoustic field. The set of equations is then solved for the harmonic components of the scattered field.

Ingenito and Williams (1971) assumed that the fundamental and the second harmonic are the only significant frequency components

$$\begin{aligned}\phi(x,y,z,t) &= \sum_{i=1}^{\infty} \phi_i(x,y,z,t) \\ &\cong \phi_1(x,y,z,t) + \phi_2(x,y,z,t) \quad ,\end{aligned} \tag{1.38}$$

where ϕ_1 is the solution of the linear wave equation; ϕ_1 and ϕ_2 are the fundamental and the second harmonic of the velocity potential, respectively. A differential equation that governs ϕ_2 was given as

$$\left(\nabla^2 - \frac{1}{c_0^2}\frac{\partial^2}{\partial t^2}\right)\phi_2 = -\frac{1}{2c_0^2}\frac{\partial}{\partial t}\left[\left(\nabla^2 - \frac{1}{c_0^2}\frac{\partial^2}{\partial t^2}\right)\phi_1^2 + \frac{\gamma+1}{c_0^2}\left(\frac{\partial \phi_1}{\partial t}\right)^2\right] \quad . \tag{1.39}$$

Assuming ϕ_1 and ϕ_2 are time harmonic, their format is

$$\begin{aligned}\phi_1 &= \varphi_1(x,y,z)\ e^{-j\omega t} \\ \phi_2 &= \varphi_2(x,y,z)\ e^{-j\omega t} \quad .\end{aligned} \tag{1.40}$$

Equation (1.39) was then solved, in cylindrical coordinates (r,θ,z), for the second harmonic acoustic field generated by a circular disc centered at the r=0 and z=0 plane. Then $\varphi_2(r,z)$ can be expressed in terms of $\varphi_1(r,z)$

$$\varphi_2(r,z) = -\frac{k^2(\gamma+1)}{8c_o}\int_{\sigma=0}^{z} e^{jk\sigma}\,\varphi_1^2\left(r, z - \frac{\sigma}{2}\right) d\sigma \quad , \tag{1.41}$$

where $\gamma = (B/A + 1)$ and c_o is the speed of sound. For a disc receiver of radius a, the output voltage resulting from the second harmonic is proportional to the average of φ_2 over its surface

$$\langle \varphi_2(r,z) \rangle = -\left[\frac{k^2(\gamma+1)}{8c_o}\right] \int_{\sigma=0}^{z} e^{jk\sigma} \left\langle \left| \varphi_1\left(r, z - \frac{\sigma}{2}\right) \right| \right\rangle^2 d\sigma \ , \tag{1.42}$$

where < > represents the spatial average over the transducer face. The integrand had been evaluated by Bass (1958) as

$$\langle \varphi_1 \rangle = -\frac{u_o^2}{k^2} e^{2jkz} \left[1 - 2\left(1 - \frac{\zeta^2}{2k^2a^2}\right) \sqrt{\frac{2}{\pi\zeta}}\, e^{-j\frac{\pi}{4}} \right] \ , \tag{1.43}$$

where u_o is the velocity amplitude of the vibrating source disc, and ζ is given by

$$\zeta = \left(\frac{k}{2}\right)\left[\sqrt{(z^2 + 4a^2)} - z\right] \ . \tag{1.44}$$

Substituting Equations (1.43) and (1.44) into Equation (1.42) produces another integral equation

$$\langle \varphi_2(r,z) \rangle = \frac{u_o^2\,(\gamma+1)}{4c_o} e^{2jkz} \left(\frac{z}{2} + I\right) \ , \tag{1.45}$$

where

$$I = -\frac{4}{\sqrt{\pi k}} e^{-j\frac{\pi}{4}} \int_{\frac{z}{2}}^{z} \left[\left(\sqrt{\theta^2 + 4a^2} - \theta\right)^{-0.5} - \frac{1}{8a^2}\left(\sqrt{\theta^2 + 4a^2} - \theta\right)^{1.5} \right] d\theta \ . \tag{1.46}$$

Converting the velocity potential into acoustic pressure, using the planar small-signal dissipationless relationship, $p_2 = -j\omega\rho_o\varphi_2$, and $p_o=\rho_o c_o u_o$, gives

$$|\langle p_2\rangle| = \omega\rho_o|\langle\varphi_2\rangle|$$

$$=\frac{\omega p_o^2(B/A+2)}{2\rho_o c_o^3}\left|\frac{z}{2}+I\right|$$

$$=\frac{\pi f p_o^2(B/A+2)}{2\rho_o c_o^3}z\left|1+\frac{2I}{z}\right| . \qquad (1.47)$$

The finite aperture diffraction effects depend on B/A and the distance of propagation.

1.2 Acoustic Nonlinearity Parameter B/A of Biological Media and Its Significance

The B/A parameter is related to the mechanical properties of a biological medium. The B/A values for various liquids and biological media have been compiled by Zhang (1990) and Everbach (1989). The reported B/A parameter ranges from 5 to 12. Linear dependence of the B/A parameter on concentration has been reported in aqueous solutions of bovine serum albumin, hemoglobin, dextran T2000, dextrose, sucrose and polyethylene glycols (Law, 1984; Law et al., 1985; Cobb, 1982; Gong et al., 1984).

A mixture's B/A value can be calculated using the mixture laws (Apfel, 1983, 1986; Sehgal et al., 1986a). These mixture laws have been used to model tissues as mixtures of the three components-- water, fat, and protein-- from which the chemical composition of tissues can be determined from the measurements of density, velocity and B/A (Apfel, 1986; Sehgal et al., 1986a; Dong et al., 1987).

The B/A values for protein and carbohydrate, in solid state, are estimated from the B/A data of their aqueous solutions, of known composition, using the mixture laws. The

B/A parameter of single-component liquids takes values close to 5 for inorganic liquids and 10 for organic liquids. The B/A value for pure fat has been determined to be between 9.9 and 11.5 (Everbach, 1989; Errabolu et al., 1987; Apfel, 1983). Fat, protein, and carbohydrate have essentially very similar B/A values (Zhang, 1990). For pure substances known as constituents of tissues, water has a B/A value of about five, while fat, protein, and carbohydrate have values of about ten. The mixtures of these components have intermediate B/A values. Investigation of the B/A parameter of tissue has also shown a dependence on structural features. Law et al. (1985) reported the decrease of the B/A value from 7.7 of intact beef liver to 6.8 of the same beef liver homogenized.

Researchers have found that the B/A value of blood is slightly higher than that of a solution containing the same amount (dry weight) of protein (Law et al., 1985). The explanation is that the red cells of blood are composed of a hemoglobin solution contained in a membrane, thus placing blood in a higher structural hierarchy. The intact liver, which is much more complex in structure than blood, has a correspondingly greater B/A value. Homogenization of the liver, which destroys the structure to some extent, leads to a decrease in the B/A value (Law et al., 1985).

Several research results indicate a possible relationship between B/A and tissue composition, particularly in the relative amounts of water and fat (Law, 1984; Bjorno, 1986; Sehgal et al., 1984, 1986a). This raises the possibility of estimating the tissue composition from B/A and sound speed (Sehgal et al., 1986a). Tissue is composed mostly of water which is either bound or unbound (free). The state of water in biological tissue plays an important role in the cellular structure and the health of tissue. The B/A of bound water is estimated to be approximately 0.4, whereas the B/A of free water is approximately 8.0 (Yoshizumi et al., 1987). The ratio of free water to bound water in malignant tissue such as in a multiple myeloma is higher than in the surrounding healthy tissue. The state of water in tissue has been imaged by NMR imaging and has been useful in medical diagnosis

(Sehgal et al., 1985). Determination of the state of water using B/A might also be possible and more economical.

Several investigators have studied the nonlinear propagation of acoustic waves in biological media (Bacon, 1986; Dunn et al., 1981; Law, 1984; Cobb, 1982; Zhang 1990). One aspect of these studies has been the measurement and analysis of the acoustic nonlinearity parameter, B/A, of biological media. The acoustic nonlinearity parameter relates the diverse nonlinear phenomena observed in ultrasound propagation to the general nonlinear wave propagation theory. Extensive work has been performed on the measurement and the investigation of the B/A parameter (Beyer, 1974; Beyer, 1960; Cobb, 1982; Coppens et al., 1965; Dong et al., 1987; Errabolu et al., 1987; Everbach, 1989; Gong et al., 1984; Law et al., 1985; Narayana and Swamy, 1981; Sehgal et al., 1984, 1986b; Sun and Zhao, 1985; Zhu et al., 1983; Zhang, 1990). One of the goals of studying the acoustic nonlinearity parameter B/A has been to provide more accurate modeling of the propagation of finite amplitude waves in biological media. The accurate modeling of ultrasound propagation through biological media may allow a more effective administration of therapeutic ultrasound dosage (Swindell, 1985) and the production of higher-quality images (Bjorno and Lewin, 1982; Rugar, 1984).

1.3 Simulation of Nonlinear Wave Propagation

1.3.1 Nonlinear distortion

Studies by Pestorius and Blackstock (1974) of finite amplitude noise propagation in tubes have produced software packages useful in studying general nonlinear waveform distortion in acoustics. The waveform distortion depends on the rate of wave propagation. The rate of propagation dy/dt of a given displacement velocity u is given by

$$dy/dt = c_o + \beta u \ , \tag{1.48}$$

where β is (1+B/2A). This equation can be rewritten and approximated as

$$\frac{dt}{dy} = \frac{1}{c_o + \beta u} \cong \frac{1}{c_o}\left(1 - \frac{\beta u}{c_o}\right) . \qquad (1.49)$$

At the discontinuity of a shock wave, this equation becomes

$$dt/dy \cong (1/c_o)\,[\,1 - (\beta/c_o)\,((u_a + u_b)/2)\,]\ , \qquad (1.50)$$

where u_a and u_b are the values of u just ahead of and just behind the shock. Pestorius and Blackstock began with Equation (1.49) and wrote it in the form of a difference relation, solving the latter using a computer. The computer program evaluates the propagation time of the wave through a small distance y; the new time, space relationship is

$$t_{new} = t_{old} - \beta\, u_{old}\, y / c_o^2 \cdot \qquad (1.51)$$

This updated time is associated with a particular point on the waveform. The new waveform is tested for multiple values. If it is still single-valued, the process is repeated. If it has multiple values, Equation (1.50) is used; the shock is located and particle velocities are corrected.

This program was used to simulate situations with known experimental outcomes. The experimental problem to which Pestorius and Blackstock addressed themselves involved propagation in a tube and required the introduction of a computational procedure to take into account both the attenuation and dispersion that are characteristic of tube propagation. The algorithm developed made it possible to predict very closely the behavior of both single pulses and noise in propagation through an air-filled aluminum tube of 96-ft. length by 2-in width. The received pulse shapes, experimental and computed, matched each other very closely.

1.3.2 Absorption

The close match between theory and experiment was partly due to incorporating absorption into the computer program. To formulate the absorption algorithm, it is necessary to consider a single frequency component of an arbitrary spherical wave. If the complex amplitude of the component is U_o at a distance r_o, the amplitude U at a distance r is, in the absence of nonlinear distortion, given by

$$U = \frac{r_o U_o}{r} e^{-\vartheta(r-r_o)} \quad . \tag{1.52}$$

The factor $\exp(-j(2\pi/\lambda)(r-r_o))$ does not appear because the wave is represented in the time domain in terms of the retarded time $t'=t-(r-r_o)/c_o$. If $r=r_o+\Delta r$, where Δr is the propagation distance step, Equation (1.52) becomes

$$U = \frac{r_o}{r_o + \Delta r} U_o e^{-\vartheta \Delta r} \quad , \tag{1.53}$$

where ϑ is the attenuation parameter.

1.3.3 Wave propagation algorithm

Orenstein and Blackstock (1982) used these formulas (Equations (1.53) and (1.51)) to simulate the propagation of acoustic signals in air. The initial waveform representing the acoustic signal is the input at $r=r_o$. The waveform is transformed from the time domain to the frequency domain via a fast Fourier transform (FFT), and absorption is applied (Equation (1.53)). The waveform is then transformed back to the time domain by an inverse FFT, and the nonlinear distortion is applied (Equation (1.51)). The waveform propagation distance becomes $r_o+\Delta r$, and the process is repeated until *r* equals a specified propagation distance.

Small time, or propagation distance, steps are taken to ensure that no shocks form during a nonlinear distortion step. The absorption step is applied before the distortion step to handle occasions in which the initial waveform contains a discontinuity (shock). The shock formation distance is calculated after each absorption step. The next value of Δr is chosen as one-tenth of the shock formation distance. This formulation ensures that multiple values do not occur in the nonlinear distortion step. After the distortion step, the time increments between the points in the waveform are no longer equally spaced. The FFT routine requires that the time increments be equally spaced. An interpolator is used to find equally spaced time increments. Cotaras and Blackstock (Beyer, 1974) used a similar algorithm for numerically implementing the weak shock theory for an attenuating inhomogeneous ocean. This algorithm took into account the change in absorption coefficient with ocean depth.

1.4 Nonlinear Interaction of Sound Waves

1.4.1 Formulation of the scattered wave solution

The simulation program described in Section 1.3 deals with the nonlinear distortion of a single waveform; however, the work here is directed towards the nonlinear interaction of two ultrasound pulses. The ultrasound waves interact in a nonlinear manner and produce mixing products. One of the oldest observations in nonlinear acoustics was made by Sorge in 1745 and independently reported by Tartini in 1754. These two musicians found that the sounding of two musical tones of high intensity results in the appearance of a lower tone whose frequency is equal to the difference between the two original tones. The sound is known as the Tartini tone. The signals had to be quite intense before a difference tone could be observed, and this tone was weak. Helmholtz (Beyer, 1974) undertook an analytical study of this problem and discovered the existence of a sum frequency as well as a difference frequency. Rücker and Edser (Beyer, 1974) excited a tuning fork at the sum frequency, thus identifying the interaction as an objective one, that is, actually occurring in

the medium. Lamb (Beyer, 1974) used a perturbation technique to show the existence of both the sum and the difference frequencies. His work was confirmed experimentally by Jenkins, O'Neil, and Thuras (Beyer, 1974). Two sound beams traveling in the same direction produce sum and difference frequencies in the medium.

The interaction of two sound beams has been studied analytically. Almost all of the theoretical work on the nonlinear interaction of two sound beams (scattering of sound by sound) began with the paper by M.J. Lighthill on sound produced by turbulence (Beyer, 1974). In this paper Lighthill presented the exact equations of motion for an arbitrary fluid in the form

$$\frac{\delta \rho}{\delta t} + \frac{\delta(\rho u_i)}{\delta x_i} = 0$$

$$\frac{\delta(\rho u_i)}{\delta t} + c_0^2 \frac{\delta \rho}{\delta x_i} = - \frac{\delta T_{ij}}{\delta x_i}$$

$$\frac{\delta^2 \rho}{\delta t^2} - c_0^2 \nabla^2 \rho = \frac{\delta^2 T_{ij}}{\delta x_i \delta x_j} \quad , \tag{1.54}$$

where the stress T_{ij} is defined by the relation

$$T_{ij} = u_i u_j + p_{ij} - \rho c_0^2 \delta_{ij} \quad . \tag{1.55}$$

Here $\rho u_i u_j$ is the instantaneous Reynolds stress tensor, p_{ij} the compressive stress tensor, and δ_{ij} the Kronecker delta. In effect, the sound field radiated by fluid flow (including the interacting sound beams) is equivalent to one produced by a static distribution of acoustic quadrupoles with source strength density given by T_{ij}.

Westervelt (1963) solved the equations by Lighthill for collinear beams and formulated the equation for the scattered pressure as

$$p_s = \omega_s^2 \rho_o \frac{F}{8\pi R} \frac{e^{i(\omega_s t - k_s R)}}{i(\frac{\alpha_1+\alpha_2}{2} + k_s \sin^2 \frac{\theta}{2})} \quad . \tag{1.56}$$

The quantity F is

$$F = - \frac{i\omega_s}{\rho_o^2 c_o^4} (1 + \frac{B}{2A}) p_1 p_2 \quad , \tag{1.57}$$

where p_1 and p_2 are the pressures of the primary sources, R is the distance from the source to the receiver, θ is the angle between the receiver and the acoustic axis of the source (the observation angle), and α_1 and α_2 are the attenuation coefficients at the primary frequencies.

Equation (1.56) provides the beam profile. The beam profile could be used to calculate the half pressure point. The half-width of the beam $\theta_{1/2}$ at the half pressure point was theoretically derived by Westervelt as

$$\theta_{1/2} \cong 2 \times 3^{1/4} (\frac{\alpha}{k_s})^{1/2} \quad , \tag{1.58}$$

where α is the attenuation coefficient of the primary beam. This equation could be utilized to calculate the beam width of the scattered wave. The beam width and the beam pattern of the scattered waves have been studied extensively. The numerical and experimental research by Bellin and Beyer (Beyer, 1974) and Benet (Beyer, 1974) showed that the beam pattern of the (sum) scattered frequency in the nearfield equaled the product of the beam patterns of the primary beams.

1.4.2 Beam profile at the farfield of a plane piston

The beam pattern at the farfield of a plane piston has been calculated theoretically. The problem of the nonlinearities of the farfield of a plane piston is taken to be that of a spherical source with boundary conditions at the effective starting point of spreading. Lockwood, Muir and Blackstock (Beyer, 1974) assumed that the particle velocity amplitude at this point is given by $(u_o/c_o)D(\theta)$, where $D(\theta)$ is the infinitesimal amplitude directivity function in the farfield of a circular, baffled, plane piston.

$$D(\theta) = \frac{2J_1(ka\sin\theta)}{ka\sin\theta} , \tag{1.59}$$

where a is the radius of the source, k is the wave number, and θ is the angle between the receiver and the source. In the weak nonlinearity region, the analysis based on the weak shock theory of Blackstock results in

$$D^n(\theta) \cong [D(\theta)]^n , \tag{1.60}$$

where $D^n(\theta)$ is the directivity of the nth harmonic. The harmonic components of the wave become progressively narrower.

1.5 Proposed Nonlinear Ultrasonic Imaging Systems and Definition of System Parameters

1.5.1 Imaging methods based on dependence of sound speed on pressure

The methods in this category take advantage of the change in the sound speed caused by pressure. The change in the sound speed is also related to the value of the nonlinearity parameter in the region where the pressure has been changed. A change in the pressure is generated by a relatively high-intensity acoustic wave at low frequency. This acoustic wave is called the pump. A high-frequency, low-intensity coherent wave probes

the portion of the medium where the sound speed has been changed by the pump. If the probe propagates along the y-axis, the propagation time of the probe is given as

$$t = \int_0^L \frac{1}{c}\,dy = \int_0^L \frac{1}{c_o + \frac{1}{2\rho_o c_o}\frac{B}{A}p}\,dy \quad , \tag{1.61}$$

where L is the length of the medium and p is the change in pressure caused by the pump.

Equation (1.61) could be approximated (for pump pressures less than 50 atm) as

$$t = \int_0^L \frac{1}{c_o}\left(1 - \frac{\frac{B}{A}p}{2\rho_o c_o^2}\right) dy = \frac{L}{c_o} - \int_0^L \frac{\frac{B}{A}p}{2\rho_o c_o^3}\,dy \quad , \tag{1.62}$$

where the approximation is valid, since $(B/A)p / 2\rho_o c_o^2$ is much smaller than one for pump pressures less than 50 atm. The time of flight of the probe depends on the acoustic nonlinearity parameter of the medium, as seen in Equation (1.62).

Equation (1.62) forms the basis for many proposed imaging systems. Different imaging systems have been proposed depending on the pump and probe geometry. Ichida et al. (1984) have used a perpendicular pump and probe geometry. The instantaneous time delay for this geometry becomes

$$\Delta t(\tau) = -\int_0^L \frac{\frac{B}{A}(y)\ p(y - c_o\tau)}{2\rho_o(y)c_o^3(y)}\,dy \quad . \tag{1.63}$$

The time delay is very small and could be multiplied by the angular frequency of the probe to provide the phase shift. The instantaneous phase shift and the pump pressure can be measured leading to an estimate of the nonlinear parameter.

Sato et al. (1985) proposed a counterpropagation geometry for the imaging system. In this system, the pump and the probe propagate towards each other. The instantaneous time delay experienced by a point on the probe is

$$\Delta t(\tau) = -\int_0^L \frac{\frac{B}{A}(y)\ p(c_o\tau - y/2)}{2\rho_o(y)c_o^3(y)}\,dy \quad . \tag{1.64}$$

This time delay could be considered as a phase modulation of the probe. Deconvolution of the phase function with the pump pulse leads to an estimate of the acoustic nonlinearity. Two-dimensional images of the nonlinear parameter are provided by the mechanical or electrical scanning of the pump and probe waves.

Cain (1986) proposed a reflection mode imaging system. A probe followed by a pump is launched towards a planelike or a pointlike reflector. The probe can have a coherent or a chirp waveform. The pump can have an intense short duration or a coded long duration pulse. The pump interacts with the reflected probe and the probe phase is modulated. The acquired phase of the probe was shown in a numerical example to be very small (less than a few degrees; Cain, 1986) and no phase wrapping occurred. The instantaneous phase of the probe is given as

$$\Delta\varphi(\tau) = -\pi f \int_0^{c_o\tau/2} \frac{B/A(y)}{\rho_o(y)c_o^3(y)}\, p(\frac{c_o\tau}{2} - y)\,dy \quad . \tag{1.65}$$

Deconvolution of the extracted phase of the probe with the pump leads to an estimate of the nonlinearity parameter profile.

1.5.2 Tomographic techniques based on the parametric array by Westervelt

Nakagawa et al. (1984) proposed the utilization of the scattered wave resulting from the nonlinear interaction of two copropagating ultrasound pulses for imaging the B/A parameter. The average value of the scattered wave over the receiver surface is (Cai, 1988)

$$|\langle p_s(\vec{r})\rangle| \approx \frac{p_o^2\,\omega_s}{2}|F|\int_0^Y \frac{1+\frac{B}{2A}(y)}{2\rho_o(y)c_o^3(y)} e^{-\int_0^Y [\alpha_1(y)+\alpha_2(y)]dy} dy \quad , \tag{1.66}$$

where p_o is the amplitude of the wave launched into the medium, $\vec{r}$ is the position vector, $|F|$ represents diffraction loss, and Y is the length of the medium. Projections of the nonlinear parameter are obtained from different angles. The line integral formulation in Equation (1.66) is then used to reconstruct the nonlinear parameter image. This nonlinear ultrasonic imaging system produced images of the nonlinear parameter (Nakagawa et al., 1986).

1.6 Scope and Purpose of the Thesis

The reflection mode nonlinear ultrasonic imaging system will be systematically analyzed building on the theory and the simulation material presented in this chapter. The different components of the reflection mode imaging system will be elaborated upon, including time-delay formulation of the nonlinear interaction of ultrasound pulses, beam profiles of the acoustic signals, methods of demodulation, simulation techniques, and experimental methods. A signal processing method for producing B/A images in the reflection mode is presented.

Reflection mode imaging of the B/A parameter is developed in this dissertation. Chapter 2 discusses the mathematical modeling of the reflection mode nonlinear interactions. These nonlinear interactions are modeled either as counterpropagation or copropagation reflection. The nonlinear interactions are simulated in Chapter 3. The simulation results for the two possible cases of nonlinear interaction, namely, the counterpropagation and copropagation reflections, are shown. Copropagation reflection experiments are described in Chapter 4. These experiments are presented for various materials to verify the mathematical model produced in Chapter 2. The results of the comparison between the mathematical models and the experiments are discussed in Chapter 5. Chapter 5 also contains the suggestions for future work and discusses the limitations of the present study.

CHAPTER 2

MATHEMATICAL MODELING

In this chapter, the counterpropagation model is investigated to identify nonlinear interaction mechanisms which have not been taken into account previously. Specifically, past counterpropagation models have not taken the pump reflections into account. These reflections generate nonlinear interactions through copropagation of the reflected pump with the probe. This chapter will demonstrate that the sensitivity of the probe to phase modulation by copropagation reflection is higher than with counterpropagation.

2.1 Counterpropagation

A mathematical expression is derived for the instantaneous phase shift in a sinusoidal probe (Cain, 1986). This instantaneous phase shift is proportional to the convolution of the pump with the spatial distribution of the nonlinear parameter B/A.

Determining the ratio B/A, from Equations (1.5) and (1.4), gives

$$B/A = \frac{\left(\rho_o^2(\delta^2 p/\delta\rho^2)_{s,\rho=\rho_o}\right)}{\rho_o c_o^2} = 2\,(\rho_o c_o)\left(\frac{\delta c}{\delta p}\right)_{s,\rho=\rho_o} . \qquad (2.1)$$

This definition of B/A forms the analytical basis of the time-delay formulation of the B/A imaging system.

The reflection mode imaging system is shown in Figure 2.1.a. An acoustic waveform, composed of a high-frequency sinusoidal probe, $s(\tau,y)$, is followed by a pump, $p(\tau,y)$. The probe is reflected from a plane at y=L. A probe of duration $T_d=2L/c_o$ must be used to image the entire line along the propagation path from y=0 to y=L. In this case, the probe duration is equal to twice the signal transit time between the transmitter/receiver and

the reflector plane. Figure 2.1.a. shows the situation at T_d after beginning the signal transmission. Thus, the pump, $p(\tau,y)$, interacts with the reflected probe, $s(\tau,y)$, over the image line from y=0 to y=L. If B/A varies over this space, the probe waveform, $s(\tau,y)$, will undergo a phase variation over its entire duration, $T_d=2L/c_o$. The situation at $3L/c_o$ is shown in Figure 2.1.b. Note that the time between the beginning of the probe transmission and the reception of the trailing edge of the probe is $4L/c_o = 2T_d$.

A relationship between an arbitrary pump, $p(\tau,y)$, and an arbitrary distribution of B/A(y) is now developed. It is useful to begin by noting that a sinusoidal signal, propagating over a path of length L with a speed c_o, undergoes a phase shift,

$$\phi = 2 \pi f L / c_o \quad . \tag{2.2}$$

Consider the step response of the system in Figure 2.2, in which a unit step of pressure, $u(\tau,y)$, is propagated to the right over the image line from y=0 to y=L, and a sinusoidal probe propagates in the opposite direction. The step response of the system, that is, an expression for the instantaneous phase shift at any point along the received probe, $s(\tau)$, can be derived. It is important to observe that, while the step discontinuity of pressure propagates over the length L in time L/c_o, it interacts with the probe over a duration of $2L/c_o$. Thus, the received signal, $s(\tau)$, will carry information in the form of instantaneous phase changes over the interval from $\tau=0$ to $\tau=2L/c_o$, where $\tau=0$ is the instant when the pump discontinuity begins moving to the right and the leading edge of the probe is received at y=0.

Making use of Equations (2.1) and (2.2), the instantaneous phase, $\phi_+(\tau)$, of the probe, $s(\tau)$, after interacting with the step pump, $u(\tau,y)$, has the form

$$\phi_+(\tau) = 2\pi f \int_0^{c_o\tau/2} \left(c_o + \frac{u(\tau c_o/2 - y)B/A(y)}{2\rho_o c_o}\right)^{-1} dy + 2\pi f \int_{\tau c_o/2}^{L} \left(\frac{1}{c_o}\right) dy \quad . \tag{2.3}$$

The instantaneous phase $\phi_-(\tau)$ of the probe propagating without the pump is

$$\phi_-(\tau) = 2\pi f \int_0^L \left(\frac{1}{c_o}\right) dy \quad . \tag{2.4}$$

The phase difference $\phi_+(\tau)$ - $\phi_-(\tau)$ can be attributed entirely to the nonlinear interaction between the probe and the pump. This phase difference is

$$\Delta\phi_u(\tau) = \phi_+ - \phi_- = 2\pi f \int_0^{c_o\tau/2} \left[\left(c_o + \frac{u(c_o\tau/2 - y)B/A(y)}{2\rho_o c_o}\right)^{-1} - \frac{1}{c_o}\right] dy \quad , \tag{2.5}$$

which can be written as

$$\Delta\phi_u(\tau) = -\frac{\pi f}{\rho_o c_o} \int_0^{c_o\tau/2} \left(\frac{u(c_o\tau/2 - y)B/A(y)}{c_o^2 + [u(c_o\tau/2 - y)B/A(y)]/2\rho_o}\right) dy \quad . \tag{2.6}$$

The denominator of Equation (2.6) can be approximated by c_o^2, since the other term is at most an order of magnitude smaller. Therefore,

$$\Delta\phi_u(\tau) = -\frac{\pi f}{\rho_o c_o^3} \int_0^{c_o\tau/2} u(c_o\tau/2 - y)B/A(y) dy \quad . \tag{2.7}$$

This is a convolution integral, from which the impulse response of the system is derived as

$$\Delta\phi_b(\tau) = -\frac{\pi f}{\rho_o c_o^3}\int_0^{c_o\tau/2} \delta(c_o\tau/2-y)B/A(y)dy \quad , \tag{2.8}$$

and becomes

$$\Delta\phi_b(\tau) = -\frac{\pi f}{\rho_o c_o^3} B/A(c_o\tau/2) \quad , \tag{2.9}$$

where $\delta(y)$ is the unit impulse function. Given the impulse response, an arbitrary pump, $p(\tau,y)$, and an arbitrary variation of B/A along an image line, the phase difference, $\Delta\phi(\tau)$, can be computed using the convolution integral

$$\Delta\phi(\tau) = -\frac{\pi f}{\rho_o c_o^3}\int_0^{c_o\tau/2} p(c_o\tau/2-y)B/A(y)dy \quad . \tag{2.10}$$

This is the counterpropagation model. This equation forms a basis for the reflection mode B/A imaging, when reflections of the pump and probe from only one reflector are considered.

2.2 Analytical Formulation of the Nonlinear Interaction of Copropagating Ultrasonic Pump and Probe Signals

This section proves that copropagation of the pump and the probe leads to nonlinear interaction. The time delay of a probe wavelet (a point on the waveform) is derived for a plane probe propagating in the same direction as a broadband plane pump. The extension to arbitrary beam profiles is also provided.

The pump and the probe are propagating in the y-direction. The sound speed in a nonlinear medium is derived from Equation (2.1),

$$c(y) = c_o(y) + \frac{B/A(y)}{2\rho_o(y)c_o(y)} p(y) \quad . \tag{2.11}$$

This equation relates the speed of a probe wavelet at location y in space, $c(y)$, to the nominal sound speed c_o, the nominal medium density ρ_o, and the acoustic nonlinearity parameter B/A. The pump is denoted by $p(y)$ and modulates the time delay of the probe in the medium. A probe wavelet propagates in the medium, with a specific portion of the pump, along the y-direction.

The time delay of a probe wavelet is the difference between the nominal propagation time and the modulated propagation time. This time delay is given, when the pump and probe pulses interact between y_o and y_1, as

$$\Delta t = \int_{y_o}^{y_1} \frac{dy}{c_o(y)} - \int_{y_o}^{y_1} \frac{dy}{c(y)} \quad , \tag{2.12}$$

where the sound speed equation is given in Equation (2.11). Substituting for the speed equation leads to

$$\Delta t = \int_{y_o}^{y_1} \frac{dy}{c_o(y)} - \int_{y_o}^{y_1} \frac{dy}{c_o(y) + \frac{B/A(y)}{2\rho_o(y)c_o(y)} p(x,y-c(y)\tau,z,t_o)} \quad , \tag{2.13}$$

where the pressure field is taken to be that of the pump. The portion of the pump field, which is copropagating with the probe wavelet entering its field at time t_o, is represented

by $p(x,y-c(y)\tau,z,t_o)$. In this function's argument, $(y-c(y)\tau)$ emphasizes the point that a specific pressure is copropagating with a single probe wavelet. The following steps simplify this integral equation.

Factoring out the nominal sound speed from the denominator term leads to

$$\Delta t = \int_{y_o}^{y_1} \frac{dy}{c_o(y)} - \int_{y_o}^{y_1} \frac{dy}{c_o(y)\left(1 + \frac{B/A(y)}{2\rho_o(y)c_o^2(y)}\, p(x,y-c(y)\tau,z,t_o)\right)} \quad . \tag{2.14}$$

The term $(B/A)p/2\rho_o c_o^2$ is much smaller than one; it is less than 0.01 for soft-tissue imaging with pressures less than 20 atm. A Taylor series expansion of the integrand is performed and terms up to the first order are kept.

$$\Delta t = \int_{y_o}^{y_1} \frac{dy}{c_o(y)} - \int_{y_o}^{y_1} \frac{1 - \frac{B/A(y)}{2\rho_o(y)c_o^2(y)}\, p(x,y-c(y)\tau,z,t_o)}{c_o(y)}\, dy \quad . \tag{2.15}$$

This ratio is divided to yield

$$\Delta t = \int_{y_o}^{y_1} \frac{dy}{c_o(y)} - \int_{y_o}^{y_1} \left(\frac{1}{c_o(y)} - \frac{B/A(y)}{2\rho_o(y)c_o^3(y)}\, p(x,y-c(y)\tau,z,t_o)\right) dy \quad . \tag{2.16}$$

The first term in the second integral cancels with the first integral to yield the time retardation, due to the nonlinear interaction of the probe with the pump,

$$\Delta t = \int_{y_o}^{y_1} \left(\frac{B/A(y)}{2\rho_o(y)c_o^3(y)} p(x,y-c(y)\tau,z,t_o) \right) dy \quad . \tag{2.17}$$

This integral represents the time retardation (or time advance) of a probe wavelet copropagating with the pump from a location y_o to a location y_1. The pump pressure is assumed to be a constant for a given probe wavelet and is factored out of the integral.

$$\Delta t = p(x,y-c(y)\tau,z,t_o) \int_{y_o}^{y_1} \frac{B/A(y)}{2\rho_o(y)c_o^3(y)} dy \quad . \tag{2.18}$$

The probe modulation is a function of the pump and is given as

$$\Delta t(\tau) = p(x,y,z,\tau) \int_{y_o}^{y_1} \frac{B/A(y)}{2\rho_o(y)c_o^3(y)} dy \quad . \tag{2.19}$$

The time delay of the probe is proportional to the spatial pressure field along the y-axis, the distance of copropagation of the probe with the pump, and the integral of the acoustic nonlinearity over that distance.

2.2.1 Beam profile

If the probe has a much smaller beam width than the pump, the pump appears as a plane wave and Equation (2.19) applies. However, if the pump has a narrower beam width than the probe, then the probe receiver would experience the lateral pressure variations of this pump. In this case, the analysis needs to be extended to take into account the effect of the pump diffraction pattern. The interaction occurs along the y-axis, and the

effective pressure is an average of the pump pressure in the x and z plane over the lateral width of the probe beam. Hence, Equation (2.19) is extended to

$$\Delta t(\tau) = \int_x \int_z p(x,y,z,\tau)\, dxdz \int_{y_o}^{y_1} \frac{B/A(y)}{2\rho_o(y)c_o^3(y)} dy \quad . \tag{2.20}$$

In Section 1.5, it was reviewed that the scattered beam profile is the spatial product of the copropagating pump and probe beam profiles. The mathematical example below derives the beam profile of the scattered beam using that assertion. The beam profiles of the pump and probe are approximated to have the form of a Gaussian function in the following analytical example.

Since the beam profiles are given as

$$D_1(\theta) = \exp(-\frac{\theta^2}{2\sigma_1^2}) \tag{2.21}$$

$$D_2(\theta) = \exp(-\frac{\theta^2}{2\sigma_2^2}) \quad , \tag{2.22}$$

the scattered field is

$$D_s(\theta) = D_1(\theta)\, D_2(\theta) \tag{2.23}$$

which leads to

$$D_s(\theta) = \exp(-\frac{\theta^2}{2\sigma_1^2}) \exp(-\frac{\theta^2}{2\sigma_2^2}) \quad , \tag{2.24}$$

and equals

$$D_s(\theta) = \exp\left(-\frac{\theta^2}{2\sigma_1^2} - \frac{\theta^2}{2\sigma_2^2}\right) = \exp\left(-\frac{\theta^2}{2\sigma^2}\right) , \tag{2.25}$$

where the new beam profile is characterized by the parameter

$$\sigma = \frac{\sigma_1 \sigma_2}{\sqrt{\sigma_1^2 + \sigma_2^2}} . \tag{2.26}$$

This result shows that, if one of the primary beams is much more directed than the other primary beam, the scattered beam will have a width similar to the more directed beam. If the two widths are identical, the above equation shows that the resulting width is 0.707 of the primary width.

2.2.2 Spectrum of the modulated probe

To complete the discussion of the nonlinear interaction of copropagating pump and probe pulses, the spectral properties of the modulated probe are discussed. The received probe waveform is given as

$$s(\tau) = \sin(\omega_o \tau + \Delta\phi(\tau) + \theta_o) , \tag{2.27}$$

where ω_o is the probe frequency, $\Delta\phi(\tau)$ is the acquired phase because of the nonlinear interaction with the pump, and θ_o is due to the propagation delay. The maximum value of $\Delta\phi(\tau)$ is small (less than a few degrees) for a narrow-band phase modulated signal. This allows the use of small angle approximations. Separating the phase, due to the nonlinear interaction from the other phase terms, and expanding the trigonometric expression, leads to

$$s(\tau) = \sin((\omega_o\tau + \theta_o) + \Delta\phi(\tau)) = \sin(\omega_o\tau + \theta_o)\ \cos(\Delta\phi(\tau)) + \cos(\omega_o\tau + \theta_o)\ \sin(\Delta\phi(\tau)) \tag{2.28}$$

Applying the small-signal approximation (since the modulation is narrow-band FM) to Equation (2.28), leads to

$$s(\tau) = \sin(\omega_o\tau + \theta_o) + \cos(\omega_o\tau + \theta_o)\ (\Delta\phi(\tau)) \ . \tag{2.29}$$

The spectrum of this signal is a delta function at the carrier frequency plus the spectrum of the nonlinear modulation, due to the nonlinear interaction of the probe with the pump. This spectrum is centered at the carrier frequency. An example of the spectrum of the pump and the modulated probe is shown in Figure 2.3. The amplitude of the phase deviation, $\Delta\phi(\tau)$, is proportional to the amplitude of the sidebands of the probe.

2.3 Copropagation Reflection

The nonlinear interaction between the pump reflections and the probe is mathematically formulated in this section. This formulation leads to the following result: pump reflections lead to a probe phase proportional to the convolution of the pump with the integral of the acoustic nonlinearity.

2.3.1 Step response

An analytical relationship is derived between the phase of the probe and an arbitrarily shaped pump, $p(y,\tau)$, which interrogates a medium with an arbitrary B/A parameter profile. This is derived from the step response of the system which leads to the impulse response of the system. A unit step pressure, $u(y,\tau)$, propagating to the right on the image line, while the sinusoidal probe is counterpropagating, is shown in Figure 2.4. The underlying B/A parameter is not shown; it can have any desired function. The sound

speed and the medium density could also have any desired profile. The reflection profile has only one reflector for this initial derivation.

This single reflection of the step pump is used to derive the step response of the system. This analysis is then extended to multiple reflections or a continuum of reflectors. The step response, that is, an instantaneous phase shift at any point along the received probe signal, $s(\tau)$, is now derived. Let $\tau=0$ be the moment that the pressure discontinuity begins moving to the right and the leading edge of the probe is received at $y=0$. The analysis in Section 2.2 showed that the excess phase of the probe can be derived by analyzing the time delay acquired by a single probe wavelet. The time delay is defined as the difference between the modulated propagation time and the nominal propagation time. The time delay leads to the phase, by multiplying the time delay by the temporal frequency of the coherent probe.

The first integral in Equation (2.30) is the phase acquired by the probe while copropagating with the reflected pump. The amplitude of this reflected pump is the step pump multiplied by the reflection coefficient. The reflection plane is fixed at a distance y from the probe transmitter/receiver plane. The argument of the step pump, $u(c_o\tau/2 - y)$, involves the running time, τ, and a fixed distance, y. The product of the nominal sound speed and the running time is the distance that the step pump has propagated since it was launched, at $\tau=0$. This quantity is divided by two, leading to the round-trip propagation distance. The step pump is zero, until the running time exceeds the time required for the reflected pump to reach the probe receiver. This is because the nonlinear modulation is not received at the probe receiver until the reflected pump reaches the receiving plane. In Equation (2.30), ξ is the integration variable.

$$\Delta\phi_u(\tau) = 2\pi f \int_{c_o\tau/2}^{0} \frac{d\xi}{\left(c_o(\xi) + \frac{B/A(\xi)}{2\rho_o(\xi)c_o(\xi)} r_y\, u(\frac{c_o\tau}{2} - y)\right)} - 2\pi f \int_{c_o\tau/2}^{0} \frac{d\xi}{c_o(\xi)} \quad , \quad (2.30)$$

where r_y represents the reflection coefficient at plane y. This phase difference is entirely due to the nonlinear interaction of the copropagated pump and the probe. The first integral is the phase of a probe wavelet copropagating with the pump. The second integral is the nominal phase acquired by the probe because of its propagation.

Because the second term in the denominator of the first integral is small compared to the first term, the following mathematical steps take advantage of this fact to simplify the equation:

$$\Delta\phi_u(\tau) = 2\pi f \int_{c_o\tau/2}^{0} \frac{d\xi}{c_o(\xi)\left(1 + \frac{B/A(\xi)}{2\rho_o(\xi)c_o^2(\xi)} r_y\, u(\frac{c_o\tau}{2} - y)\right)} - 2\pi f \int_{c_o\tau/2}^{0} \frac{d\xi}{c_o(\xi)} \quad . \quad (2.31)$$

The nominal sound speed is factored out of the denominator. This produces an expression in which the second term is much smaller than one. This ratio is expanded in a Taylor series, and the first and the linear term are kept, thereby reducing the equation to

$$\Delta\phi_u(\tau) = 2\pi f \int_{c_o\tau/2}^{0} \frac{1}{c_o(\xi)}\left(1 - \frac{B/A(\xi)}{2\rho_o(\xi)c_o^2(\xi)} r_y\, u(\frac{c_o\tau}{2} - y)\right)d\xi - 2\pi f \int_{c_o\tau/2}^{0} \frac{d\xi}{c_o(\xi)} \quad .(2.32)$$

Multiplying the quantities in the integrand and distributing the integration over the summation leads to

$$\Delta\phi_u(\tau) = 2\pi f\int_{c_o\tau/2}^{0} \frac{d\xi}{c_o(\xi)} - 2\pi f\int_{c_o\tau/2}^{0} \frac{B/A(\xi)}{2\rho_o(\xi)c_o^3(\xi)} r_y\, u(\frac{c_o\tau}{2} - y)d\xi - 2\pi f\int_{c_o\tau/2}^{0} \frac{d\xi}{c_o(\xi)} \quad . \tag{2.33}$$

The first and last integrals in Equation (2.33) are identical and cancel out. The remaining term is the excess phase acquired by the coherent probe, because of its nonlinear modulation by the pump. The result of subtraction of like terms leads to

$$\Delta\phi_u(\tau) = -2\pi f\int_{c_o\tau/2}^{0} \frac{B/A(\xi)}{2\rho_o(\xi)c_o^3(\xi)} r_y\, u(\frac{c_o\tau}{2} - y)d\xi \quad . \tag{2.34}$$

This equation relates the excess phase of the probe to the nonlinearity parameter. This formulation is for a single pump reflection. This pump reflection is from a location at a distance y from the probe receiver. The argument of the integrand contains the scaled step pump. The argument of this step function depends on a fixed quantity, y, and the running time. The step function is factored out of the integral. The reflection coefficient also depends only on the quantity y and is taken out of the integral. This leads to a new equation

$$\Delta\phi_u(\tau) = -2\pi f\, r_y\, u(\frac{c_o\tau}{2} - y)\int_{y}^{0} \frac{B/A(\xi)}{2\rho_o(\xi)c_o^3(\xi)} d\xi \,. \tag{2.35}$$

The integration limit of the integral in Equation (2.34) depends on the time that has elapsed from when the pump entered the medium. The integrand in Equation (2.34), however, contains the step pump which is evaluated to be zero, if the time delay that has elapsed corresponds to a distance smaller than the distance from the reflector plane to the receiver. The limit of the integral is changed in Equation (2.35) to incorporate this fact. If the elapsed time is shorter than the round-trip time to a reflector, the contribution from that reflector to the received nonlinearly modulated phase is zero. After the round-trip propagation time to the reflector has elapsed, the phase contribution from that reflector becomes a constant for a step pump. This contribution is the integral of the acoustic nonlinearity from the reflector plane to the receiver. The negative sign is absorbed into the integral in Equation (2.36). This equation is used to extend the analytical model to the case of discrete or continuous reflectors,

$$\Delta\phi_u(\tau) = 2\pi f\, r_y\, u\left(\frac{c_o\tau}{2} - y\right) \int_0^y \frac{B/A(\xi)}{2\rho_o(\xi)c_o^3(\xi)}\, d\xi\,. \qquad (2.36)$$

The derivation above is for a single reflector situated at a distance y from the receiver. For a continuum of reflectors, the phase contributions from all of the reflected pumps are integrated. The natural variable to use for this integration is the distance of the reflector to the probe receiver. The received phase contribution corresponding to a given reflector is zero, until the round-trip time for reaching that reflector has elapsed. The outer integral's upper bound depends on the distance corresponding to the round-trip depth for the elapsed time. This outer integration takes into account the contributions from the reflectors within the round-trip travel distance for the current running time,

$$\Delta\phi_u(\tau) = 2\pi f \int_0^{c_o\tau/2} dy\ r_y\ u(\frac{c_o\tau}{2} - y) \int_0^{y} \frac{B/A(\xi)}{2\rho_o(\xi)c_o^3(\xi)} d\xi \quad . \tag{2.37}$$

2.3.2 Impulse response

This derivation, for a step pump, leads to the formulation of the imaging equation for an arbitrary pump. To formulate such an equation, the impulse response of the system is needed. The step response leads to the impulse response as given in the following equation:

$$\begin{aligned}\Delta\phi_\delta(\tau) &= 2\pi f \int_0^{c_o\tau/2} dy\ r_y\ \delta(\frac{c_o\tau}{2} - y) \int_0^{y} \frac{B/A(\xi)}{2\rho_o(\xi)c_o^3(\xi)} d\xi \\ &= 2\pi f\, r(c_o\tau/2) \int_0^{c_o\tau/2} \frac{B/A(\xi)}{2\rho_o(\xi)c_o^3(\xi)} d\xi \quad .\end{aligned} \tag{2.38}$$

This equation represents the response of the system to a delta pump. It integrates the phase contributions corresponding to all of the pump reflections in the medium. Evaluating the integral, with a delta function in its integrand, leads to the evaluation of the integrand at a value that makes the argument of the delta function zero. Evaluating the integrand for $y=c_o\tau/2$ leads to the second integral equation in Equation (2.38). The reflection coefficient is multiplied by the integral of the acoustic nonlinearity from the corresponding reflector to the receiver. The excess phase of the probe is proportional to the product of the reflection coefficient and the integral of the acoustic nonlinearity.

The convolution of the impulse response with an arbitrarily shaped pump produces the general imaging equation. This imaging equation is valid for any profile of the acoustic

nonlinearity, of the nominal sound speed, and of the nominal medium density. In this equation, the probe can be a single frequency or a swept sinusoid, and the pump can be any desired acoustic signal. The phase of the probe is given as

$$\Delta\phi(\tau) = 2\pi f \int_0^{c_o\tau/2} dy\ r_y\, p(\frac{c_o\tau}{2} - y) \int_0^{y} \frac{B/A(\xi)}{2\rho_o(\xi)c_o^3(\xi)}\, d\xi \quad . \tag{2.39}$$

This is the copropagation reflection model.

In general, the modulated phase is the convolution of the pump with the integral of the acoustic nonlinearity multiplying the reflection coefficient. For a delta pump (Equation (2.38)), the modulated phase is an estimate of the integral of the acoustic nonlinearity for any depth where a reflector exists, multiplied by the reflection coefficient peculiar to that reflector. The desired quantity in this imaging system is the acoustic nonlinearity, or, equivalently, the integral of the acoustic nonlinearity. The information about the acoustic nonlinearity needs to be separated from the reflection coefficient profile.

2.3.3 Scaling with respect to the reflection coefficient

The reflection coefficient profile is needed to scale the probe phase given in Equation (2.38). The reflection coefficient profile can be extracted from pump echoes. The received echoes are formulated as

$$\Gamma(\tau) = \int_0^{c_o\tau/2} dy\ r_y\, p(\frac{c_o\tau}{2} - y) \quad . \tag{2.40}$$

This integration, which is the accumulated reflections caused by the pump, is over a region

in space which corresponds to the round-trip delay time, and, represents the added, time-delayed, and scaled pump echoes.

The pump echoes are a scaled version of the pump with their amplitudes scaled by the reflection coefficient profile. The reflection coefficient profile could be directly obtained using a delta pump. A delta pump leads to

$$\Gamma_\delta(\tau) = \int_0^{c_o\tau/2} dy\ r_y\ \delta(\frac{c_o\tau}{2} - y)\ = r(\frac{c_o\tau}{2})\ . \tag{2.41}$$

The delta pump is substituted for the arbitrary pump. This delta function sifts out the reflection coefficient profile. This evaluation of the integral produces the reflection coefficient which is then used to scale the recovered phase of the probe from Equation (2.38).

The recovered probe phase, due to a delta pump, is the multiplication of the reflection coefficient by the integral of the acoustic nonlinearity. Dividing the reflection profile into the phase given in Equation (2.38) removes the reflection coefficient profile and leads to the integral of the acoustic nonlinearity. This division leads to

$$S(\tau) = 2\pi f \int_0^{c_o\tau/2} \frac{B/A(\xi)}{2\rho_o(\xi)c_\delta^3(\xi)}\ d\xi\ . \tag{2.42}$$

The integral of the acoustic nonlinearity is available as a continuous function of time. Since the integral is available for various integration limits, the integrand can be extracted. The extraction of the integrand is possible since the upper bound is a running variable. The upper bound of Equation (2.42) is a function of depth. Since the variable

representing depth has been preserved, the image information has been preserved. The image information is the integrand which is obtained by differentiating the integral.

The next step is to differentiate the integral Equation (2.42) to obtain an estimate of the acoustic nonlinearity,

$$\frac{dS(\tau)}{d\tau} = 2\pi f \frac{B/A(c_o\tau/2)}{2\rho_o(c_o\tau/2)c_o^3(c_o\tau/2)} \quad . \tag{2.43}$$

The acoustic nonlinearity is multiplied by the radian frequency of the probe. If the probe frequency is a swept sinusoid, the estimate becomes

$$\frac{dS(\tau)}{d\tau} = 2\pi f(\tau) \frac{B/A(c_o\tau/2)}{2\rho_o(c_o\tau/2)\, c_o^3(c_o\tau/2)} \quad . \tag{2.44}$$

The radian frequency in cases of both coherent or wide band probes is compensated for by dividing the estimate by the radian frequency of the probe. The final estimate is

$$\text{Estimated Profile} = \frac{B/A(c_o\tau/2)}{2\rho_o(c_o\tau/2)\, c_o^3(c_o\tau/2)} \quad . \tag{2.45}$$

The equations that lead to Equation (2.45) use the copropagation reflection method as a basis for nonlinear imaging, when the multiple pump reflections are taken into account.

2.4 Comparison Between Copropagation and Counterpropagation

The mathematical models for copropagation reflection (Equation (2.39)) and counterpropagation (Equation (2.10)) are evaluated numerically and compared. The pump in Equation (2.10) is chosen as a 10 atm peak pressure, with a 0.5 μsec duration, and is one cycle of a sinusoid. This pump interacts with a 2 MHz probe. This pump, while

counterpropagating the probe, nonlinearly modulates its phase. The phase change, due to counterpropagation nonlinear interaction, is less than 0.02 deg (Equation (2.10)) for a B/A change from 10 to 9. To compare the sensitivity of Equation (2.10) to the sensitivity of Equation (2.39), the reflection coefficient profile is needed. If the reflection coefficient is 1/100, a copropagation reflection over 2 cm contributes a phase of 0.21 deg (Equation (2.39)).

Copropagation reflection produces a much larger phase modulation than counterpropagation. One reason for the low sensitivity of counterpropagation is that the pump and the probe are propagating past each other, which reduces the interaction time to half the pump duration. Another reason is evident from Equation (2.10); taking the nonlinearity to be positive, a bipolar pump would lead to a bipolar integrand, which reduces the cumulative effect of the nonlinear interaction.

The nonlinear interaction is scaled if the peak pump pressure or the probe frequency is changed. The copropagation reflection and counterpropagation nonlinear interactions in this case do not change their relative values. The conclusion from the above numerical example, and its extensions regarding changing pump pressure or probe frequency, is that copropagation reflection is more sensitive than counterpropagation.

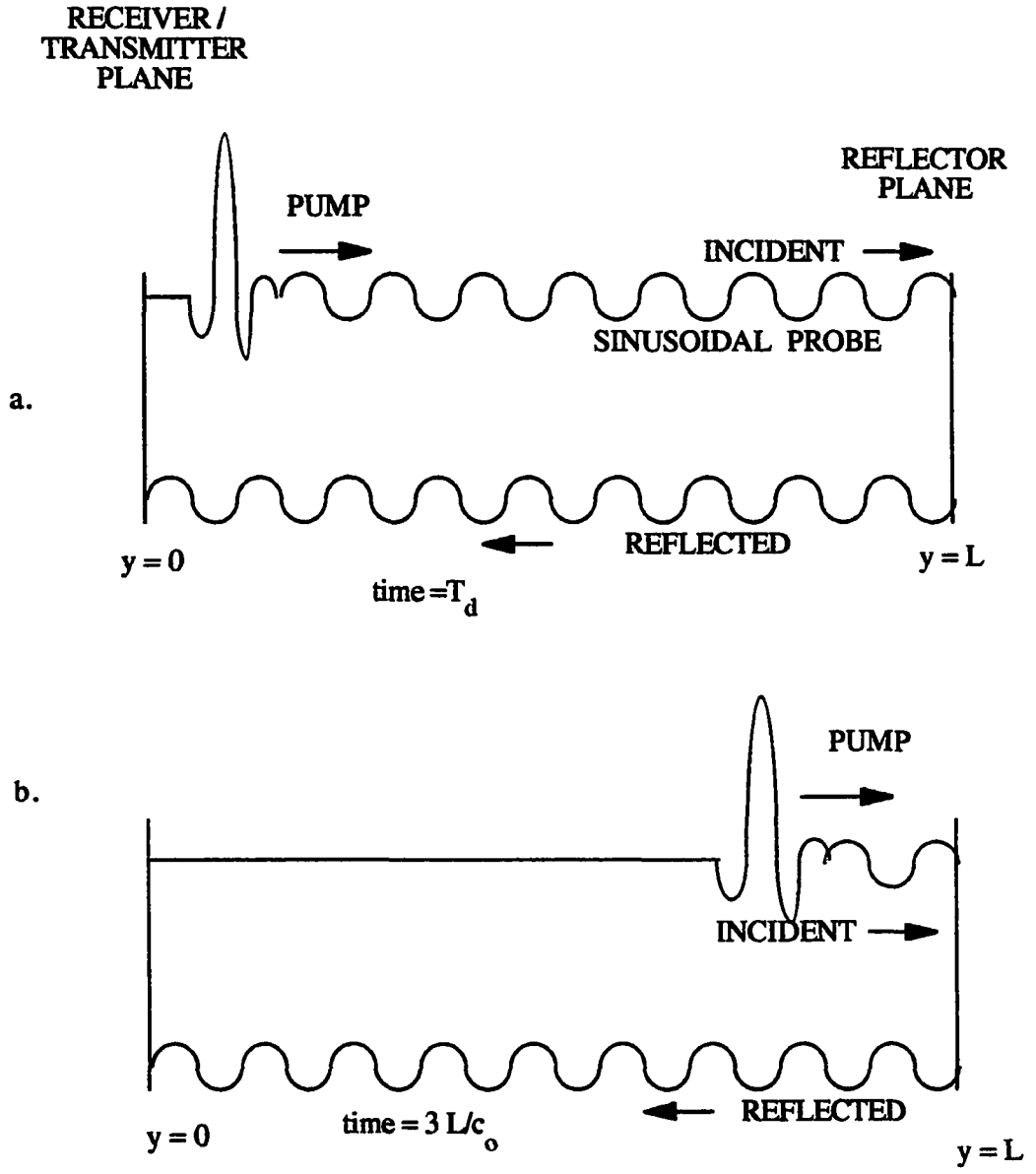

Figure 2.1 The imaging system: a. The probe has filled the medium. b. The pump has propagated into the medium and nonlinearly interacted with the counterpropagating probe.

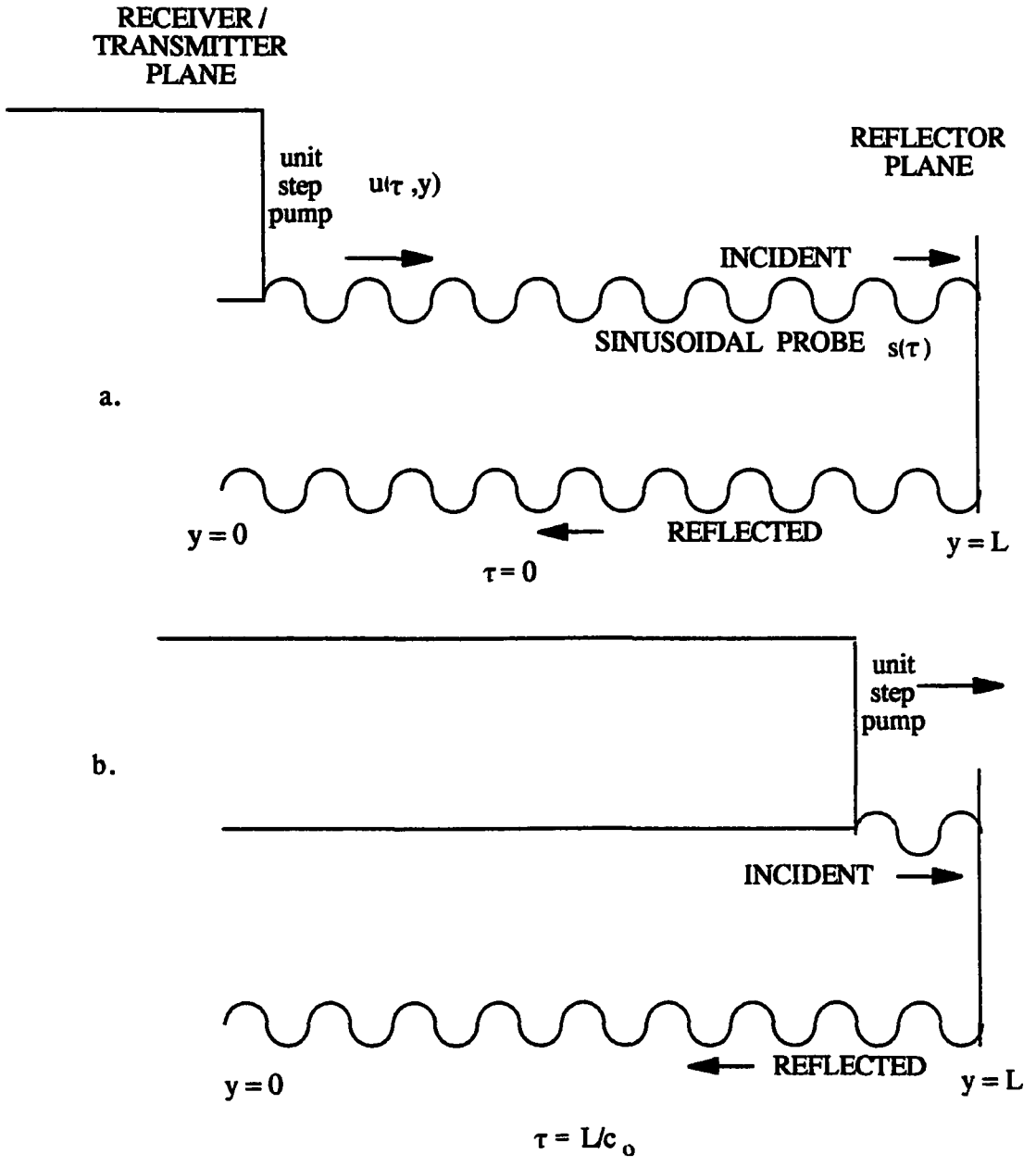

Figure 2.2 A step pump interrogates the medium: a. The probe has filled the medium and the step pump is introduced into the medium. b. The step pump counterpropagates the probe.

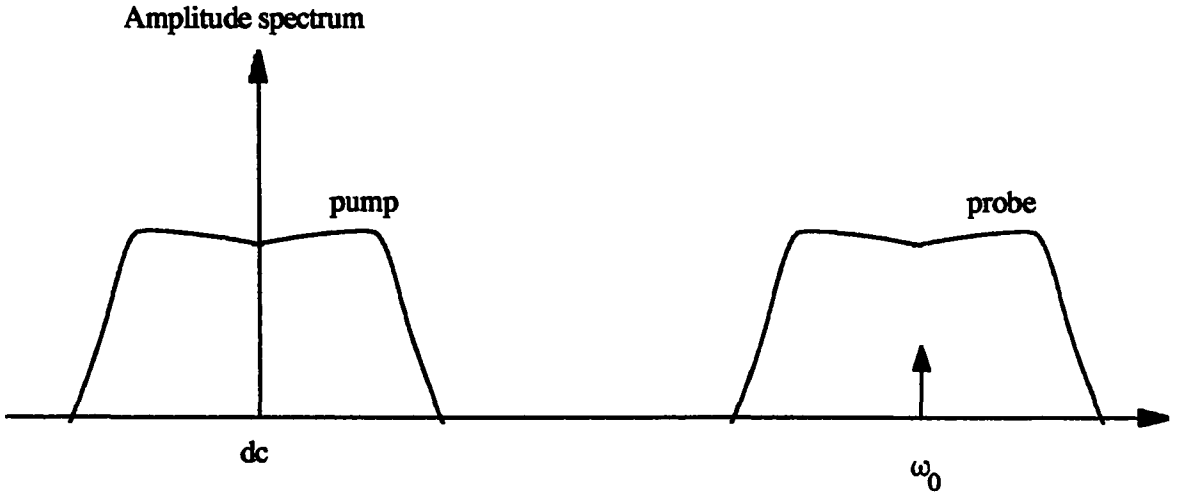

Figure 2.3 The spectral profile of the pump and the nonlinearly modulated coherent probe.

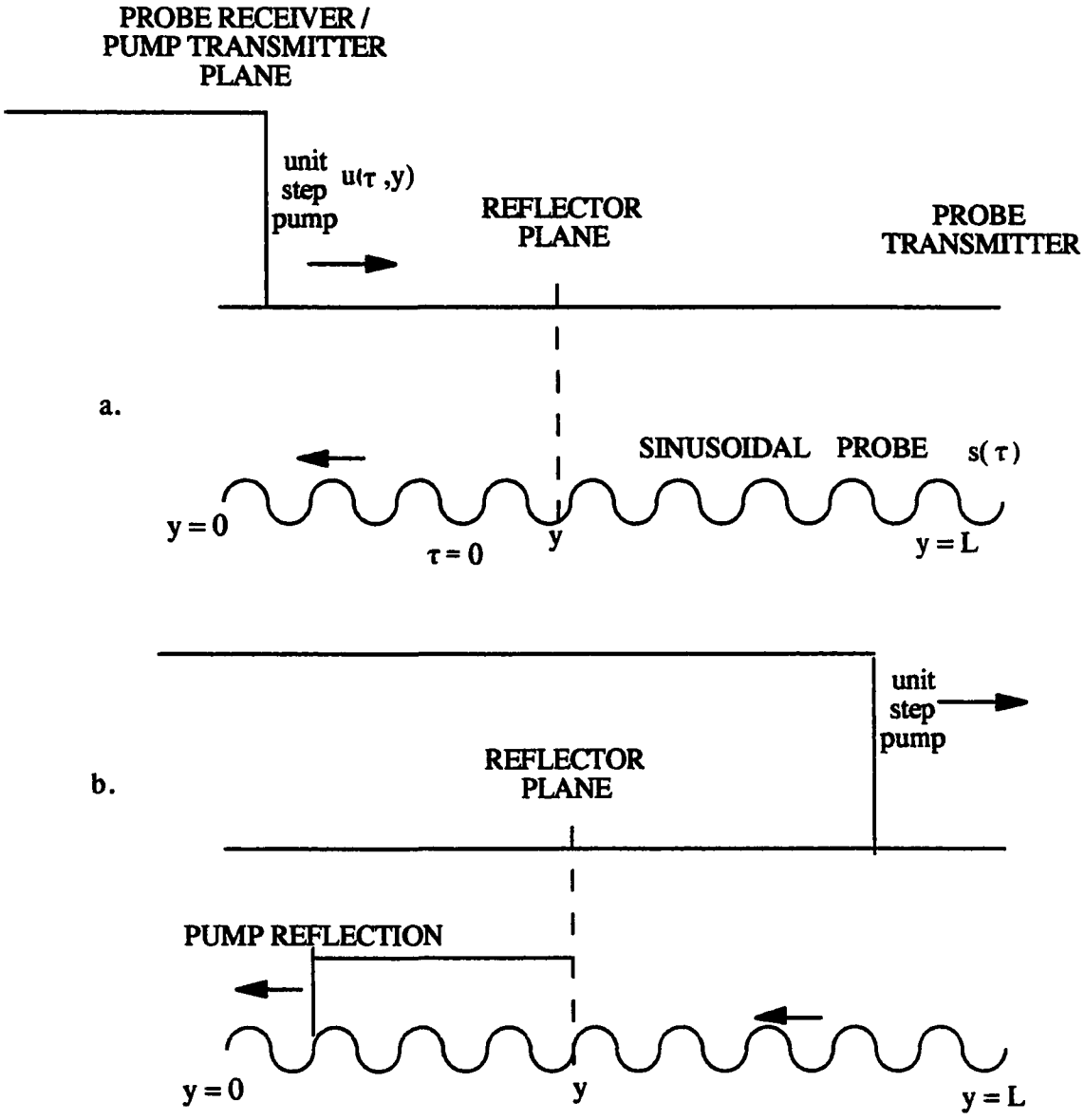

Figure 2.4 a. A sinusoidal probe has filled the medium and a step pump is introduced into the medium. b. The step pump is reflected by a reflector plane and copropagates with the probe to the probe receiver.

CHAPTER 3

SIMULATION

This chapter provides the nonlinear propagation algorithm for the simulation of nonlinear interaction. This algorithm is applied to the counterpropagation nonlinear interaction of pump and probe and to the copropagation nonlinear interaction of pump and probe; the comparison between the sensitivity of counterpropagation and copropagation reflection is discussed.

The simulation uses the mathematical solution to the nonlinear wave equation. The purpose of the simulation is to interact the pump and the probe nonlinearly, and to compare the sensitivity of copropagation versus counterpropagation. The underlying simplification is a plane wave assumption. The algorithm is validated by comparing it with the Fubini solution. The simulations in this chapter show that the copropagation reflection method is more sensitive than the method using counterpropagating waveforms.

3.1 Simulation Algorithm

3.1.1 Introduction

The simulation program propagates plane ultrasound waves of finite amplitude in an attenuating, inhomogeneous medium, taking into account propagation dependence on the B/A parameter. The program's flow chart is provided, and the individual modules are described. The output of the simulation program is compared with the Fubini solution for a coherent plane wave input. The simulation algorithm nonlinearly interacts a plane finite amplitude pump with an infinitesimal amplitude probe. The probe and the pump either copropagate or counterpropagate. Both of these situations are discussed in this chapter.

3.1.2 Analytical basis of the simulation algorithm

In a nonattenuating fluidlike medium, the general nonlinear wave equation is (Section 1.1, Equation 1.27)

$$\frac{\partial^2 \zeta}{\partial t^2} = \frac{c_o^2}{(1+\frac{\partial \zeta}{\partial x})^{2+\frac{B}{A}}} \frac{\partial^2 \zeta}{\partial x^2} \quad , \tag{3.1}$$

where ζ is particle displacement and c_o is the sound speed of vanishingly small disturbance (Beyer and Letcher, 1969). In terms of pressure, the general solution of Equation (3.1) is

$$p = F(\omega (t \pm x/v)) \quad , \tag{3.2}$$

where v is the rate of propagation of the wave as a function of pressure and is given by

$$v = c_o \left(1 + \frac{B}{2A} \frac{p}{\rho_o c_o^2}\right)^{2A/B + 1} \quad . \tag{3.3}$$

As seen from this equation, the B/A parameter, the nominal sound speed, the nominal medium density, and the change in acoustic pressure all have been taken into account. The algorithm to be presented below uses Equation (3.3) to propagate a plane pump, taking into account nonlinear distortion and absorption of the acoustic energy.

The first module of the algorithm is the application of attenuation to the pump. This step is placed before the propagation step to remove the possibility of the wave having multiple values. The attenuation function is a function of frequency and is calculated in the frequency domain. The pump is Fourier transformed to obtain the complex Fourier coefficients. These coefficients are multiplied by the attenuation appropriate for the frequency of the Fourier coefficient and the nominal propagation distance.

The time interval for attenuation should be small compared to the time it takes for the pump to become substantially distorted. The degree of distortion depends upon the source pressure, the frequency, and the nonlinear and attenuation properties of the medium. In making the distortion and attenuation calculations for each short propagation step, the step size needs to be small enough that the waveform remains single-valued. For the simulations in this chapter, the amount of attenuation is calculated and applied to the pump every 0.5 cm.

The second module is wave propagation. The pump is represented as $p(x,\tau)$, where x is the spatial coordinate and τ is the time. The pump is digitized in space and is represented by $p(X_i,\tau_j)$, where X_i represents a vector of the spatial positions of the pump wavelets (pump samples). The vector $p(X_i)$ contains the pressure associated with the wavelets. The vectors X_i, $p(X_i)$ and the quantity τ_j define the pump for the time τ_j. The spatial profile of the pump for the next time update, τ_{j+1}, is represented by $p(X_{i+1}, \tau_{j+1})$. The vector X_{i+1} represents the new spatial positions of the wavelets. The vectors X_{i+1} and X_i are related to each other by the nonlinear distortion step.

The calculation of the vector X_{i+1} updates the spatial position of each single pump wavelet. Taking x_i to be an element of the vector of spatial positions X_i, the updated location x_{i+1} is given by

$$x_{i+1} - x_i = \int_{\tau_j}^{\tau_{j+1}} c(x,\tau)\, d\tau \quad , \tag{3.4}$$

where $c(x,\tau)$ represents the sound speed that the wavelet experiences while traveling in the time interval (τ_j,τ_{j+1}). In the above equation, Equation (3.3) is substituted for $c(x,\tau)$ to yield

$$x_{i+1} - x_i = \int_{\tau_j}^{\tau_{j+1}} c_o(x) \left(1 + \frac{B}{A}(x) \frac{p(x,\tau)}{2\rho_o(x)\, c_o^2(x)}\right)^{2A/B(x)+1} d\tau \cdot \qquad (3.5)$$

For a given wavelet, $p(x,\tau)$ is approximated as $p(x_i)$, provided the propagation time interval, (τ_j,τ_{j+1}), is small. The pump wavelet propagates through an inhomogeneous medium where the nominal speed of sound, the medium density and the B/A parameter change.

The updated pump position for a fairly small propagation time interval is

$$x_{i+1} - x_i \cong \left\{c_o(x_i) \left(1 + \frac{B}{A}(x_i) \frac{p(x_i)}{2\rho_o(x_i)\, c_o^2(x_i)}\right)^{2A/B(x_i)+1}\right\} (\tau_{j+1} - \tau_j) \cdot \qquad (3.6)$$

The time updates are chosen at regular time intervals. These time intervals, (τ_j,τ_{j+1}), are fixed at the initialization step. For the time intervals, the nonlinear distortion calculation is performed for all of the elements of the spatial vector X_i, which leads to the propagated spatial positions X_{i+1}.

After the nonlinear distortion step, the program iterates back to the attenuation step. The attenuation function is applied, in the frequency domain, to the Fourier transform of the pump. The vector X_i is initially a uniformly sampled vector, but, after the nonlinear propagation step, the sample spacings become nonuniform. Because of the nonlinear propagation, the different wavelets propagate at different speeds, leading to the vector X_{i+1}-X_i, which has different values corresponding to the individual x_i. This nonuniform sampling is seen from Equation (3.6), where the spatial position (and spacing between wavelets) depends on the wavelet pressure. The Fourier transform requires that the spatial position vector elements, X_i, are on a uniform grid. The matrix $[X_i, p(X_i)]$, with X_i representing nonuniform sampling, is interpolated to produce a uniformly sampled spatial

vector $p(\underline{X}_i,\tau_j)$. Fourier transform of $p(\underline{X}_i,\tau_j)$ produces $P(k_i,\tau_j)$, where k_i represents the vector of Fourier coefficients. This complex function is multiplied by the attenuation function in the frequency domain. The attenuation function is represented as $A(k_i, x_{j+1}-x_j)$, where $x_{j+1}-x_j$ is the distance of propagation (here x_j represents a wavelet with a pressure of zero). The spectrum of the attenuated pump is represented by $P(k_i,\tau_j)$ $A(k_j, x_{j+1}-x_j)$. This spectrum is then inverse Fourier transformed to produce the pump.

The pump is described as a function of distance, which facilitates simulating the spatial interaction of the pump and the probe. These waveforms are sampled on a uniform spatial grid. The computer program keeps track of the waveform pressures and their corresponding spatial plane coordinates. The memory requirement depends on the desired sampling frequency and the spatial extent of the waveforms. Higher sampling frequencies and longer spatial extents lead to larger array sizes. The pump is attenuated in the attenuation module for a desired propagation time. The spatial location of the pump wavelets is updated in the nonlinear propagation step, by small time steps. Provided that these time steps are small, the calculation represents the physical interaction occurring in space and evolving in time. Next, the physical interaction between the pump and the probe is mathematically formulated.

The probe wavelets are represented as $B(X_k)$, where X_k represents the spatial sample locations and $B(X_k)$ represents the amplitude of the probe. The wave propagation algorithm (Equation (3.6)) is extended as follows: Given that the time interval for propagation is small, the pressure for each x_k is given as the pump pressure at that spatial location. The spatial value of x_k might not be exactly the same as an x_i in the X_i vector representing the spatial samples of the pump. In this situation, the acoustic pressure at the spatial location x_k is obtained from the pump samples, $p(X_i)$, by interpolation. After obtaining the pump pressure, the spatial position of the probe wavelet is updated as

$$B(x_{k+1}) - B(x_k) = \int_{\tau_j}^{\tau_{j+1}} c_o(x) \left(1 + \frac{B}{A}(x) \frac{p(x,\tau)}{2\rho_o(x)\, c_o^2(x)}\right)^{2A/B(x)+1} d\tau \ , \quad (3.7)$$

where x in the integrand represents the spatial position of the probe wavelet in the time interval of (τ_j,τ_{j+1}). Given that the time interval, (τ_j,τ_{j+1}), is very small, the integral could be approximated as

$$B(x_{k+1}) - B(x_k) \cong \left\{c_o(x_k) \left(1 + \frac{B}{A}(x_k) \frac{p(x_k)}{2\rho_o(x_k)\, c_o^2(x_k)}\right)^{2A/B(x_k)+1}\right\} (\tau_{j+1} - \tau_j) \ . \quad (3.8)$$

The nominal sound speed, the B/A parameter, and the medium density are evaluated at the initial spatial position of the probe wavelet, x_k. The pump is calculated, at time τ_j, as the pressure at this spatial location of the probe wavelet.

Equation (3.8) provides the nonlinearly propagated probe. The updating of the probe and pump wavelets is done sequentially. Initially, the pump is propagated for a small time interval. Next, the probe wavelets are propagated for the same small time interval using the updated pump. This process is repeated until the pump and the probe are propagated for the desired interaction time. The attenuation and the nonlinear distortion steps are continued until the pump has propagated for the desired time.

3.1.3 Program flow chart

A compact reference for the different modules of the wave propagation and the wave interaction algorithm is provided in Figure 3.1. This flow chart shows the major modules of the wave propagation algorithm. The pump, the probe, the medium parameters, the sampling rate, and the propagation time are entered in the initialization module. The program acts on the initialization information, the attenuation module

attenuates the waveforms, the wave propagation nonlinearly distorts the waves, and the nonlinear wave interaction module simulates the nonlinear interaction of the pump with the probe. The algorithm iterates between the nonlinear distortion, the nonlinear interaction, and the attenuation steps.

3.1.4 Testing

A comparison is made between the Fubini solution and the simulation program propagating coherent plane waves of finite amplitude. Excellent agreement is found between these solutions. The Fubini solution involves an infinite sum which is truncated to the first ten terms. It is evaluated for various time instances versus distance. The Fubini solution is approximated by the following equation

$$p(x) = p_o \sum_{n=1}^{N} \frac{J_n(n\sigma)}{n\sigma/2} \sin n(2\pi ft - kx) \qquad x \angle 1 \ , \tag{3.9}$$

where p_o is 20 atm, f is 1 MHz, k is the wavenumber which for water is $2\pi/1.5$mm, and σ is given by $\sigma = x/l$; l is called "shock forming distance" and is 7.5 cm in water for this particular pressure and frequency (Beyer, 1974). For this calculation N is ten. The above sum is calculated on a Cray-XMP using the Bessel function calculating subroutines in the IMSL library.

The Fubini solution and the simulation are compared in Figures 3.2, 3.3, and 3.4. Wave propagation is performed for 1, 3, and 5 cm. The Fubini solution and the wave propagation algorithm are evaluated at ten spatial samples. As seen in the figures, the peak pressure of the acoustic wave is 20 atm. The waveform shown is the positive half-cycle of a 1 MHz sinusoidal signal, with a width of 0.75 mm.

The simulated and calculated data are plotted using two different symbols. The star symbol represents the output of the wave propagation algorithm. The circle symbol

represents the Fubini solution. Only the data points from the Fubini solution are interpolated. The analytical solution and the wave propagation algorithm calculate the wave on different spatial grids. This provides a separation between the samples, and keeps the graph readable.

There is a close resemblance between the waves propagated by the wave propagation algorithm and the Fubini solution. The equation used for propagating the acoustic waves in a nonlinear medium (Equation (3.3)) is from the solution to the nonlinear plane wave equation. Since this solution does not have a coherency restriction, it could be used to propagate any arbitrary waveform. This simulation is used next to nonlinearly interact a pump counterpropagating a probe.

3.2 Counterpropagation Nonlinear Interaction

This section covers the simulation study of a pump and a probe which counterpropagate and nonlinearly modulate each other. The probes used are a chirp and a sinusoid. The demodulation of the chirp probe is elaborated upon in Appendix A.

The algorithm propagates a plane ultrasound pump of finite amplitude using a step-wise spatial domain technique. The simulation takes into account both the nonlinear distortion and attenuation of the pump. Attenuation is applied in the frequency domain. The existence of the pump induces a change in the time of flight of a probe wavelet between the transmitter and the receiver. The change in the time of flight is observed as the change in the probe phase. The nonlinear interaction of the pump with the probe either slows down the probe wavelet or speeds it up. This depends on whether the probe interacts with the rarefaction or the compression part of the pump. Because of the large disparity in the amplitude of the pump and the probe, the pressure in the probe region is essentially that produced by the pump. The pump modulates the phase of the probe. The modulated phase of a single-frequency sinusoid is extracted using a simulated narrow-band FM demodulator. The recovered phase is deconvolved with the initial spatial profile of the

pump to remove the smearing effect of the finite width pump. Since the pump and probe counterpropagate, the interaction time of each probe wavelet with the pump is half the pump time duration.

3.2.1 Simulations of the counterpropagation nonlinear interaction

The simulated profile of the B/A parameter is shown in Figure 3.5, where the transmitter / receiver plane is located at 0.5 cm and the reflector plane is at 4.5 cm. The total width of the simulated medium is 4 cm. This B/A profile contains discontinuities to allow the study of the resolving capabilities of this simulated imaging system. For the first simulation a delta pump is used. In this computer experiment, the delta pump is approximated as the positive half-cycle of a 2 MHz sinusoidal pump. The peak pump pressure is 20 atm. This pump, before entering the medium and after propagating through it, is depicted in Figure 3.6. The major change in this pump is its progress toward a sawtooth waveform shape. The peak pressure has changed only slightly since the attenuation in water is negligible.

In this computer experiment, the probe is a single-frequency sinusoid with a frequency of 2 MHz. This probe is propagated into the medium, reflected, and, when it reaches the launch point, the pump is propagated into the medium. The effective spatial length of the probe is then twice the length of the medium. The probe is received and, simultaneously, a narrow-band FM demodulator detects the instantaneous phase of the probe. This phase function carries the information on the convolution of the pump with the B/A profile. This recovered phase is depicted in Figure 3.7. The maximum phase shift is 0.3 deg. This phase profile matches the underlying B/A profile very closely. The phase profile is deconvolved with the initial spatial profile of the pump. The deconvolved image of the B/A parameter is shown in Figure 3.8. As expected from Equation (2.10), the broadband nature of the δ pump has reproduced an estimate very similar to the underlying B/A parameter.

The counterpropagation of a chirp probe and a pump is also simulated. The pump used in this computer experiment is shown in Figure 3.9. The dc offset of this pump is zero. The pump nonlinearly modulates the chirp probe, while the two signals counterpropagate. The extracted phase of this chirp probe is shown in Figure 3.10.

In Figure 3.10, the interval with a B/A of 11 is 0.015 m to 0.03 m. Outside this interval, B/A is five. The pump has a zero dc offset; therefore, the resulting nonlinear interaction is zero for regions in which the B/A parameter is a constant. The nonzero offset of the phase seen in Figure 3.10 is due to numerical noise generated by the vast dynamic range of the numbers involved in the calculations. The phase fluctuations have occurred at the boundary of the regions in which the B/A parameter changes. The peak phase deviation is about 0.2 deg for a probe frequency of 2 MHz. The next section provides the phase deviation for a probe copropagating with a pump.

3.3 Copropagation Nonlinear Interaction

This section simulates the nonlinear interaction occurring between a chirp pump copropagating with a probe. The pump is shown in Figure 3.11. This pump is an LFM pulse covering the frequency range of about dc to 1.6 MHz. The vertical axis in Figure 3.11 represents pressure and is in units of Pascal (Pa). The peak pump pressure is 0.01 atm. This pump nonlinearly interacts with a probe over a spatial region of 5 cm. The effects of the pump pressure, the B/A parameter, and the distance of copropagation on the level of nonlinear interaction are presented below.

3.3.1 Effect of pump pressure on nonlinear interaction

The result of the nonlinear interaction of the chirp pump with a probe is shown in Figure 3.12. The right vertical axis shows the phase modulation of a coherent 2 MHz probe. The left vertical axis is in a pulse position modulation units. Pulse position modulation is calculated as $B(X_f)$-$B(X_i)$-5cm, where B(X) is defined in Equation (3.8),

and $B(X_f)$ and $B(X_i)$ represent the final and initial spatial positions of the wavelet. The probe wavelets are initially uniformly spaced. The nonlinear interaction of the pump and probe shifts the position of the probe wavelets.

The shape of the modulation in Figure 3.12 is similar to the profile of the pump, partly because the pressures of the probe wavelets are determined by the pump pressure with which they propagate. A probe wavelet propagates with a speed determined by the pump pressure; the larger the pump pressure, the faster the wavelet propagates and the level of nonlinear modulation increases.

The phase modulation is plotted versus pump pressure in Figure 3.13. It is observed that there is a linear relationship between the pump pressure and the modulation of the probe by this pump. For this computer experiment, the B/A was eight.

3.3.2 Effect of the acoustic nonlinearity parameter

Another parametric study of interest is the relationship between the phase modulation and the B/A parameter. The phase acquired by a 2 MHz probe, copropagating collinearly with a pump of peak pressure 1 atm for a distance of 5 cm, is shown in the right vertical axis in Figure 3.14. This computer experiment shows that, for a pump pressure of 1 atm, increasing the underlying B/A parameter increases the level of the nonlinear interaction.

3.3.3 Dependence of nonlinear modulation on the distance of copropagation

Another parameter of interest is the sensitivity of the nonlinear interaction process to the distance of copropagation of the pump and the probe. The peak pressure of the pump is chosen as 10 atm. The pump is copropagated with a probe for various distances. The modulation of the probe by the pump is shown in Figure 3.15. Since the nonlinear modulation is cumulative, the longer distances of copropagation lead to larger values of nonlinear modulation. A B/A parameter of nine was used for this computer experiment.

Several trends emerge from these sets of computer experiments. The level of nonlinear interaction is proportional to the distance of copropagation, to the B/A parameter, and to the pump amplitude. Next, the contribution to nonlinear interaction from copropagation is compared to that of counterpropagation.

3.4 Comparison Between the Sensitivities of Copropagation and Counterpropagation

The sensitivity of counterpropagation is compared with the modulation caused by the pump reflections in this section. The simulation of counterpropagation has shown that this process has low sensitivity (Section 3.2). The net counterpropagation interaction depends on the differential change in the B/A parameter, with larger changes leading to larger levels of nonlinear interaction. The examples in Section 3.2, with very large abrupt changes in the B/A parameter, provide a measure of what the largest phase contribution would be (Figures 3.7 and 3.10). This case is compared with the phase contribution from the reflected pump copropagating with the probe.

Figure 3.7 shows that a pump of peak pressure 20 atm induced a counterpropagation phase shift of 0.3 deg in a 2 MHz probe. If 1/100 of this pump is reflected and copropagates with the probe over 5 cm, the copropagation reflection phase shift is 0.96 deg (Figure 3.13). This is a typical example in the sense that increasing the pump pressure or probe frequency only scales these numbers and does not alter their relative sensitivity. The conclusion is that the sensitivity of the copropagation reflection technique is higher than that of the counterpropagation technique.

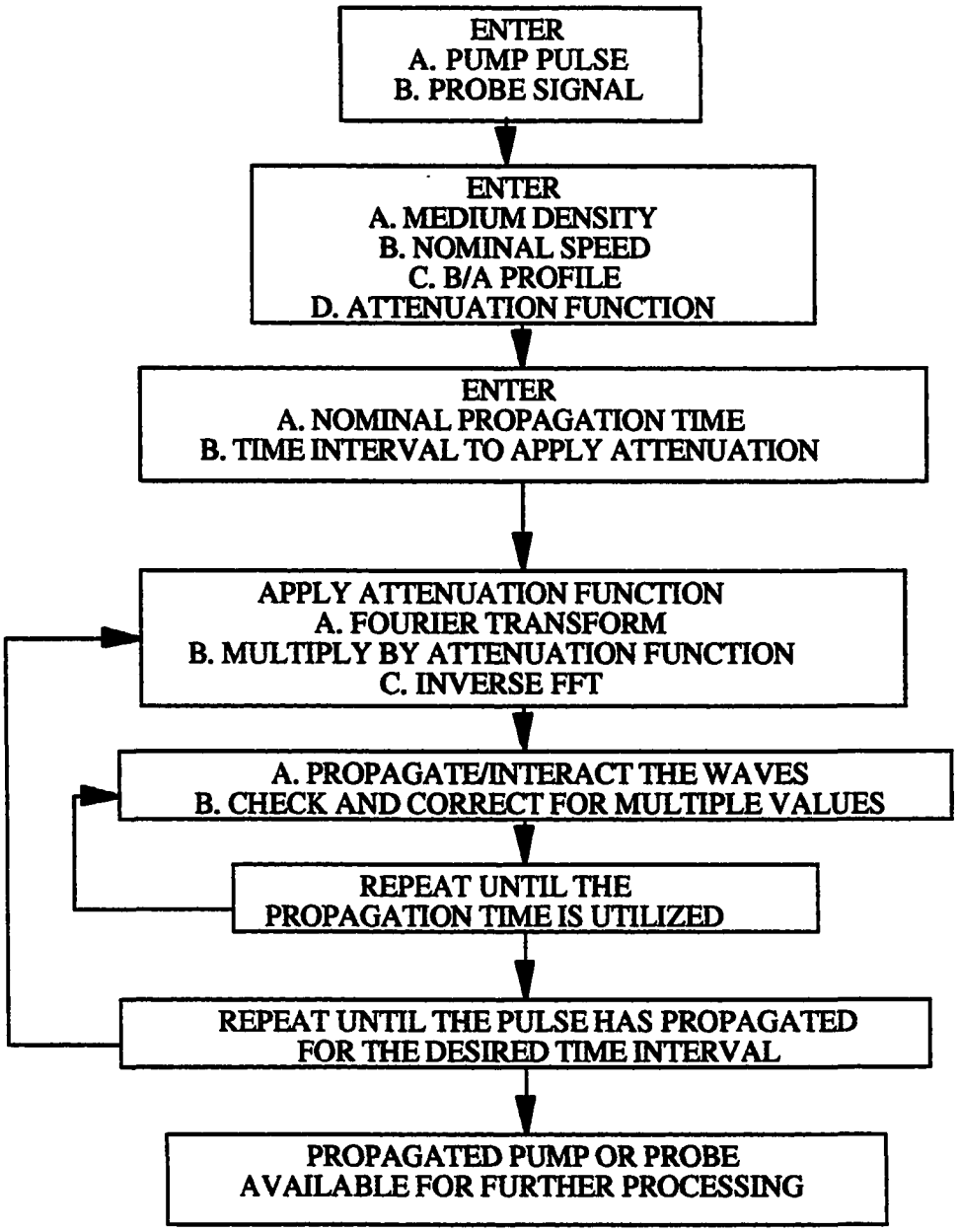

Figure 3.1 Flow chart of nonlinear wave interaction/propagation algorithm.

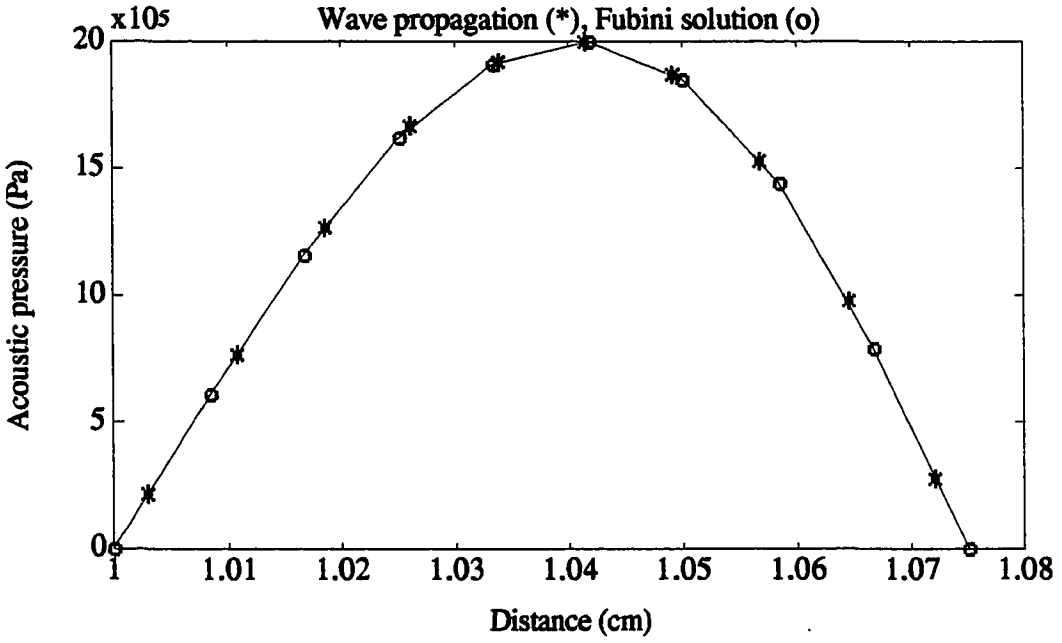

Figure 3.2 Stars represent the output of the wave propagation program. The circles are the analytical solution by Fubini. Pump is 20 atm. B/A is 5 and frequency is 1 MHz.

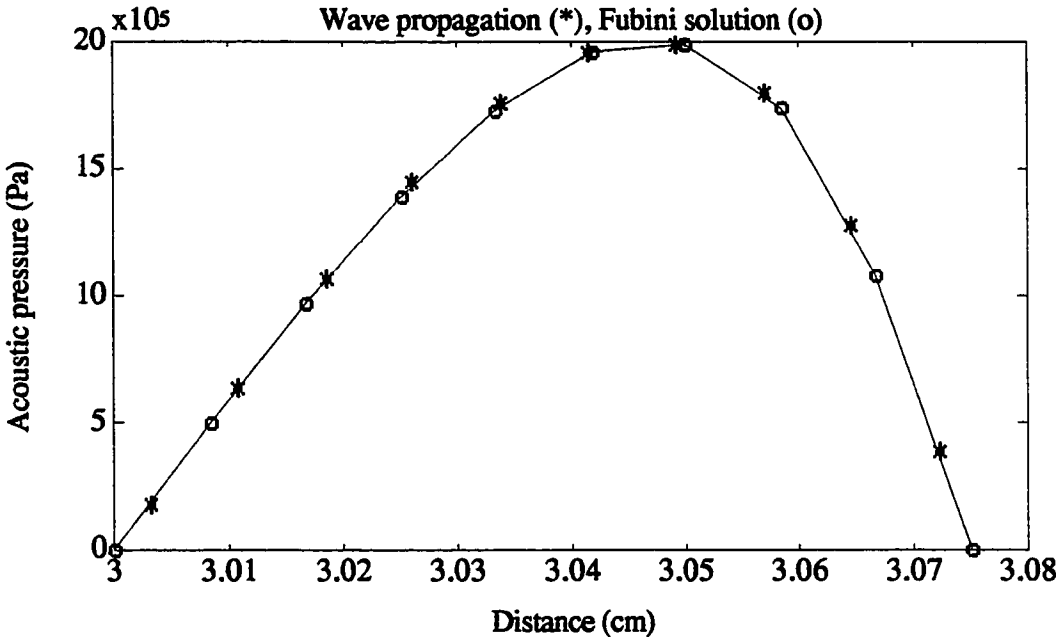

Figure 3.3 The coherent signal nonlinearly distorted. The signal has propagated 3 cm. B/A is 5. Frequency is 1 MHz and the medium is waterlike.

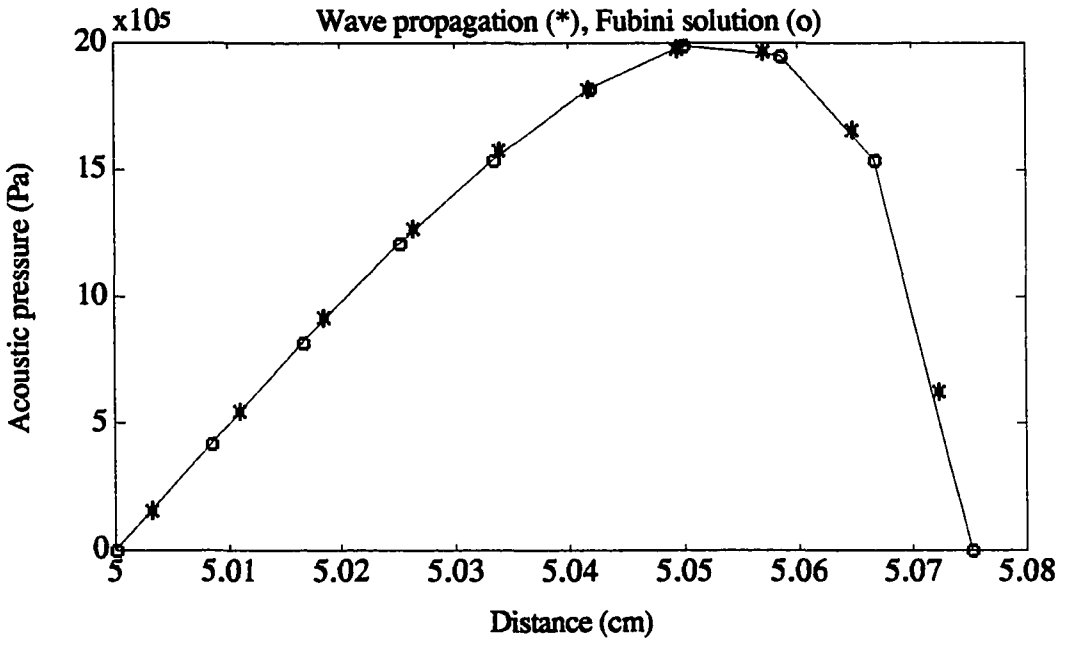

Figure 3.4 The simulated and the analytical solution of the nonlinear wave equation. The signal has propagated 5 cm. Frequency is 1 MHz. The medium is waterlike.

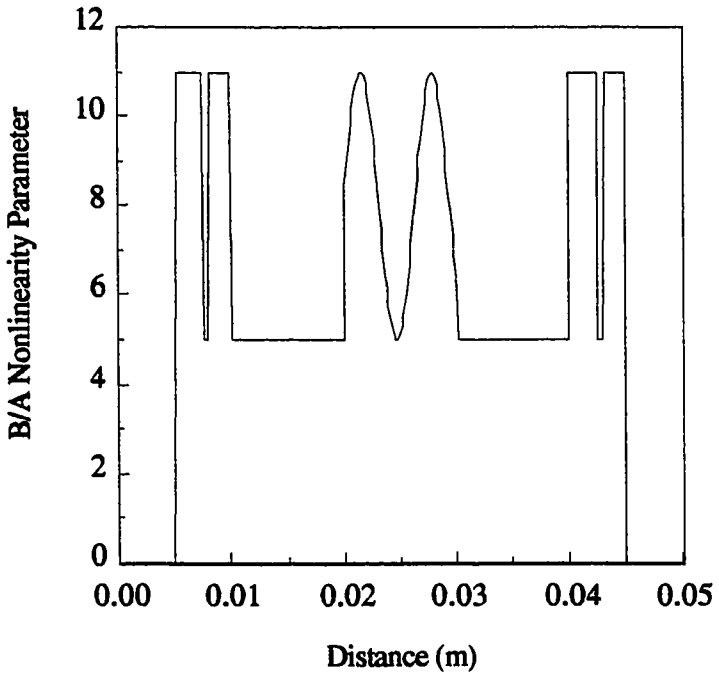

Figure 3.5 Profile of the B/A parameter.

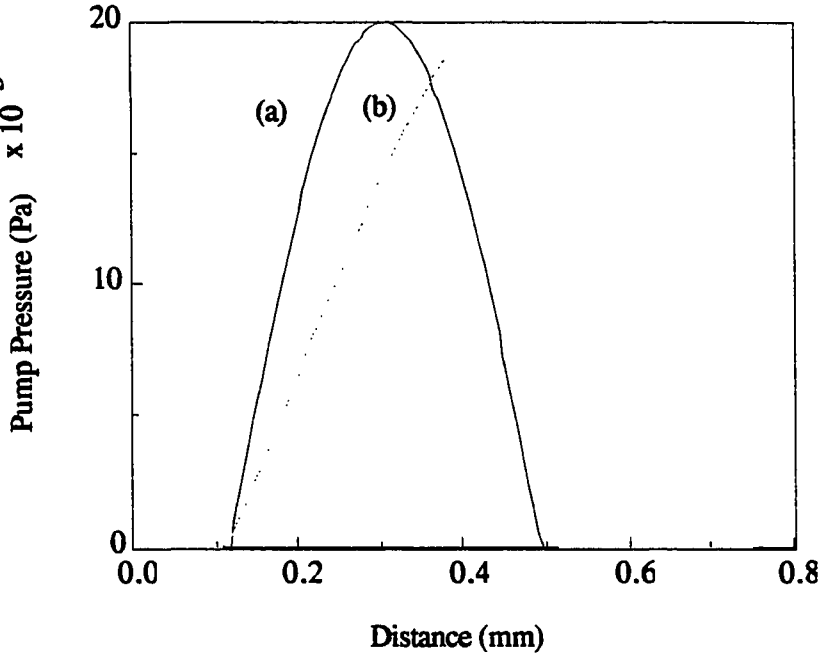

Figure 3.6 Curve (a) shows the spatial profile of a δ pump before entering the medium. Curve (b) shows the spatial profile of the δ pump propagated for 5 cm.

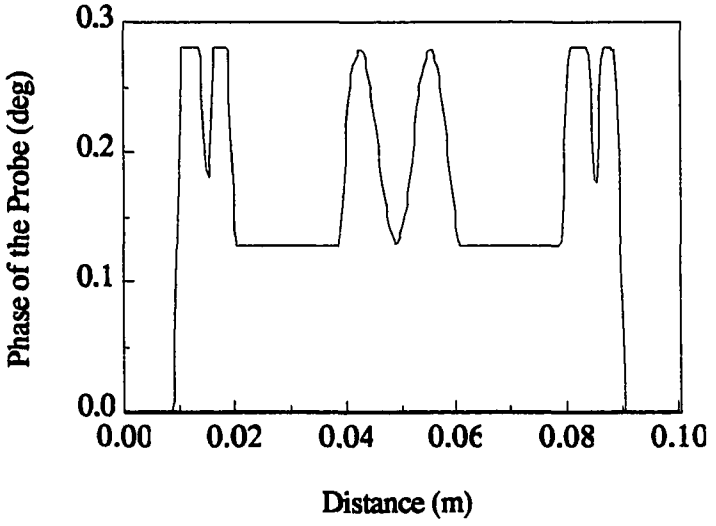

Figure 3.7 The instantaneous phase of a 2 MHz sinusoidal probe interacted with a δ pump.

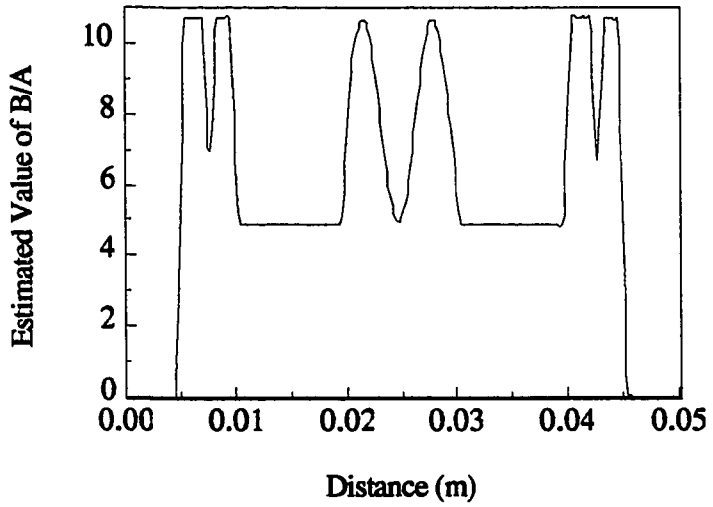

Figure 3.8 The deconvolved estimate of the B/A parameter.

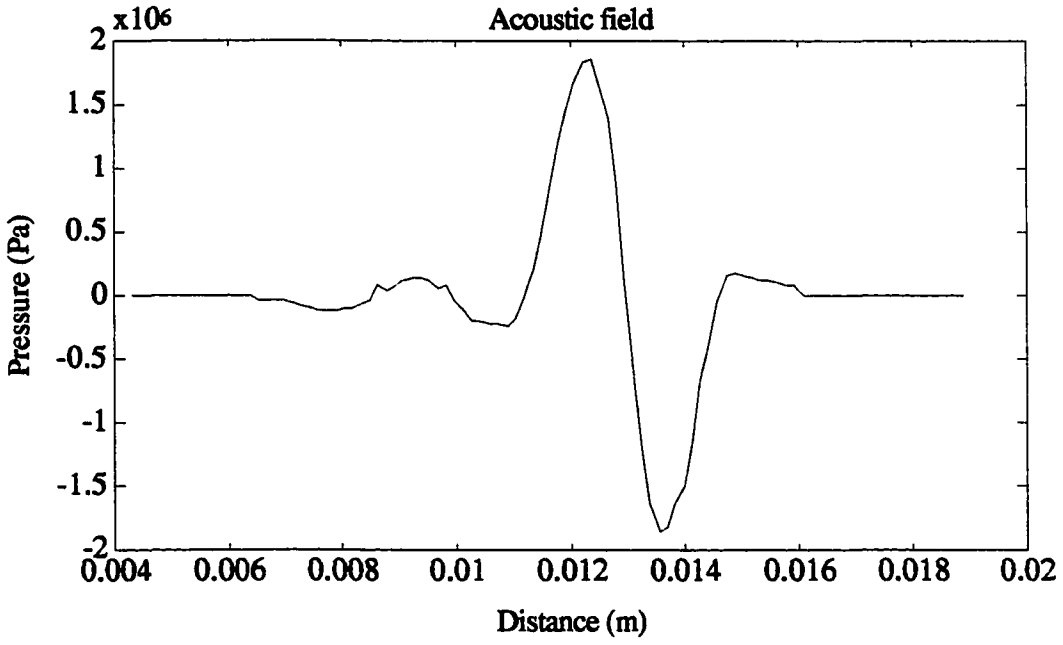

Figure 3.9 The pump used in the counterpropagation computer experiment.

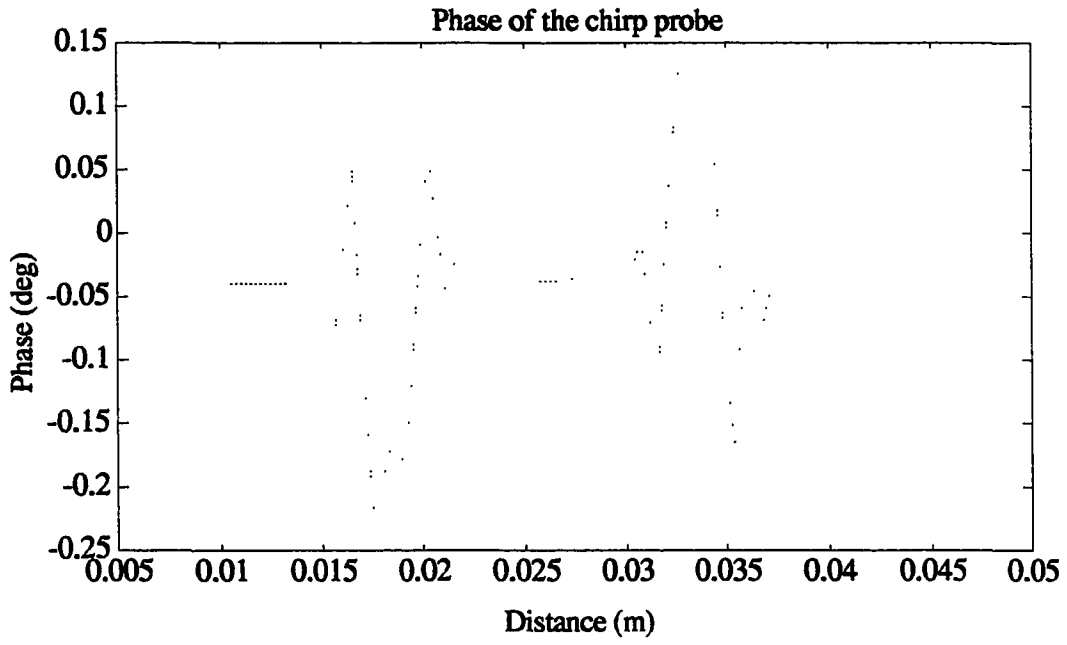

Figure 3.10 The modulated phase of the probe interacting with a 20 atm pump.

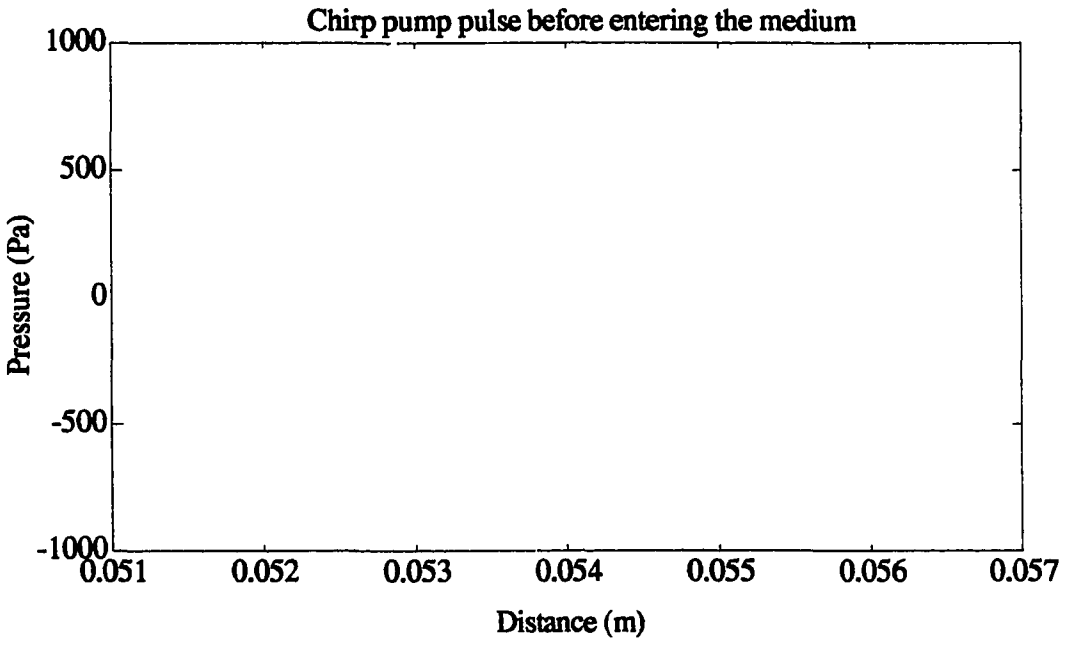

Figure 3.11 The chirp pump used in the computer experiments for the copropagation simulations.

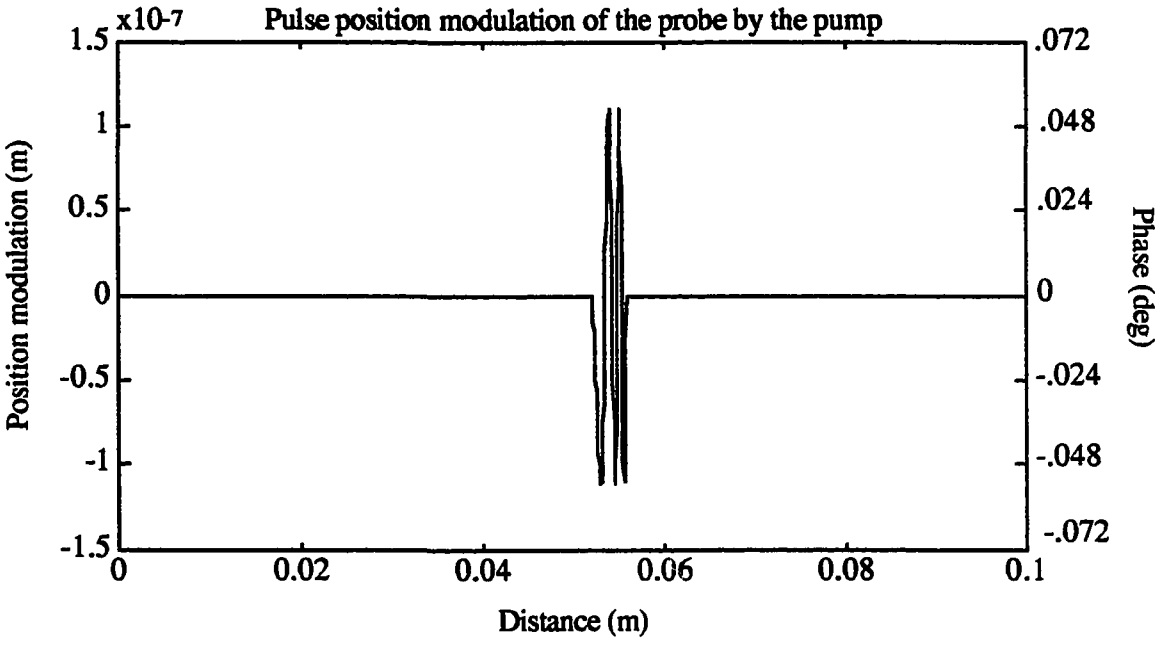

Figure 3.12 Pulse position modulation of the probe by the chirp pump. Pump pressure is 0.01 atm. Pump and probe are copropagated for 5 cm.

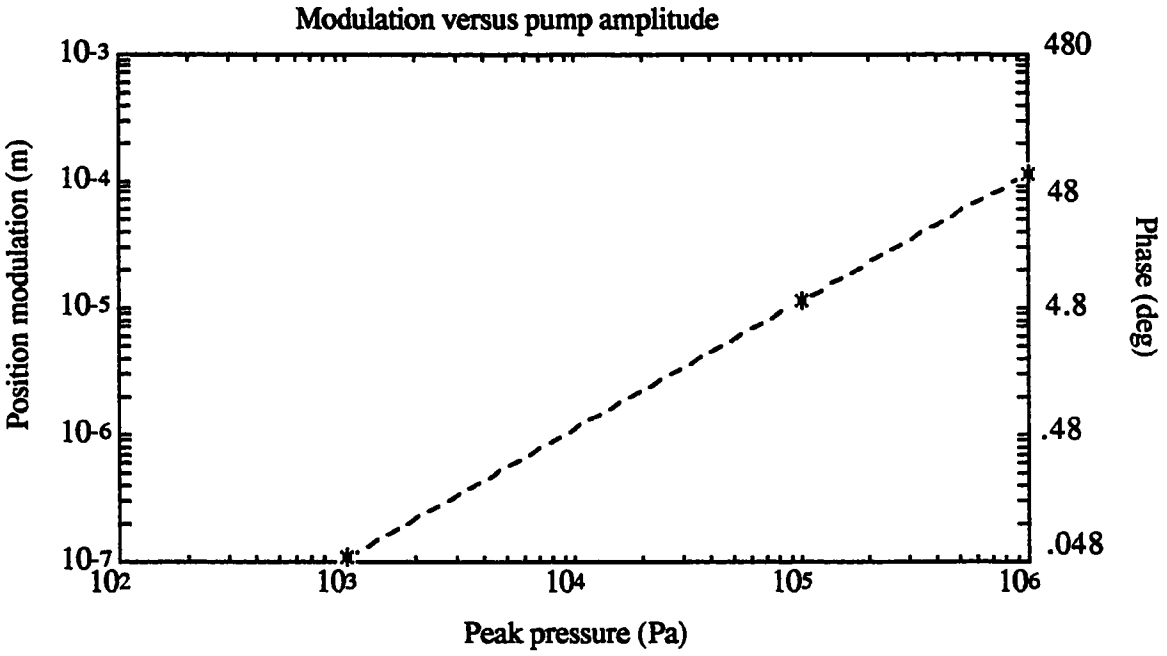

Figure 3.13 Nonlinear modulation versus pump peak pressure. B/A is 8. Distance of copropagation is 5 cm. Probe frequency is 2 MHz.

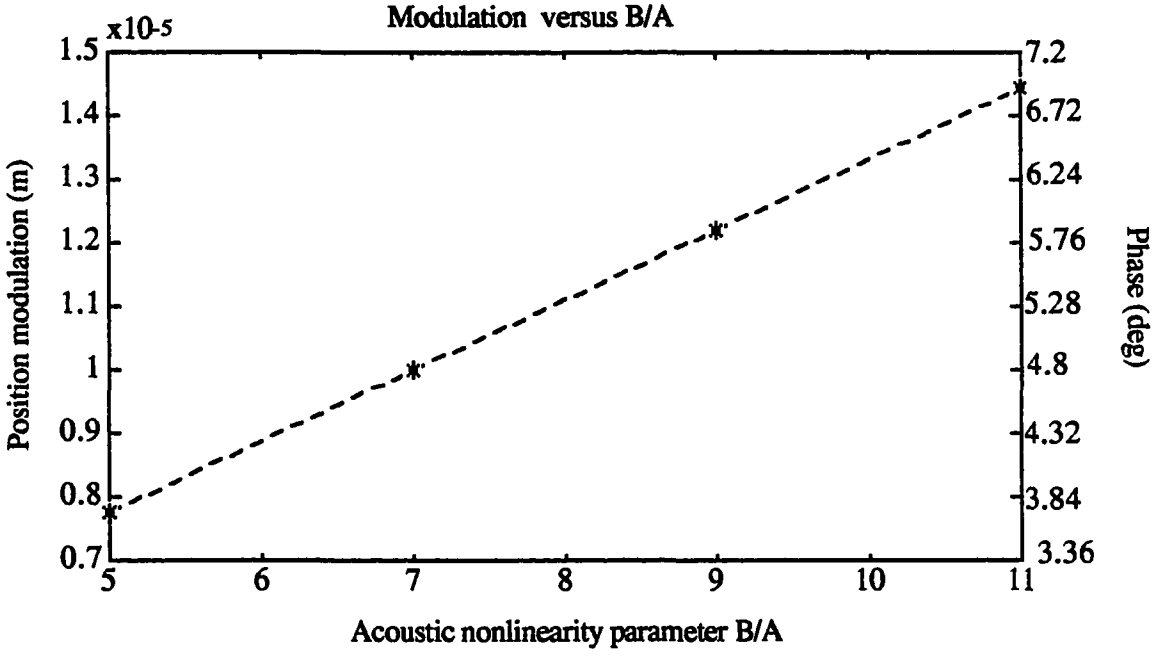

Figure 3.14 Nonlinear modulation amplitude versus the B/A parameter. Pump pressure is 1 atm. Distance of copropagation is 5 cm.

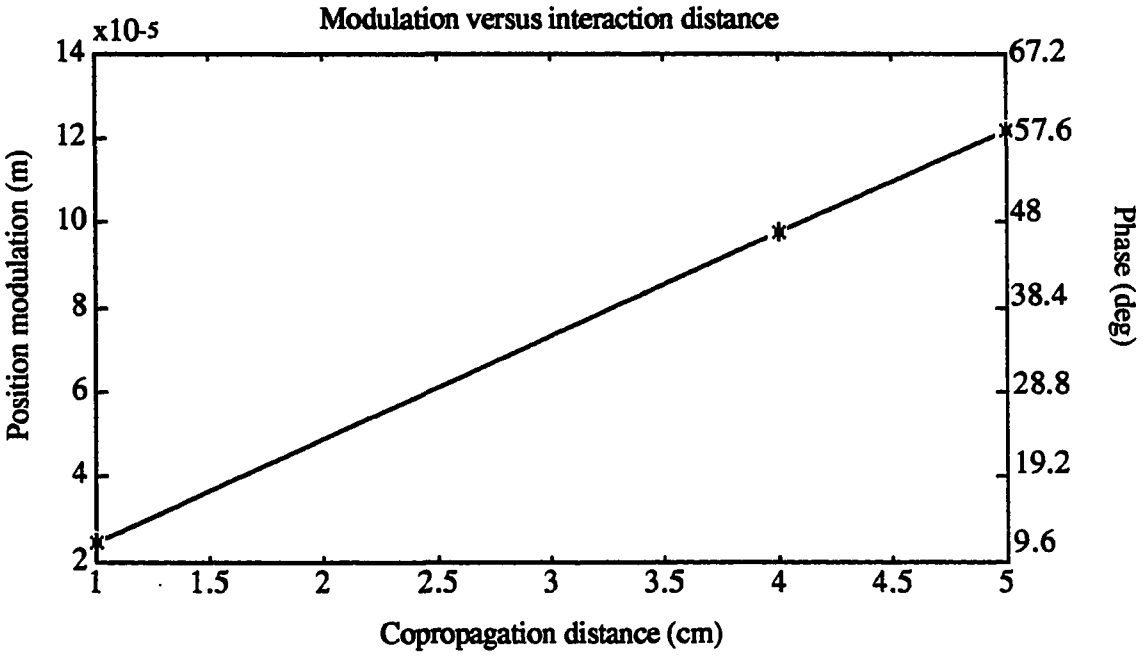

Figure 3.15 Nonlinear interaction versus propagation distance. The pump is 10 atm. The B/A is 9.

CHAPTER 4

COMPARISON BETWEEN THEORY AND EXPERIMENT

This chapter provides experimental examples to show the limitations of the analytical and simulation results. Specifically, Equation (2.19) on copropagation of pump and probe, Equation (2.23) on beam profile of the scattered beam, and Equation (2.39) on copropagation reflection are discussed experimentally. In the case of copropagation, limitations of both the theory and the experimental setup are described (Section 4.1). The scattered beam profile is discussed to provide more insight into the resolution concepts in a nonlinear imaging system (Section 4.2). For the case of copropagation reflection, experiments are performed under various idealized experimental conditions to verify the theoretical derivations (Section 4.3). One example of how these data could be used under idealized experimental conditions to provide an image of the nonlinearity shows the limitations of the existing theory (Section 4.4).

4.1 Experimental Characterization of the Nonlinear Interaction of Copropagating Pump and Probe Pulses

This section discusses the copropagation of the pump and probe (Equation (2.19)). The goal of this experiment is to verify the proportionality relationship between the phase of the probe function and the pump shape. The limitations of the theory and the experimental setup are accentuated by using a broadband pump pulse. The limitations of the plane wave nature of the theory and the limitations of the detection transducers and signal processing modules are discussed.

4.1.1 Materials and Method

The experimental system is shown in Figure 4.1. The pump is produced by a Panametrics transducer (V392) with a 1 MHz center frequency and a diameter of 1.5 in. This transducer is an immersion type and operates in water. It is factory-wired to accept a negative electrical pulse. The inversion of the electrical driving signal is accomplished using a one-to-one inverting transformer (Ritec model RT-HI). The pump transducer is excited by a Ritec BP-9400 ultrasonic pulser (serial #107, peak output voltage: 400 V). The electrical driving pulse width is set to 250 ns, which is a quarter of the transducer fundamental period. The setting is done using thumb-wheel switches with one pulse per output burst. The polarity of the output voltage is positive.

The probe is received or transmitted by 10 MHz Panametrics transducers (V312-SM, flat, 0.25 in diameter; V311-SU, flat, 0.5 in diameter). The diameters of these transducers should ideally be the same size; however, in this experiment the available transducers were used.

The probe-transmitting transducer is driven by a Hewlett Packard 3326A two-channel synthesizer. This synthesizer is operated in the two-phase sinusoidal function mode. The sinusoid's frequency, amplitude, and phase are entered digitally using a numerical keypad. This signal, from the synthesizer, is amplified 37 dB by an ENI RF power amplifier (model 400Ap, 37 dB gain over 150 kHz-300 MHz) and then applied to the probe-transmitting transducer.

The probe transmitter and receiver axis are perpendicular to the direction of pump propagation. The probe is reflected into a collinear position with the pump by a thin (.02 mm) plastic membrane (3M window insulator shrink wrap) which acts as a beam reflector. This acoustic beam reflector is stretched over a support structure which is a rectangularly machined plastic piece. This housing and the transducers are placed in a water tank filled with filtered tap water.

The received probe is the input to a high-pass filter with a lower cutoff of 7.8 MHz. This high-pass filter eliminates any portion of the pump received by the probe receiver. The output of the high-pass filter is amplified by a Nelson-Twomey-Research preamplifier (Model HP-80). This amplified signal is the input to a phase detector. The phase detector is a Mini-Circuits (ZRPD-I, model # 5542) multiplier chip. This multiplier chip has two inputs and one output. The inputs are the modulated sinusoidal signal and a coherent reference signal. The output voltage depends on the phase difference between these inputs. The reference input to the phase detector is from the HP synthesizer's second output. The output of the multiplier chip includes a double-frequency term, which is eliminated by a low-pass filter with an upper 3 dB cutoff of 1 MHz.

4.1.2 Results and Discussion

The excess phase of the probe, resulting from the nonlinear interaction of the probe with the copropagating pump, is displayed in Figure 4.2. The pump is displayed in Figure 4.3 as detected by a Marconi PVDF membrane hydrophone (model Y-33-7611). The shape of the pump is similar to the extracted phase of the probe. The difference between the shape of the probe phase and the shape of the pump is attributed to the missing spectral components in the probe phase. This is illustrated by the spectral analysis of the two waveforms. The amplitude spectrum of the detected pump is shown in Figure 4.4. The fundamental and the third harmonic are readily observed. The amplitude spectrum of the detected probe phase is shown in Figure 4.5. The third harmonic has been virtually eliminated.

There are several possible explanations; first, the phase detection system starts with a receiving transducer that has a nonflat spectral response, the correlation receiver (a multiplier followed by a low-pass filter) also has a limited bandwidth; second, the theoretical derivations are for plane waves, and, in practice, fairly complex diffracted field patterns are interacting. This would possibly create a smearing and averaging effect on the

resulting accumulated nonlinear interaction. Utilization of a broadband pump accentuates the effect of these limitations. In summary, the distortion is caused by the loss of the high-frequency components, which is caused by a combination of diffraction effects and the narrow-band nature of the detection system.

The experiment, however, does point out that nonlinear interaction takes place and that the nonlinear interaction is proportional to the pump wave, within the experimental constraints and the approximate nature of the mathematical formulation, as predicted by Equation (2.19). While the above equation is for uniform plane waves, the beam patterns of the pump, the probe, and the scattered field are discussed next.

4.2 Beam Profiles

This section verifies the assertion in Equation (2.23) that the beam profile of the scattered beam is the product of the pump and probe beam profiles. The beam profiles of the pump, the probe, the product of these beam profiles, and the beam profile of the scattered wave are presented. The beam profile of the scattered wave is compared with the product of the beam profiles of the pump and probe. This is used as a verification of the hypothesis that the scattered beam profile is the product of the beam profiles of the pump and the probe. Knowledge of the scattered beam profile could then be directly obtained from the beam profiles of the pump and probe. The pump and probe beam profiles could then be used to determine the resolution, since in this nonlinear imaging system the scattered field determines the resolution.

4.2.1 Materials and Method

The pump is a Panametrics 500 kHz transducer (V389, 1.5 in diameter). The probe is a 10 MHz transducer (Panametrics, V312, 0.25 in diameter). The pump is driven by a Ritec BP-9400 ultrasonic pulser. The electrical driving pulse width is 500 ns, which is a

quarter of the fundamental period. The probe is driven by an HP 3326A two-channel synthesizer with an electrical driving signal of a 10 MHz, 10 V peak-to-peak sinusoid.

The pump and probe transducers are mounted in a reflector structure (Figure 4.6) to produce collinear pump and probe beams. The pump is reflected by the reflector structure into a collinear position with the probe. The wavefield generated by the pump and probe is measured by a Nelson-Twomey needle hydrophone (#16110488). The hydrophone is moved using a Daedal 4534M micrometer positioning system, in the horizontal plane, perpendicular to the direction of wave propagation.

The needle hydrophone also detects the scattered field. This scattered field is processed by a correlation receiver (a synchronous multiplier followed by a low-pass filter). This correlation receiver generates a signal proportional to the amplitude of the scattered wave. A 7.8 MHz high-pass filter at the input to the correlation receiver separates the scattered wave from the pump. The correlation receiver contains a mixer (Mini-Circuits ZRPD-I, model #5542) and a 1 MHz low-pass filter. The reference signal is a 7 dBm, 10 MHz sinusoidal signal from the HP synthesizer.

4.2.2 Results and Discussion

There is a close match between the profile of the scattered wave and the product of pump and probe beams. The pump and probe pressures versus lateral distance at 4.7, 5.7, and 6.2 cm from the reflector are shown in Figure 4.7 and 4.8, respectively. The scattered field, measured as the modulated phase of the probe, is shown in Figure 4.9. A comparison between the scattered beam and the product of the pump and probe beams, shown in Figure 4.10, verifies Equation (2.23) which claims that the scattered wave profile is the product of the pump and probe profiles.

Since the resolution concepts in the nonlinear imaging system are defined in terms of the scattered wave, and the scattered wave profile could be inferred from the pump and

probe beam profiles, then knowledge of the pump and probe beam profiles could lead to quantitative numbers for the resolution concepts.

4.3 Verification of Copropagation Reflection Model

This section provides experimental verification, in an ideal case, for Equation (2.39) describing the copropagation reflection method. Various chemical solutions are used to vary the B/A and the reflection coefficient profiles. A theoretical curve representing Equation (2.39) is provided to be compared with the experimental data as far as the shape of the curve and the amplitudes are concerned.

4.3.1 Materials and Method

The system block diagram is shown in Figure 4.11. An AT&T PC 6300 computer stores the data. This computer communicates through a Metrabyte IEEE-488 (GPIB) controller card with a Data Precision model 6100 Waveform Analyzer in ASCII/DOS format. The Data Precision Model 6100 Universal Waveform Analyzer serves as the signal acquisition and processing unit. The Data Precision 6100 is triggered externally by a Ritec BP-9400 Ultrasonic burst pulser. The Ritec pulser generates a square-voltage pulse as the input to the pump. The pump output pressure is maximized by setting the pulse width to 700 ns and using a 1:3 step-up transformer. The pump is a 500 kHz Panametrics video scan (V389) immersion transducer with a diameter of 1.5 in.

The pump and probe receiver axes are aligned by an anodized aluminum reflector assembly (Figure 4.6). The reflector houses the probe receiver (Panametrics, 10 MHz, V312-SM, 0.25 in). The probe transducer diameter is dictated by the physical case size. The probe transmitter is a 10 MHz transducer (Panametrics, V311-SU, 0.5 in). This probe transmitter is driven by an HP 3326A two-channel synthesizer. The signal received by the probe receiver is processed by the phase detection system described in Section 4.1.1.

The transducers are aligned such that all waves travel collinearly, and the phantom assembly is positioned such that all waves impact the membrane at a normal incidence. For the phantom assembly, the window insulator material (shrink wrap) of 3M serves as the membrane material. The small thickness of the shrink wrap (0.02 mm) with respect to the pump wavelength (3 mm) allows unobstructed propagation of the acoustic wave. The phantom contents consist of 100% tert-butanol, a 20% tert-butanol/ 80% water mixture, and 100% ethylene glycol.

4.3.2 Results and Discussion

The comparison of the waveforms of the theory (Equation (2.39)) with the waveforms of the experiment constitutes the validity test. Figures 4.12, 4.13, and 4.14 (McGough, 1990) depict the copropagation reflection theoretical results with a dashed line and the experimental results with a solid line, for 100% tert-butanol, 20% tert-butanol / 80% water, and 100% ethylene glycol phantoms, respectively. In each figure two pulses are seen: the first pulse originates from the water-solution interface; the second pulse originates from the solution-water interface. The difference between the temporal locations of the simulated and experimental waveforms arises from the difficulty in measuring the actual phantom width when it is suspended in water.

The agreement between the theoretical (Equation (2.39)) and the experiment -- within experimental constraints -- in each of the experimental cases verifies that the nonlinear interaction has resulted from the copropagation of the reflected pump with the probe. The difference between the experimental and theoretical results, even in this idealized experimental condition, is attributed to the virtual impossibility of implementing a normal pump incidence on a flat phantom surface, as called for by the theoretical formulation. The limitations of the theory are further discussed in the next section.

4.4 An Example of How Copropagation Reflection Data May Be Used for Nonlinear Imaging

This section provides one example of how Equation (2.39) could be useful in the imaging of the nonlinear parameter, B/A. The experiment follows the steps in the mathematical derivations in Section 2.3. The limitations of the theory will become evident once the constraints on the experimental system are described. These limitations point out new issues that need to be worked out before an in vivo system can be constructed.

4.4.1 Materials and Method

The experimental system is shown in Figure 4.15. The pump transducer (Panametrics, 500 kHz, 1.5 in diameter, V389) is driven by a Polynomial Waveform Synthesizer (Model 2020, Analogic Data Precision) through an ENI power amplifier (model 400Ap, serial #522, 37dB gain over 150 kHz-300 MHz). The synthesizer generates an electrical LFM pulse, a chirp of 5 μs duration spanning the frequency band of 150 kHz to 1000 kHz. The upper frequency of 1000 kHz is used to provide a clear spectral separation between the pump and a 5 MHz probe. The probe receiver (Panametrics, 5 MHz, 0.25 in diameter, V310) and the pump are housed in a reflector structure. This pump reflection produces a virtual acoustic source behind the probe receiver. The signal received by the probe receiver is high-pass filtered (2.7 MHz lower cutoff) to remove the pump reflections. The filtered signal is demodulated by the phase detection system described in Section 4.1.1. The probe transmitter is driven by an HP two-channel synthesizer. This probe transmitter (Panametrics, 5 MHz, 0.5 in in diameter, V309) produces a continuous wave which propagates through a phantom.

The phantom is designed to produce a layered medium. The inner layer is filled with 100% ethylene glycol which has a different B/A value than water. Water surrounds the phantom and is separated from the ethylene glycol by shrink plastic wraps (3M, window insulator kit, cat#2140, thickness 0.02 mm). The water that surrounds the

ethylene glycol is separated from the rest of the water in the tank by transparency sheets (Xerox, thickness 0.06 mm). These transparencies act as reflectors and produce pump reflections.

4.4.2 Results and Discussion

The electrical driving pulse of the pump, averaged 100 times, is shown in Figure 4.16. This signal is averaged to be consistent with the averaging of the rest of the signals in this experiment. The pump propagates through the medium and is reflected from various interfaces. The pump reflections, detected by the probe receiver and averaged 100 times, are shown in Figure 4.17. The horizontal axis represents the time between when the pump transducer was electrically pulsed and when the echoes were received. These pump reflections originated from discrete reflectors. The first reflection is from the transparency sheet; the second reflection is from the water-ethylene glycol interface; the third reflection is from the ethylene glycol-water interface; and the fourth reflection is from the transparency sheet. The mathematical model for these reflections is Equation (2.40).

The nonlinearity parameter of the material between the discrete reflectors is shown in Figure 4.18. The value of the nonlinearity parameter N (= B/A / 2 $\rho_o c_o^3$) is plotted versus time with the interval (213-224 μs) representing ethylene glycol.

The probe phase, averaged 100 times, is shown in Figure 4.19. The first pulse in the figure represents the phase modulation caused by the first pump reflection. The second, third, and fourth pulses represent the phase modulations caused by the second, third, and fourth pump reflections, respectively. The mathematical model for these phase modulations is Equation (2.39).

Processing the probe phase (Equation (2.39)) and the pump reflections (Equation (2.40)), using the mathematical steps developed in Section 2.3 (Equations (2.42) and (2.43)), leads to an estimate of the nonlinearity parameter (Equation (2.45)). This estimate is scaled using the nonlinearity parameter of water and is shown in Figure 4.20.

Comparing Figures 4.20 and 4.18, the estimated value for ethylene glycol has an error of about 5%. The fractional variation of the nonlinearity estimate of water is about 20%.

The experiment described in this section serves as an example of the utilization of the copropagation reflection method to produce an image of the acoustic nonlinearity. The limitations of the method are discussed next. Proper alignment, to provide normal incidence on a planar surface, is crucial in the experiments. Oblique incidence angles would change the acoustic path length and also the reflection coefficient. Nonplanar surfaces produce a complicated reflected field, which is not modeled accurately by a plane-wave model. In addition, the lateral structure in the target would require the lateral spatial sampling of the wavefield by less than half of the spatial wavelength of this field. The limitation of normal incidence on a planar surface points to the need for a three-dimensional solution.

As seen in the B/A image (Figure 4.20), the estimated values for the regions representing water have different values. This is to be expected since the model used is only a mathematical approximation to the physical processes that characterize the system, and when this idealized model is used to process the experimental data, the reconstructed image will always be different than the underlying parameter that is being imaged. Improving the modelling of the physical processes would lead to a reconstructed image which is closer to the underlying parameter. In addition, in one of the signal processing steps (Equations (2.40) and (2.42)), the data are divided by the reflection coefficient; any error in that parameter would cause a large error in the estimated B/A value.

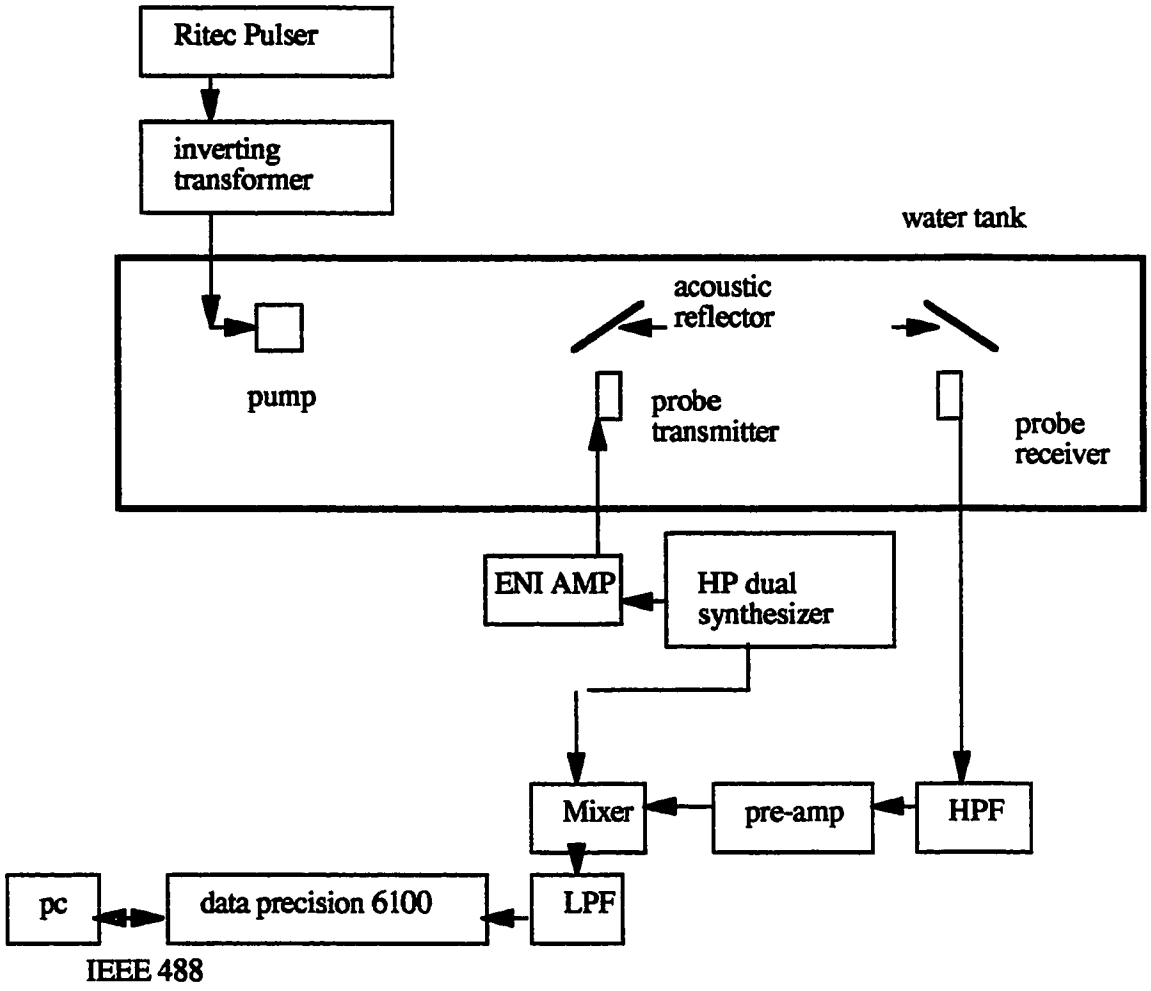

Figure 4.1 The experimental setup for the nonlinear interaction experiments.

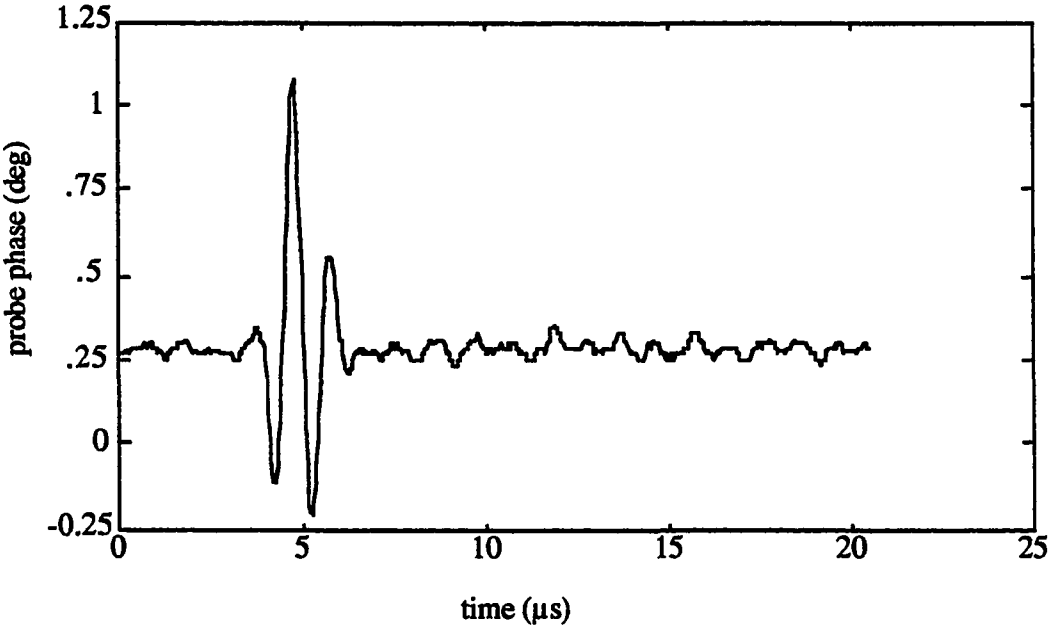

Figure 4.2 The phase of the modulated probe.

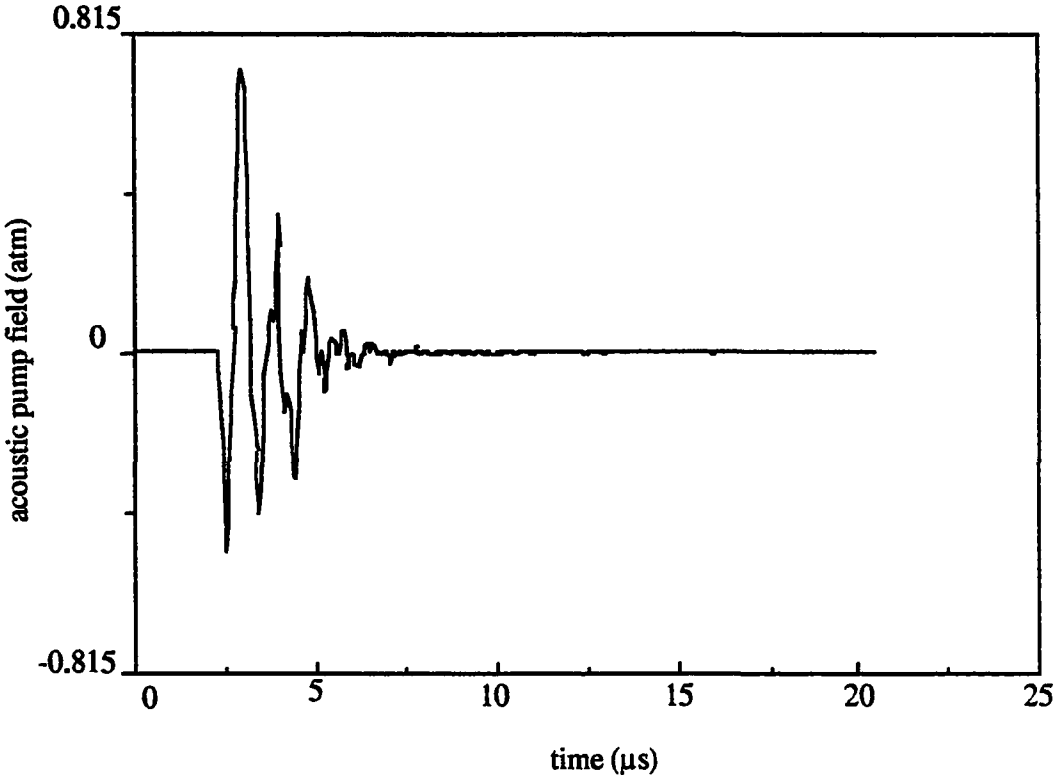

Figure 4.3 The pump detected by a membrane hydrophone.

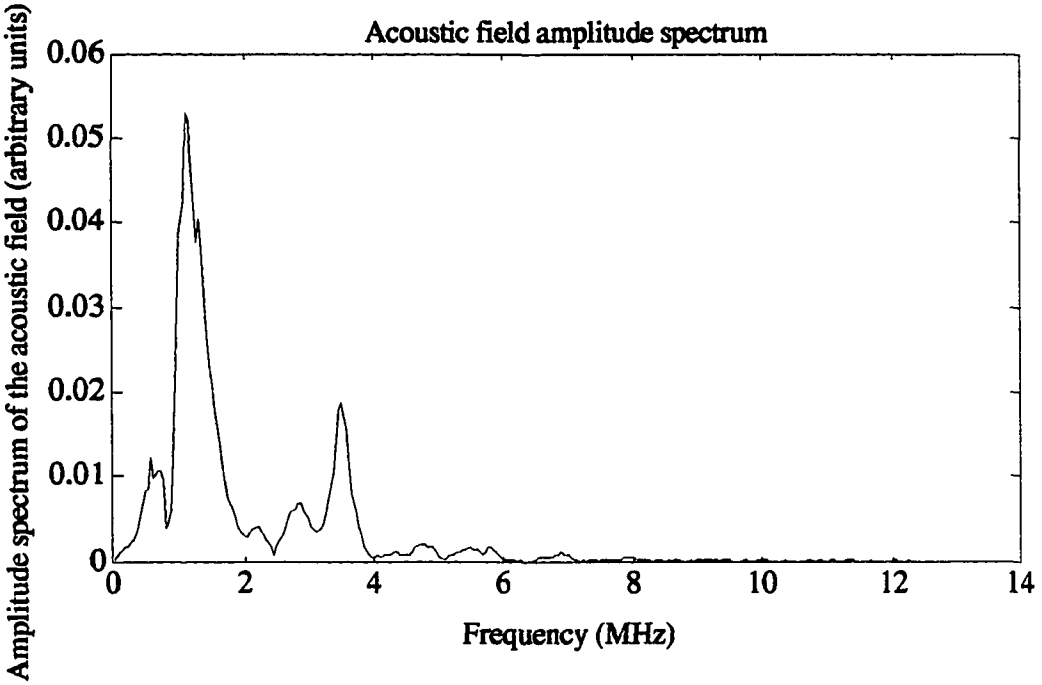

Figure 4.4 The amplitude spectrum of the pump shown in Figure 4.3.

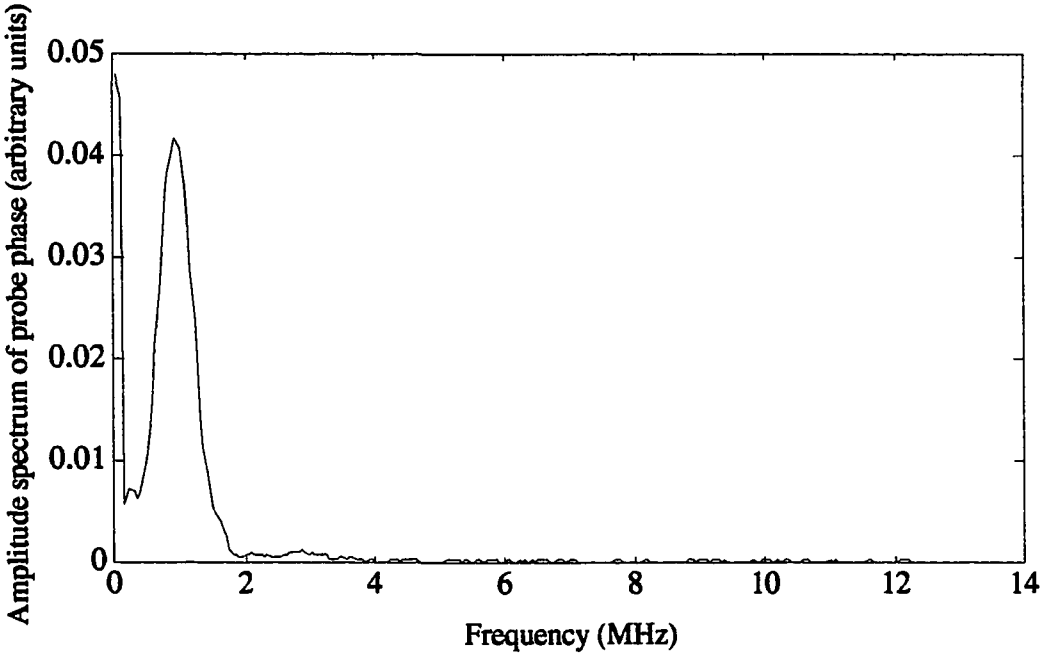

Figure 4.5 The amplitude spectrum of the detected probe phase.

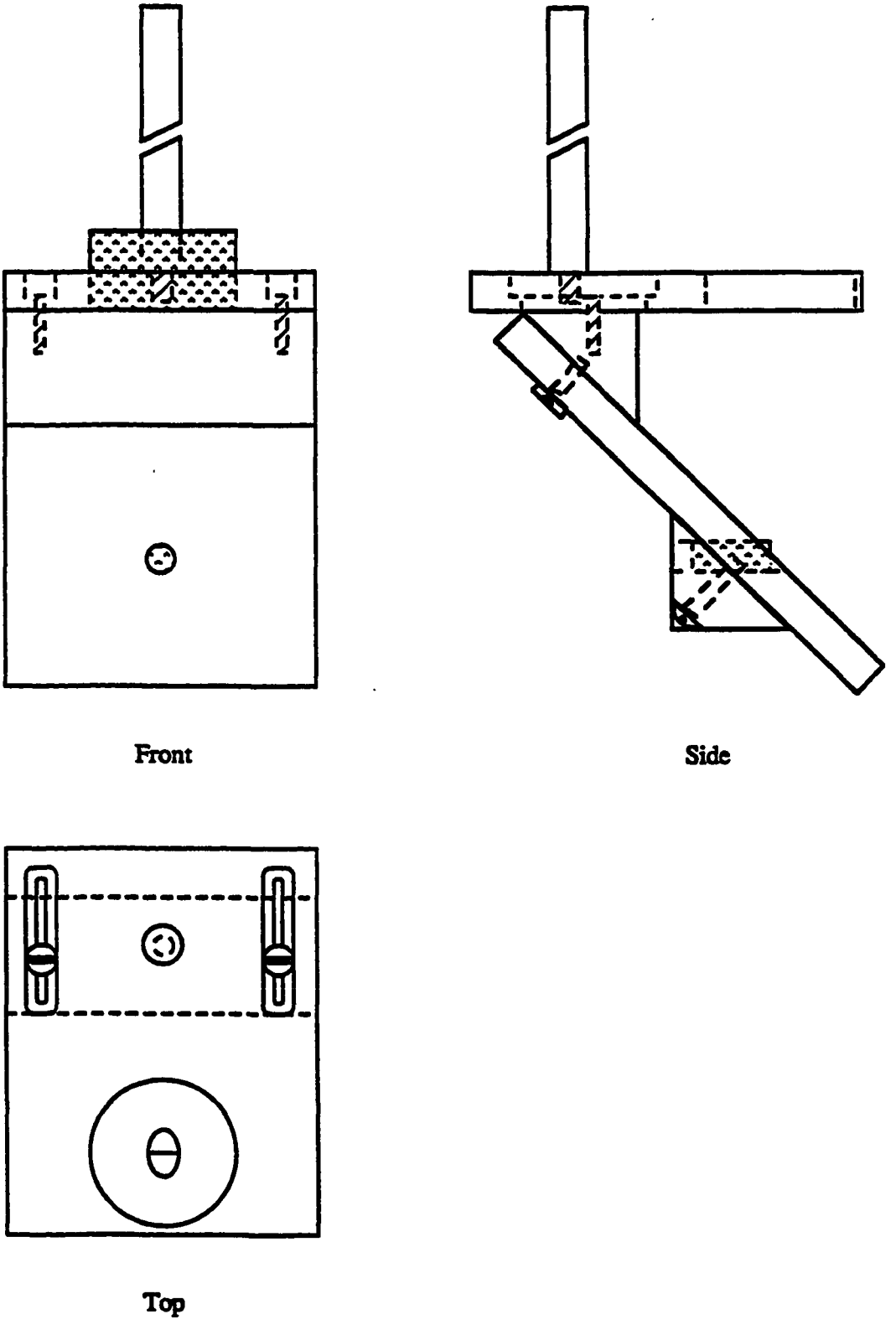

Figure 4.6 Half-size scale drawing of the reflector assembly (McGough, 1990).

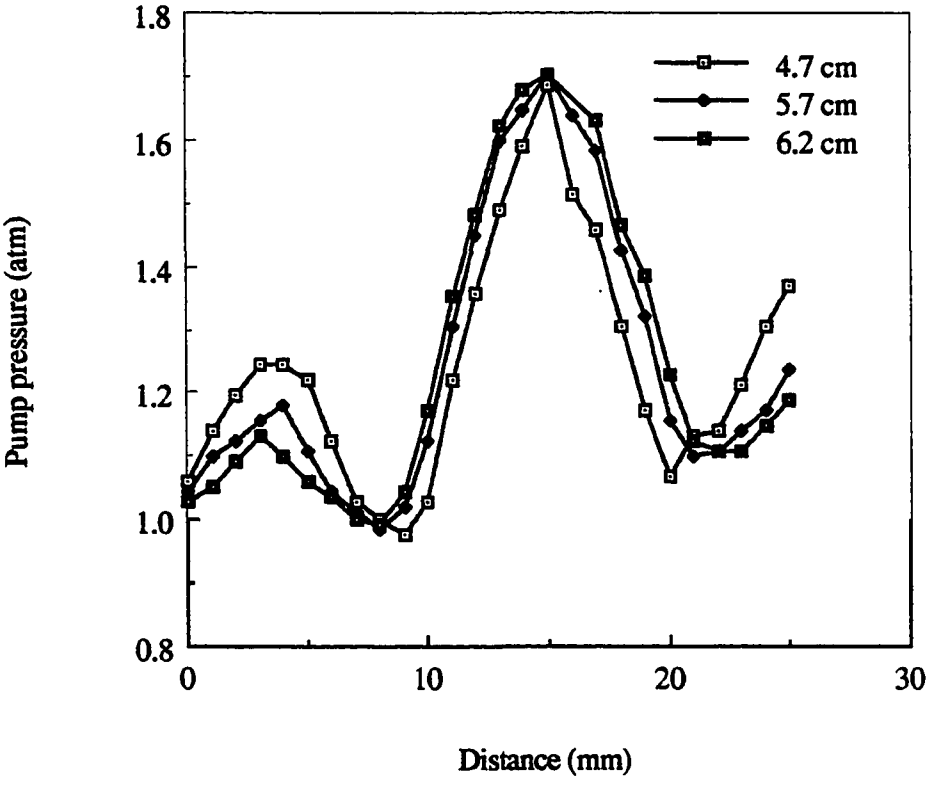

Figure 4.7 The lateral pump pressure at 4.7, 5.7, and 6.2 cm planes.

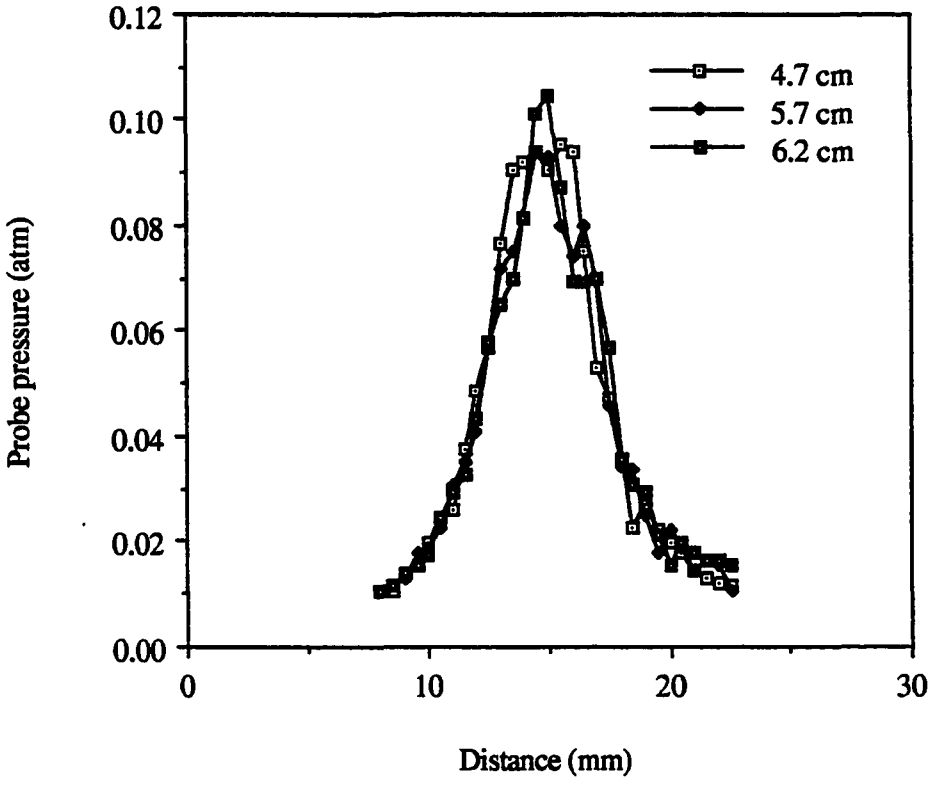

Figure 4.8 The lateral probe pressure profiles.

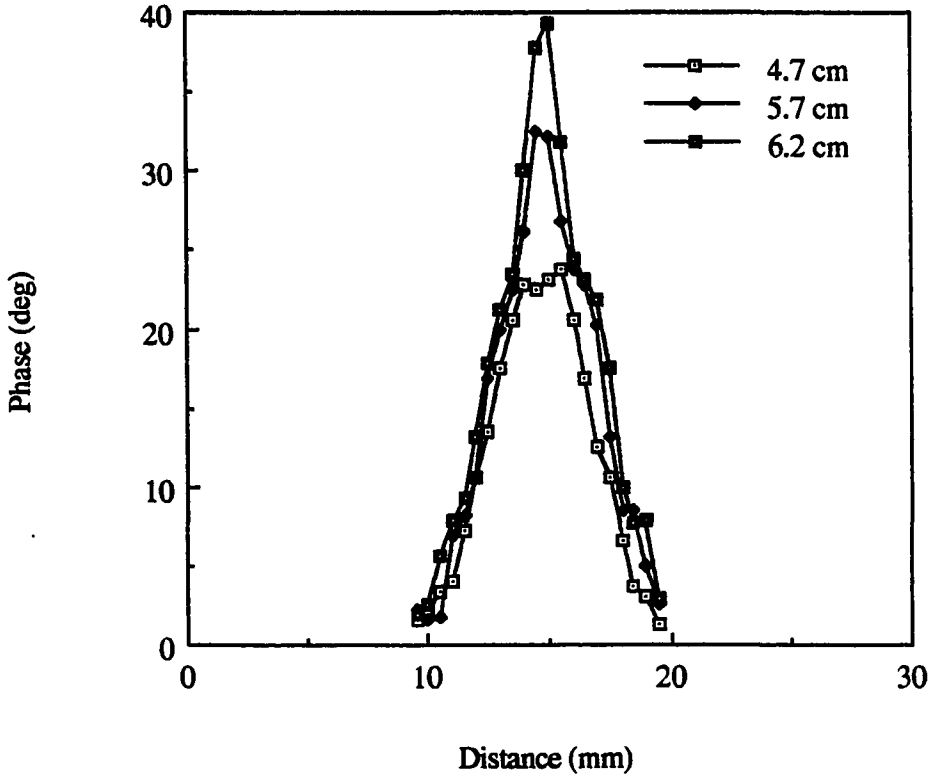

Figure 4.9 The lateral scattered field profile.

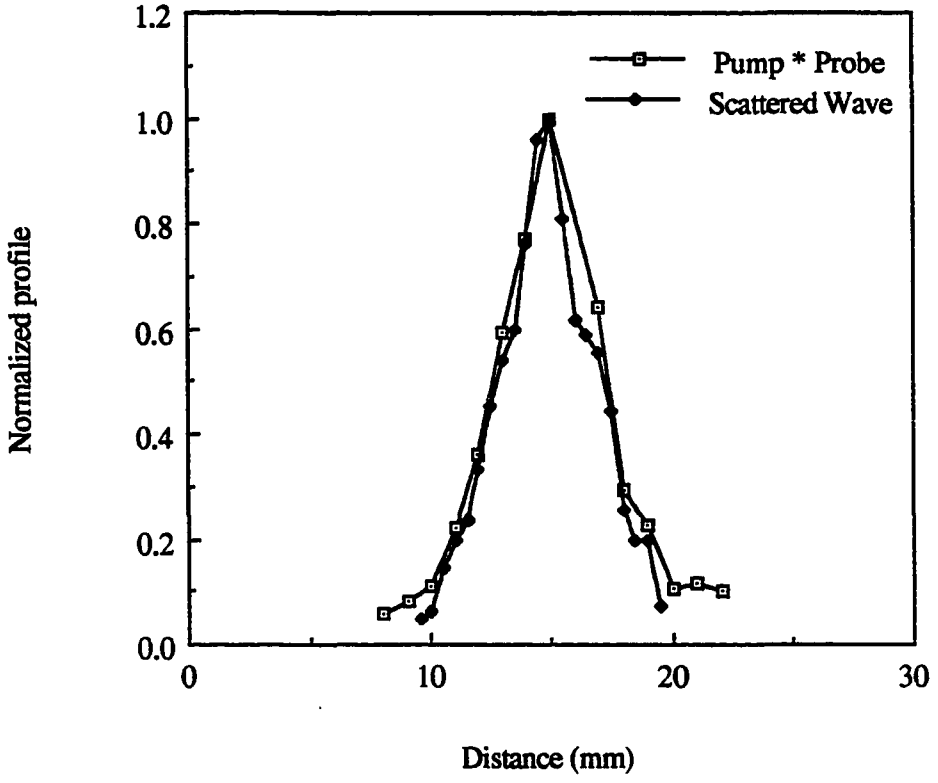

Figure 4.10 A comparison between the scattered beam and the product of the pump and probe beams.

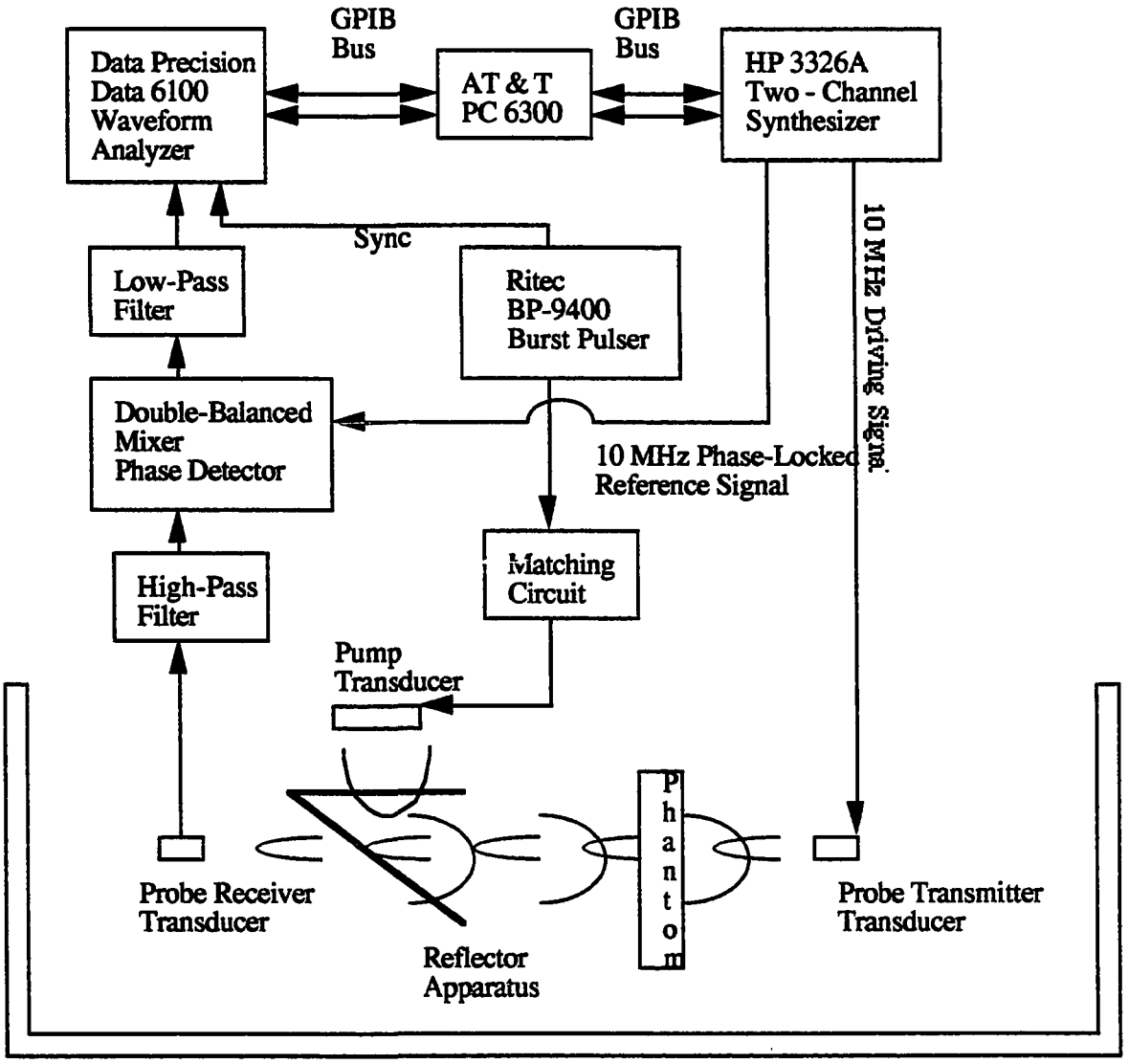

Figure 4.11 The equipment interconnection diagram (McGough, 1990).

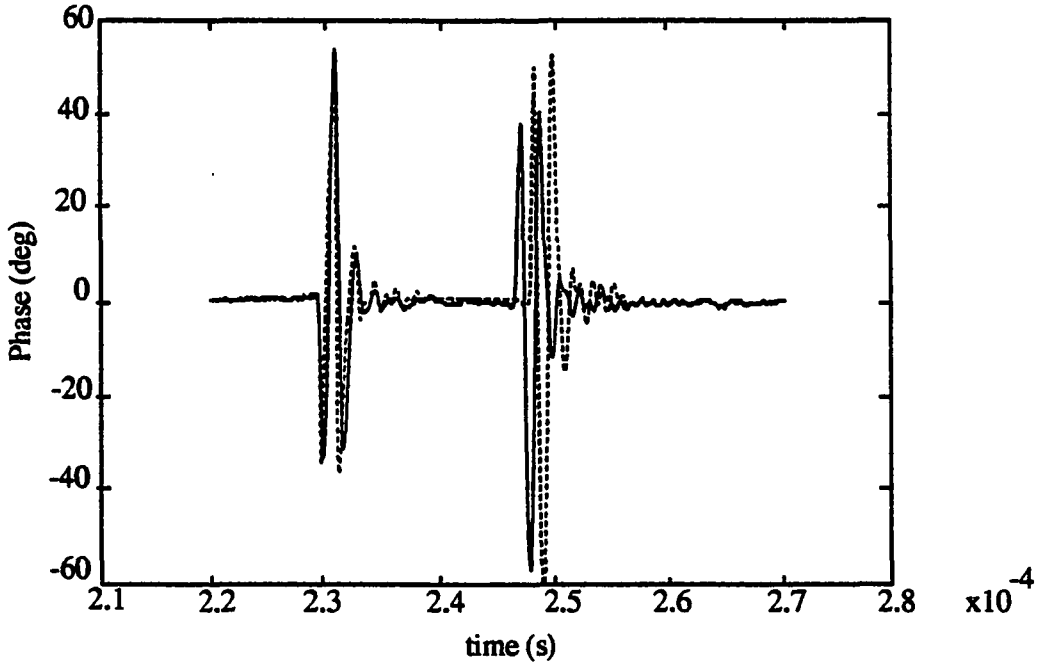

Figure 4.12 Theoretical (dashed line) and measured (solid line) phases for 100% tert - butanol phantom (McGough, 1990).

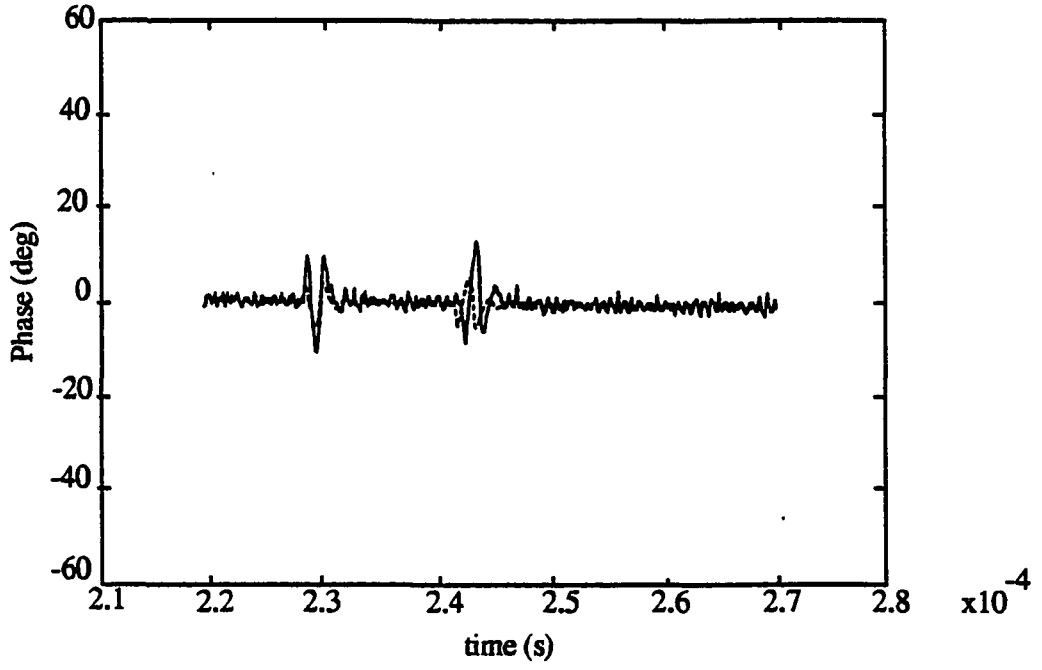

Figure 4.13 Theoretical (dashed line) and measured (solid line) phases for 20% tert - butanol / 80% water phantom (McGough, 1990).

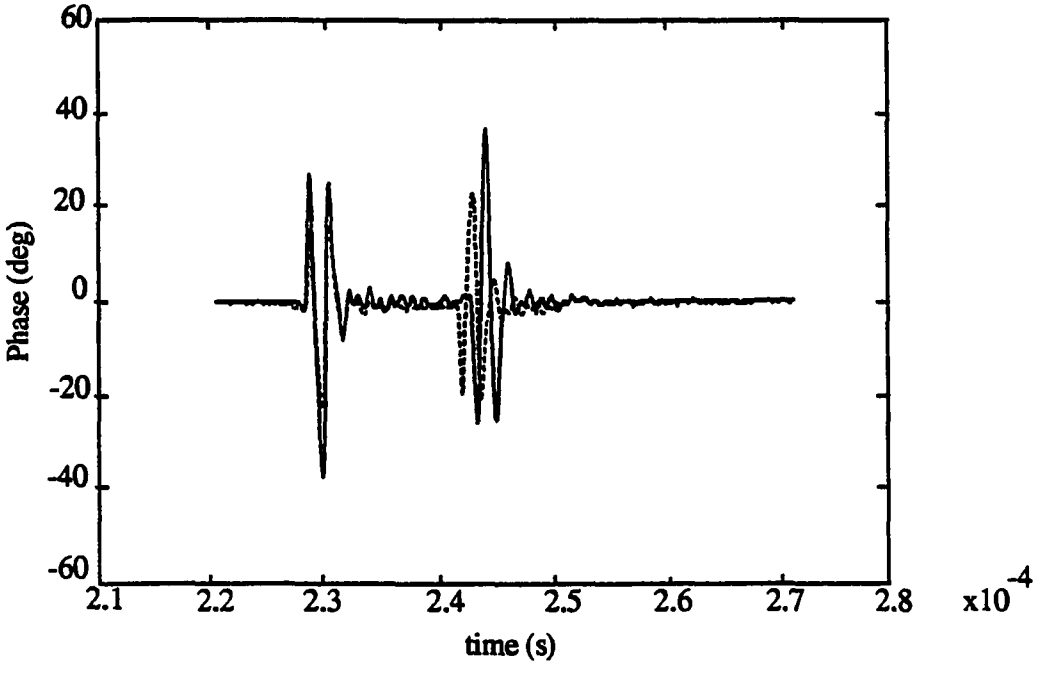

Figure 4.14 Theoretical (dashed) and measured (solid) phases for 100% ethylene glycol phantom (McGough, 1990).

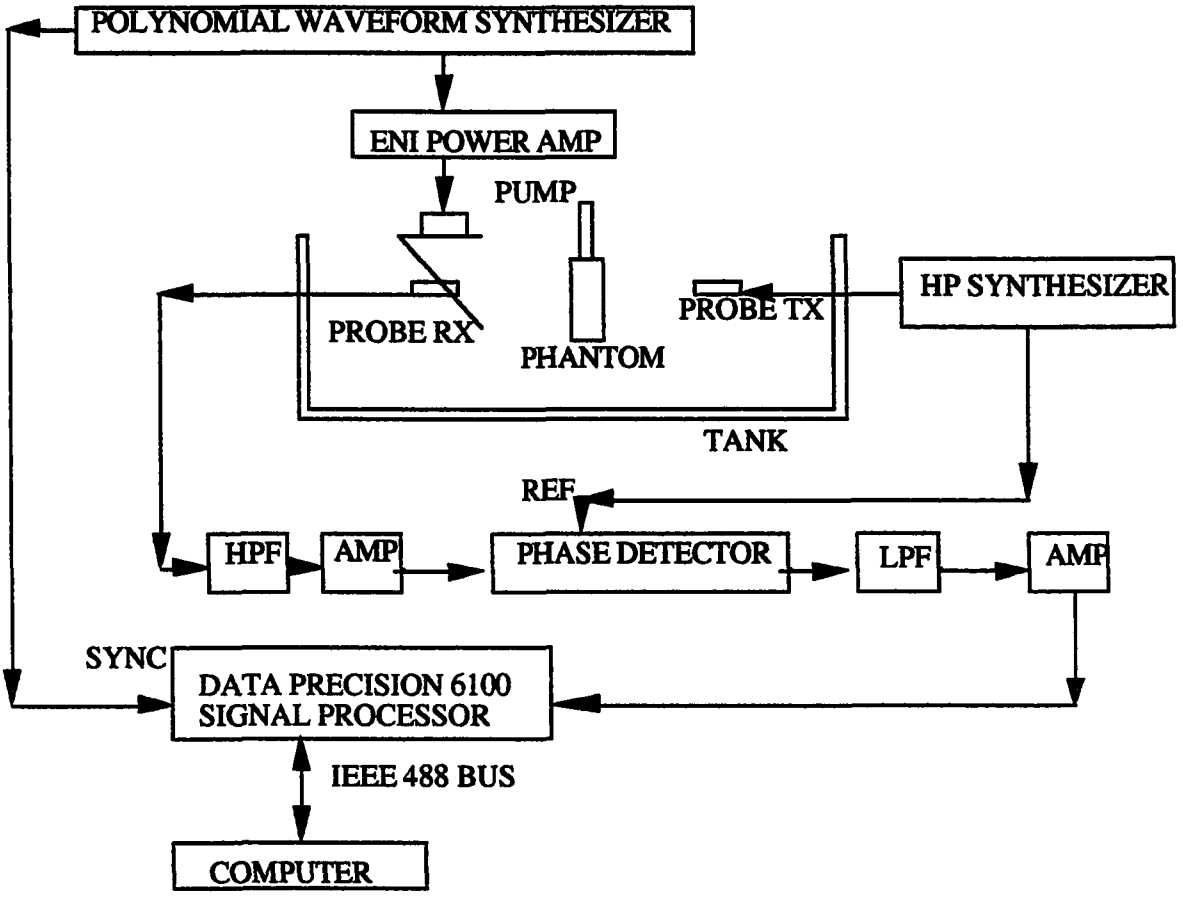

Figure 4.15 The experimental setup. The imaging system and the associated electronics are shown.

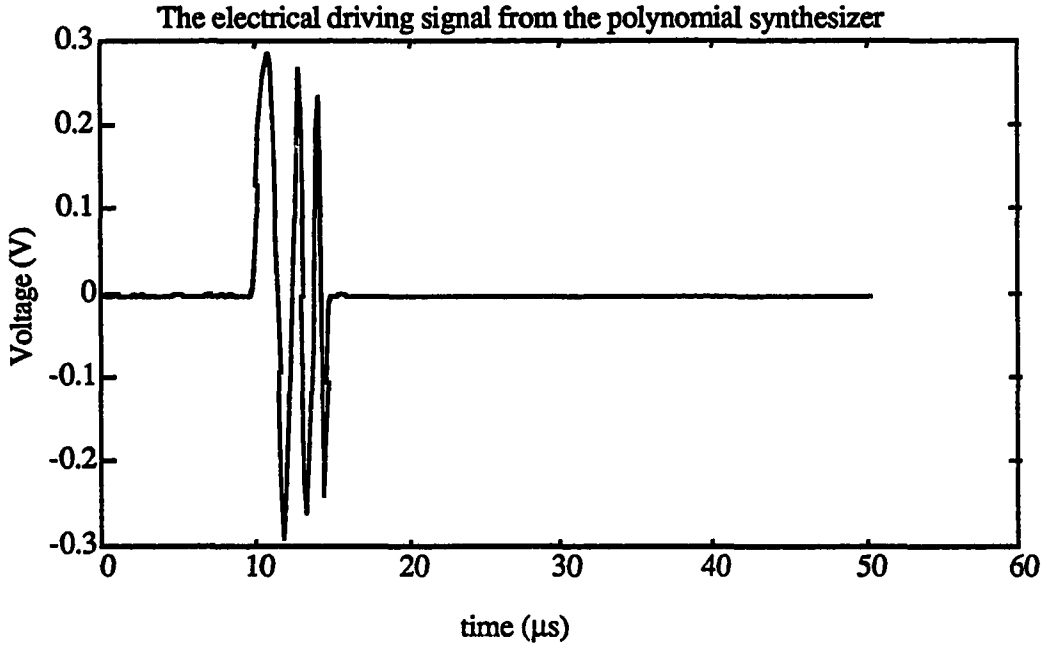

Figure 4.16 The electrical driving signal of the pump, averaged 100 times, is shown.

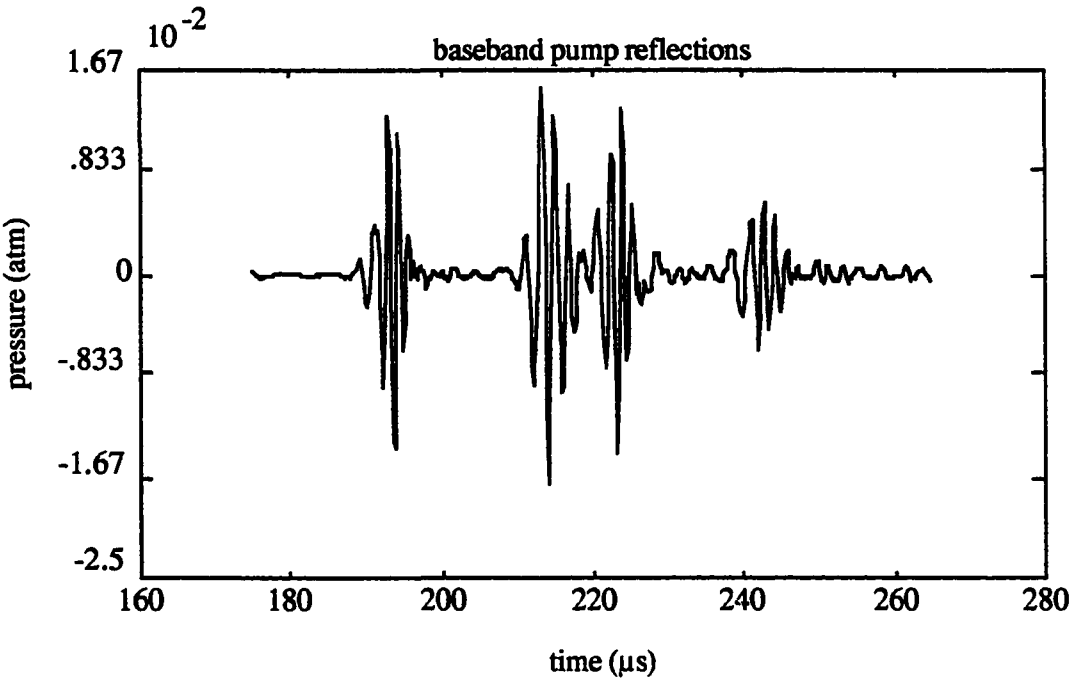

Figure 4.17 The pump echoes from the four reflectors in the medium.

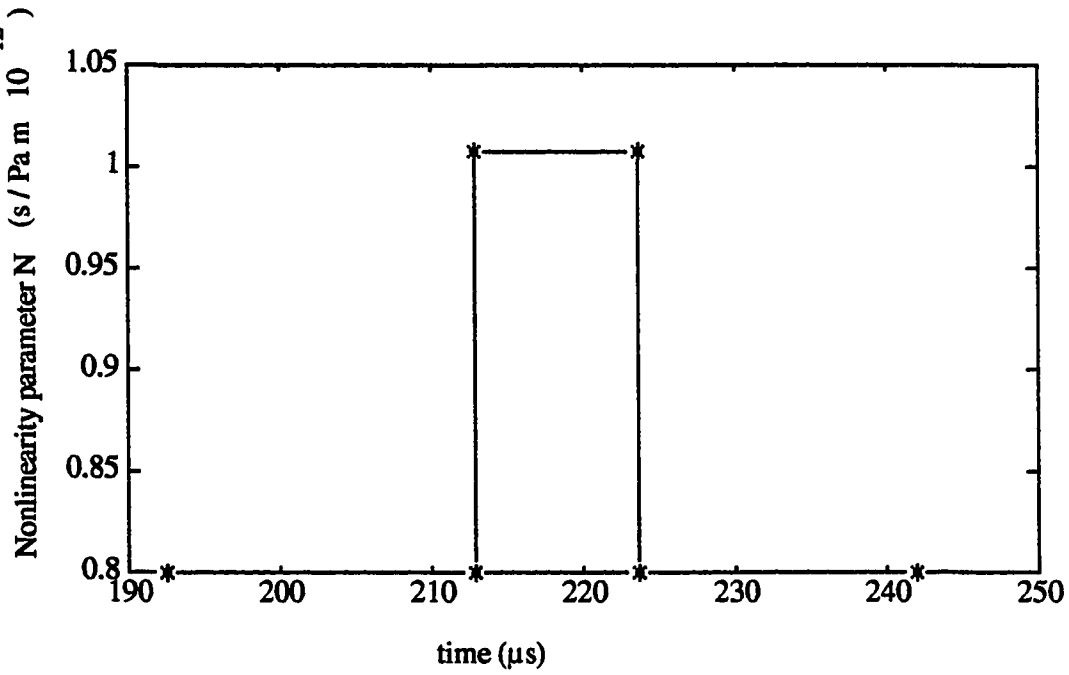

Figure 4.18 Nonlinearity parameter N for a water, ethylene glycol (213-224 μs), and water-layered medium.

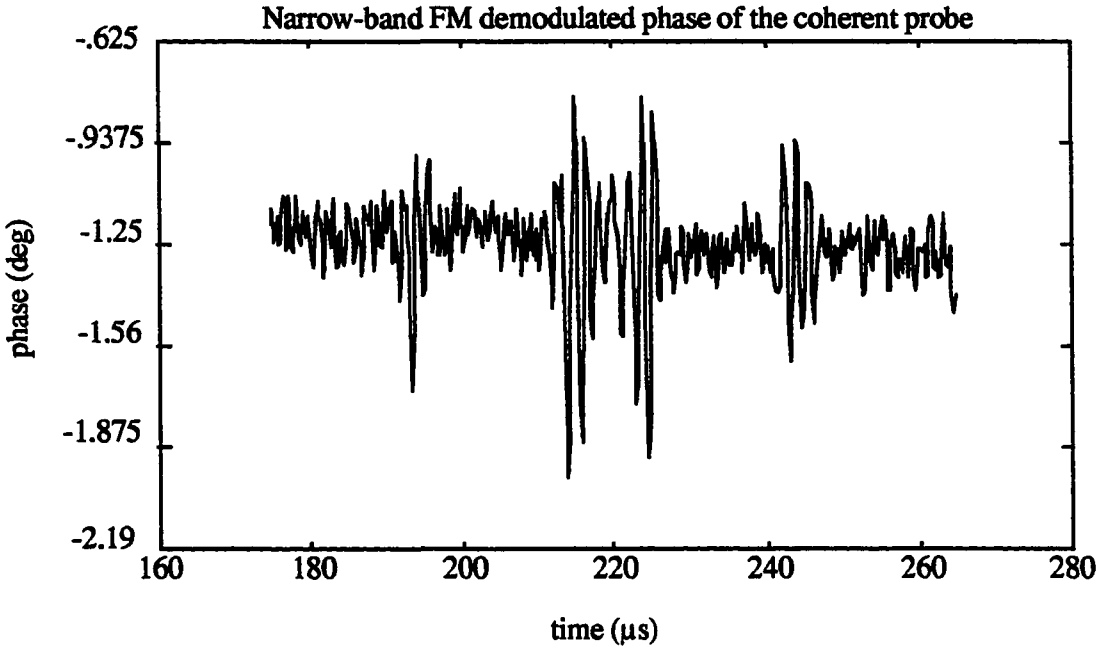

Figure 4.19 The nonlinear modulation of the probe by the reflected pump, averaged 100 times, is shown.

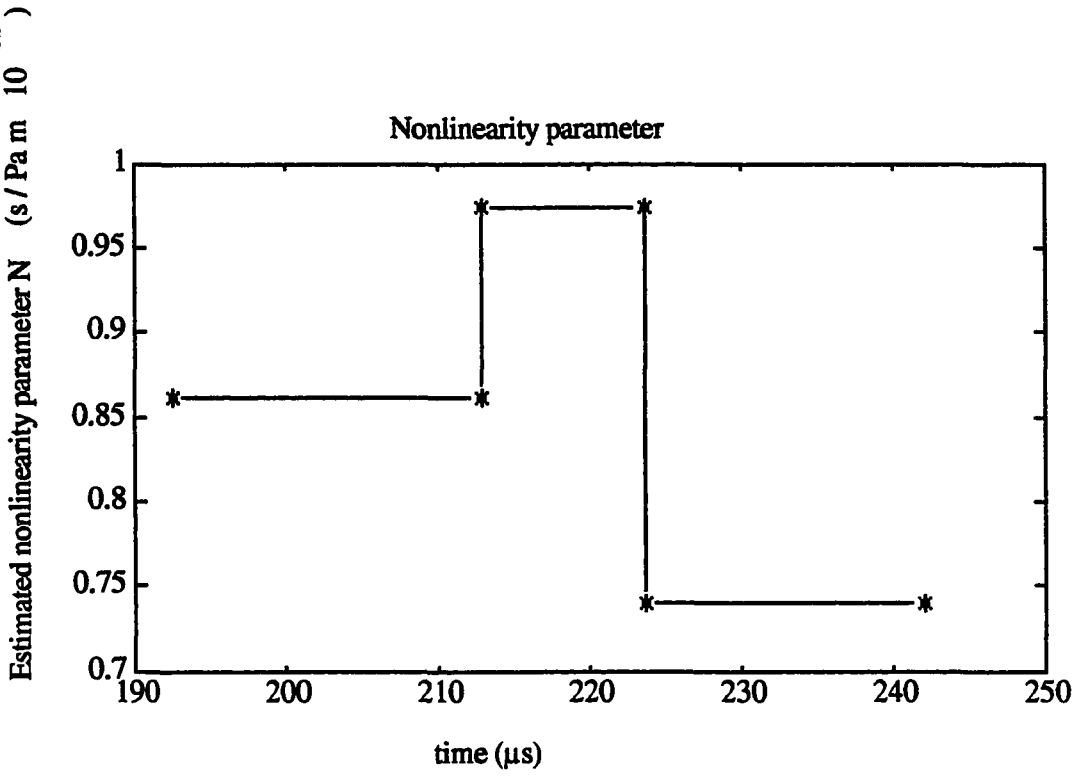

Figure 4.20 Estimated nonlinearity parameter of ethylene glycol.

CHAPTER 5

CONCLUSIONS AND DISCUSSION

5.1 Conclusions

A reflection mode B/A imaging system was systematically analyzed using simulation, mathematical, and experimental techniques. A new simulation program and a new mathematical formulation were presented. Experiments were performed to verify the new mathematical formulations. The experimental results in Chapter 4 showed a close agreement between the copropagation reflection model and the experimental data (Section 4.3). The field of nonlinear imaging could make progress by refining the analytical and simulation modeling to describe more complex phantoms and diffracted field patterns.

Analytical and simulation models need to be refined to eliminate errors caused by basic assumptions of these models. Cobb (1983) states that the Fubini plane wave approximation, similar to the approximation here, fails to hold for sources with large ka, especially in the near field. Thus, the probe field experiences large variations in phase and amplitude over the probe receiver. These diffraction effects will need to be incorporated into the simulation program.

Other limitations that are of concern in nonlinear ultrasonic imaging systems stem from problems with aberration and speckle. The solutions that have been used for these problems and those that are under current research will benefit nonlinear acoustical imaging. Using the results reported in this thesis and with the anticipation of the solution to the aforementioned limitations, future applications and the relationship to other imaging modalities and sensory systems are elaborated upon next.

5.2 Nonlinear Imaging Based on Copropagation

The imaging technique used in Chapter 4 requires a probe transmitter. For the reflection mode for the probe, multiple probe reflections are received. The reflected probes will be traveling back with the same portion of the reflected pump, but, because of the different round-trip delay times, there are differences in the nominal propagation phase acquired by the reflected probes. In a discrete medium, a quadrature detector could be employed, and the constant phase shift for the round-trip delay time could be removed. Phase unwrapping could be performed if any wrapping has occurred. In the human body, there is a continuum of reflectors, and, because of the finite width of a practical pump, the gradual change in the round-trip phase delay results in a complicated phase-wrapping problem.

A remedy for the phase-wrapping problem is to use a chirp probe. The phase demodulation of the chirp probe is accomplished by calculating its phase spectrum. After receiving the multiple probe reflections, the desired reflection can be chosen by compressing the chirp probes and removing the remaining reflections. This technique assumes that the desired reflection is from a (locally) strong reflector. The waveforms of a nonlinear imaging system, using a chirp probe and a chirp pump, are displayed in Figure 5.1.

The above systems depend on transmitting a probe signal into the human body, waiting for the desired depth of probe penetration, and, after the round-trip delay time has elapsed, introducing a pump whose multiple reflections copropagate with the probe and then phase modulate it. The copropagation data from the different reflectors provide the integral of B/A from the respective depths to the receiver (Equation (2.38)). The line integral from the different depths is needed to produce a B/A image.

This waiting problem may be solved with the development of new systems which depend on a pump and a probe signal being launched into the medium together (this will be explained in the following paragraphs). This produces more sensitivity, because the

amplitude of the transmitted pump is much higher than that of the reflected pump. Most of the nonlinear interaction modulation contribution occurs while the probe and the pump are copropagating into the medium. Therefore, the effect of individual reflectors on the nonlinear interaction processes is reduced. These systems are based on a reflection mode scheme which could allow the depth information to be preserved.

One system based on this concept would send a chirp probe superimposed on a similar time duration chirp pump or a wide band pseudorandom pump into a medium. The phase of the chirp probe is modulated as it copropagates with the pump into the medium. This scattered signal reflects from all of the reflector planes in the medium and propagates back to the receiver. The phase modulation of the probe by the pump is proportional to the integral of the acoustic nonlinearity from the transmitter to the reflector plane. The observed signal is the phase-modulated chirps reflected from the different reflectors in the medium. The received probe is phase demodulated by first calculating the phase spectrum, second compensating for the frequency sensitivity, and finally taking out the phase contribution from the time delay and the quadratic phase term (Appendix A). This phase is the phase contribution from the nonlinear interaction up to the different reflectors in the medium smeared together by the effect of the finite width pump. By compressing the data with a matched filter, which has an impulse response similar to the pump, high-resolution images could be obtained. This method has the potential for high-sensitivity images. The system is illustrated in Figure 5.2. Another technique uses a coherent probe and a chirp pump (Figure 5.3). This pump and probe combination interact nonlinearly while copropagating.

Imaging is achieved in the reflection mode. The pump and probe copropagate into the medium where they are reflected from the interfaces. The reflected combination of the pump and probe waveforms with the scattered field is detected by the receiver. This is exactly the same as the pulse echo system. The difference is that, in the pulse echo system,

the reflection of the primary field is of interest. In the nonlinear ultrasonic system, the reflection of the nonlinearly generated field is of interest.

The modulation of the probe by the pump produces spectral energy in the lower sideband of the probe. Choosing the probe frequency and the pump frequency range properly, this lower sideband falls at the baseband frequency range (Figure 5.4). This means that a simple low-pass filter is able to demodulate the received probe. This scheme avoids the problem of the nominal phase contribution from the round-trip delay time. The method is not dependent on coherent detection and uses a new kind of noncoherent detection technique. Compressing these data with a matched filter having an impulse response similar to the pump could provide high-resolution images. The signal-to-noise ratio for this system is low. Choosing the pump properly, large improvements in the signal-to-noise ratio can be achieved by compressing the received signal, as in the coding schemes used in radar. The proposed systems could operate using a single transducer. Wide-band transducers could produce both the pump and the probe, and receive the scattered field.

Many of the computational tasks in this section could be handled in realtime by the VLSI-based general purpose digital signal processing chips. The digital signal processing (DSP) chips and microprocessors have been incorporated into a wide range of medical imaging systems, CT and MRI systems for image reconstruction, ultrasound systems for computationally intensive applications such as real-time blood flow imaging. Typical of VLSI-based, midprocessors are the FFT processor for Doppler flow imaging. In some vector DSP chips, the vector operation of the fast Fourier transform (FFT) can be invoked with a single instruction. The ultrasonic signal waveforms utilized are readily generated and processed with current signal generation and processing systems. The system requires a microprocessor or a specialized signal processing module.

Other nonlinear ultrasonic imaging systems use a tomographic or a variable amplitude excitation system. The system proposed in this thesis could potentially produce

a line image of the nonlinearity with a single (pulse-echo) scan of the medium. An evolved version of this system could possibly be used to image the B/A parameter in the human body.

The extension of the system discussed in Section 4.4 to include the reflection mode for the probe allows a single transducer to produce the signals and detect them. A variation of this technique, transmitting both the pump and the probe into the medium simultaneously, has the potential of producing B/A images and B-mode images concurrently.

5.3 Parametric Hydrophone

Some of the work presented for the B/A imaging system could be utilized for monitoring high-intensity acoustic fields. The experiment in Section 4.1 opens up the possibility of using a similarly constructed parametric hydrophone system for probing acoustic fields. The acoustic field could be of a fairly high intensity such as the acoustic field at the focus of a lithotripter machine. The acoustic field could also be fairly broadband. The probe frequency needs to be at least the maximum frequency in the acoustic field being detected (Equation (2.29), Figure 2.3). This technique has the advantage that it does not change the actual field pattern being measured. The devices proposed in the parametric hydrophone system are commercially available. The detection system operates in the MHz region where many relatively inexpensive devices are available for signal amplification and phase detection. These analog devices have been used in video and radio systems.

Equation (2.20) provides an analytical relationship between the detected phase and the pressure field experienced by the probe. The acoustic pressure inferred from the detected phase is a spatial pressure function averaged over the lateral spatial region of interaction of the probe and the high-intensity acoustic field. Each probe wavelet copropagates with a different portion of the pressure field. This copropagation produces a

signal that is proportional to the pressure field. The smearing is the lateral averaging that takes place because of the finite lateral spatial spread of the probe, which represents the lateral spatial interaction region of the two acoustic pulses. The phase sensitivity is directly proportional to the distance of copropagation of the probe with the pump and to the temporal frequency of the probe.

5.4 Final Remarks

The future of nonlinear imaging depends on making progress on several fronts. These areas include a flexible simulation tool, a three-dimensional mathematical model, and an experimental system which could be used in a clinic.

A flexible simulator could possibly answer questions in the area of diffraction effects. A model for the reflections of ultrasonic beams from various tissue interfaces would need to be developed first. The computational complexity of this simulator would be enormous, requiring extensive computational and memory requirements. It is hereby recommended that a data base be generated from the simulation runs to provide simulated data for the extensive off-line study of the nonlinear interactions.

A three-dimensional mathematical model based on the nonlinear wave equation and its solution, even for simple cases, would allow a study of S/N characteristics of the system and of waveform optimization.

Finally, a potentially high-risk but possible high-payoff alternative is to program a commercial B-mode scanner to operate, based on the mathematical formulation developed in this thesis. Since the developed theory is very limited, the author does not expect that the images produced would be B/A images, but they would arise from the nonlinear interaction of sound waves in tissue, a parameter that is yet to be observed in a clinical environment.

The thrust of accomplishment in this thesis has been to discuss, bring together, extend, and define problems in nonlinear imaging. The results provide an appreciation of

the level of the complexity of the problems in nonlinear imaging. On the encouraging side, the research has provided more insight into the nonlinear inteaction processes and provided a mathematical model. The experimental system has verified that the nonlinear interactions are detectable and has provided a detection system to achieve that goal.

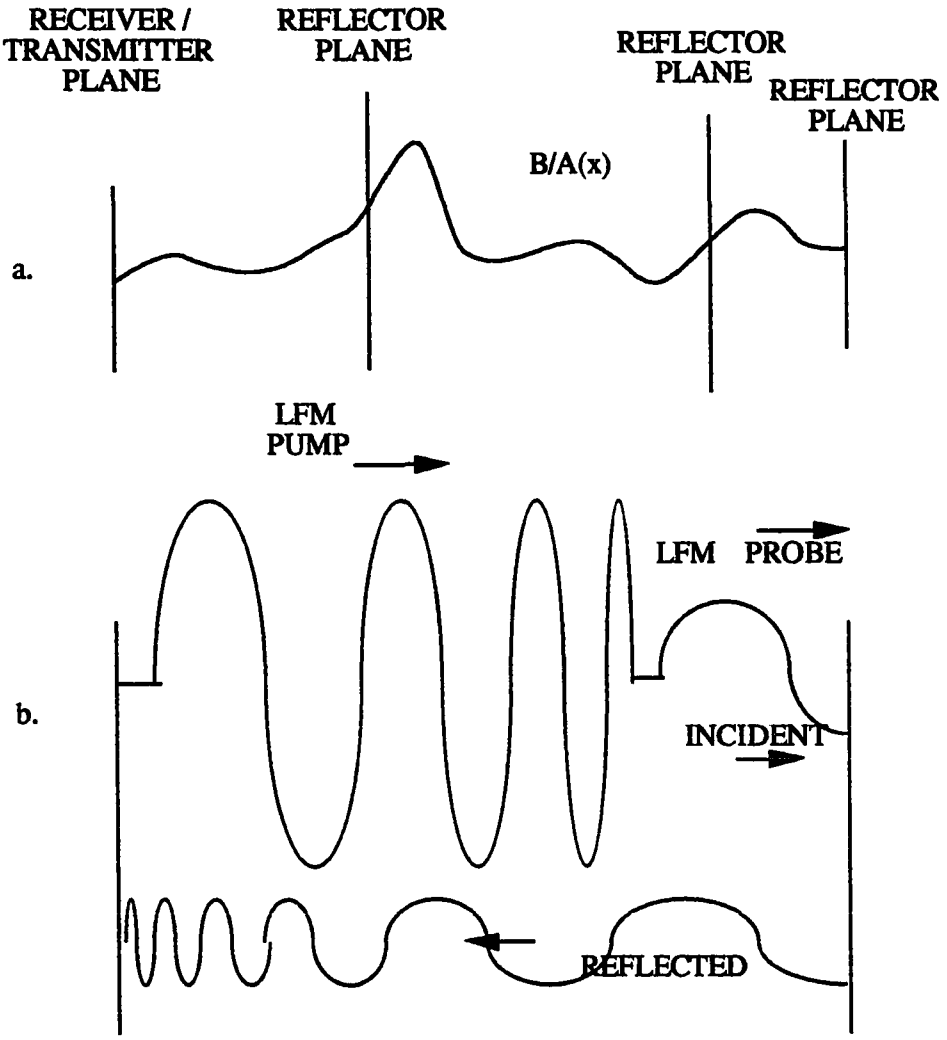

Figure 5.1 The imaging System: a. The B/A profile. b. An LFM probe followed by an LFM pump.

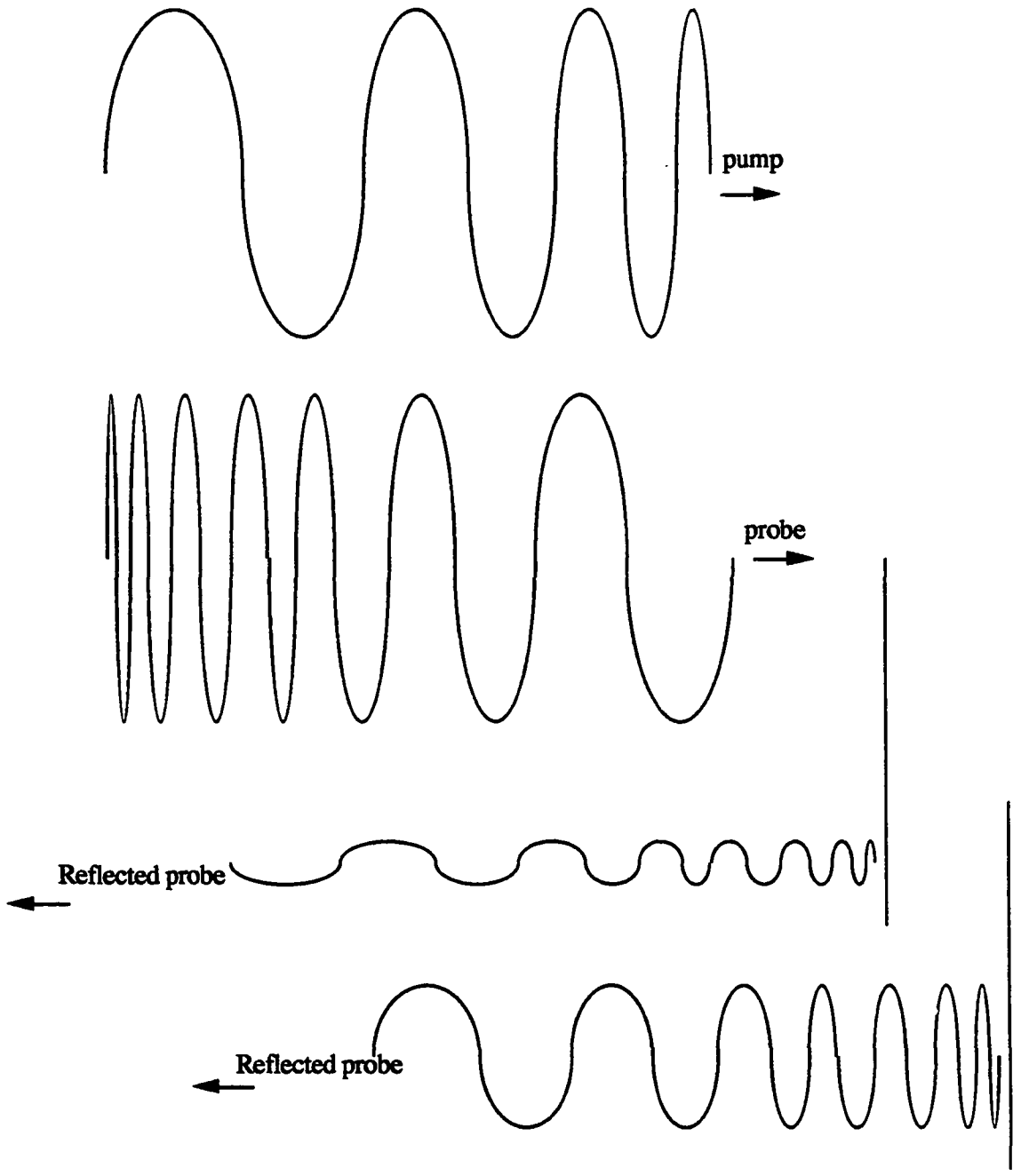

Figure 5.2 A chirp pump and a chirp probe are copropagated into the medium. The reflections of the modulated chirp probe from the different reflectors are shown.

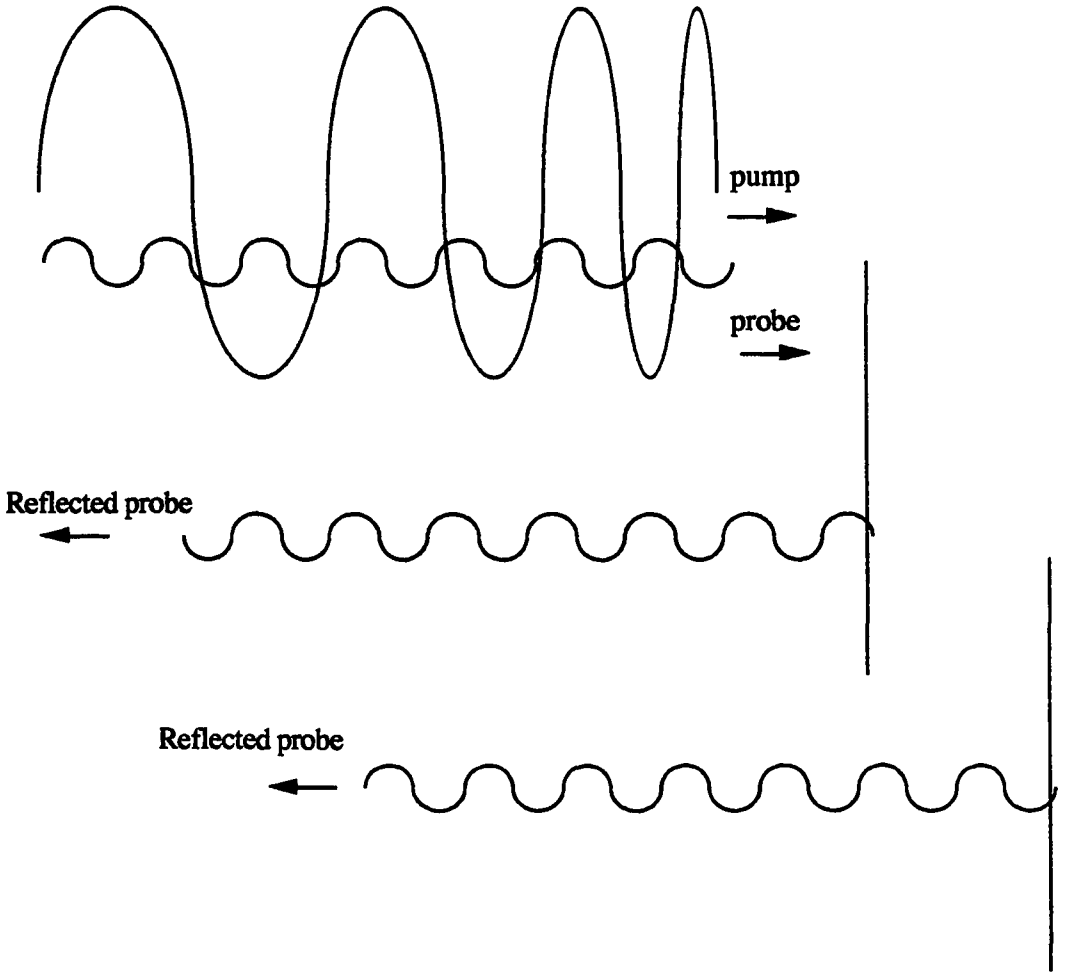

Figure 5.3 A wide-band pump is propagated into the medium with a probe. Only the reflections of the modulated probe are shown.

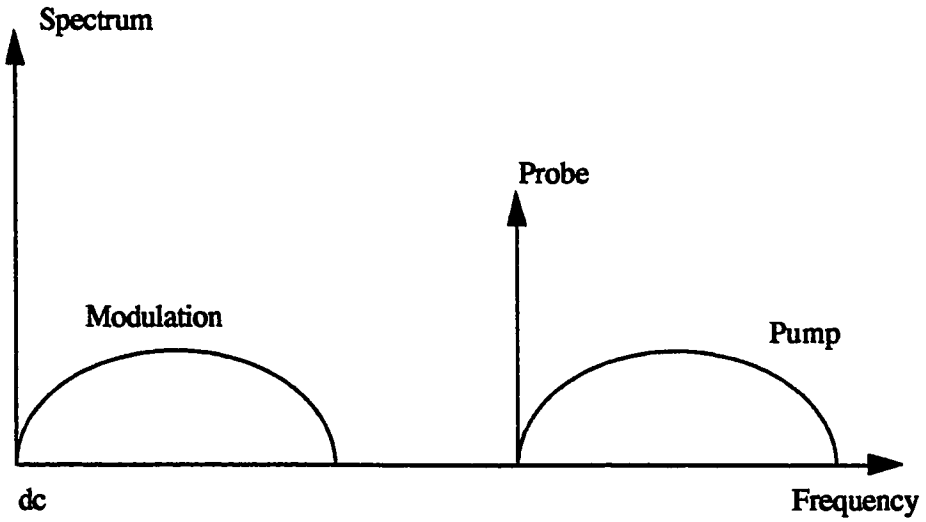

Figure 5.4 The spectra of the probe, the pump, and the probe lower sideband.

APPENDIX A

CHIRP PROBE

The instantaneous frequency of an LFM signal is

$$\omega_i(\tau) = \omega_o + \mu\tau, \qquad \frac{-T}{2} \angle \tau \angle \frac{T}{2}$$

$$= 0 \qquad \text{elsewhere.} \tag{A.1}$$

The frequency changes from $\omega_o - \mu T/2$ to $\omega_o + \mu T/2$ in a linear fashion, during the interval of the pulse. Integrating $\omega_i(t)$ and ignoring the possible constant phase angle, the angle is obtained as

$$\theta_i(\tau) = \omega_o \tau + \frac{\mu}{2}\tau^2 \quad . \tag{A.2}$$

The chirp is a cosine function lasting T seconds. The linear chirp's frequency changes linearly about ω_o.

The Fourier transform of $s(\tau)$ is given by

$$S(\omega) = \int_{-T/2}^{T/2} \cos\left(\omega_o\tau + \frac{\mu}{2}\tau^2\right) e^{-j\omega\tau} d\tau$$

$$= \frac{1}{2}\left(\int_{-T/2}^{T/2} \exp\left\{j\left[(\omega_o-\omega)\tau + \frac{\mu}{2}\tau^2\right]\right\} d\tau + \int_{-T/2}^{T/2} \exp\left\{-j\left[(\omega_o+\omega)\tau + \frac{\mu}{2}\tau^2\right]\right\} d\tau\right) . \tag{A.3}$$

The above integrals are rewritten as (Cook and Bernfeld, 1967)

$$S(\omega) = \frac{1}{2}\sqrt{\frac{\pi}{\mu}}\, e^{-j(\omega_o-\omega)^2/2\mu}$$
$$\left[C\left(\frac{(\mu T/2) + (\omega_o-\omega)}{\sqrt{\pi\mu}}\right) + j\, S\left(\frac{(\mu T/2) + (\omega_o-\omega)}{\sqrt{\pi\mu}}\right)\right.$$
$$\left. + C\left(\frac{(\mu T/2) - (\omega_o-\omega)}{\sqrt{\pi\mu}}\right) + j\, S\left(\frac{(\mu T/2) - (\omega_o-\omega)}{\sqrt{\pi\mu}}\right)\right] \quad , \tag{A.4}$$

where

$$c(x) = \int_0^x \cos\frac{\pi}{2}\alpha^2\, d\alpha \quad , \tag{A.5}$$

and

$$S(x) = \int_0^x \sin\frac{\pi}{2}\alpha^2\, d\alpha \quad , \tag{A.6}$$

are called Fresnel integrals. They occur frequently in engineering and have been tabulated (Balanis, 1982). The square law and residual phase of this signal are then given by

$$\phi(\omega) = \frac{(\omega_o-\omega)^2}{2\mu} - \tan^{-1}\left(\frac{S\left(\frac{(\mu T/2) + (\omega_o-\omega)}{\sqrt{\pi\mu}}\right) + S\left(\frac{(\mu T/2) - (\omega_o-\omega)}{\sqrt{\pi\mu}}\right)}{C\left(\frac{(\mu T/2) + (\omega_o-\omega)}{\sqrt{\pi\mu}}\right) + C\left(\frac{(\mu T/2) - (\omega_o-\omega)}{\sqrt{\pi\mu}}\right)} \right) \quad . \tag{A.7}$$

For large values of $T\Delta f$, the ratio in the argument of the inverse tangent function is approximately one.

The Fourier transform $S(\omega)$ of $s(\tau)$ yields a phase spectrum

$$\varphi(\omega) = \phi(\omega) + \Delta\varphi(\omega) \quad , \tag{A.8}$$

where $\phi(\omega)$ is the phase spectrum in the absence of the pump (Equation (A.7)), and $\Delta\varphi(\omega)$ is the phase shift associated with the nonlinear interaction between the pump and the probe. The input LFM signal determines $\phi(\omega)$ (Equation (A.7)). This phase term can be removed yielding the modulated phase function $\Delta\varphi(\omega)$.

The reception time of a chirp wavelet is related to the spatial location where this wavelet was modulated. This reception is also related to the instantaneous frequency of an LFM probe. This establishes a direct relationship between the frequency of the chirp and the spatial location in the medium where the wavelet acquired an additional phase. The Fourier transform of a frequency-modulated probe produces the modulated phase function versus the spatial variable. This allows the frequency to space and the phase retrieval operations to be performed simultaneously.

APPENDIX B

SIMULATION PROGRAM

```
C     This program simulates nonlinear wave propagation.
C
C
C
C
      DIMENSION XP1(138), PU(138)
      DIMENSION XIN(3), YIN(3), PINT(128)
      DIMENSION XP(128)
      COMPLEX A
      REAL MAG
      DIMENSION A(128), INV(128/4), M(3), S(128/4)
      DIMENSION P(128)
C
C     GENERATE THE PUMP WAVEFORM
c
      DO 10 I=1,128
10    P(I)=2*10E5*SIN(0.024737*(I-1))
C
C
C
C     GENERATE THE SPATIAL POSITION OF THE PUMP WAVELETS.
C
      DO 20 I=1,128
20    XP(I)=(I-1)*7.5E-4/127.
C
      DO 2 I=1,128
            PU(I)=P(I)
2           XP1(I)=XP(I)
c
C
      DO 1 KF=1,5
```

```
C
C       TAKE ATTENUATION INTO ACCOUNT.
C
C
        M(1)=7
        M(2)=0
        M(3)=0
C       THE ABOVE MAKES THE LENGTH OF FFT EQUAL TO 128
        IFSET=0
C       THIS GENERATES THE PROPER TABLES
        CALL HARM(A,M,INV,S,IFSET,IFERR)
C       INPUT A
        DO 30 I=1,128
30      A(I)=P(I)
        IFSET=1
C       FFT
        CALL HARM(A,M,INV,S,IFSET,IFERR)
        IF (IFERR.NE.0) PRINT *, IFERR
C       A CONTAINS THE FOURIER TRANSFORM
C
C
C       NOW APPLY THE ATTENUATION TO THE SIGNAL IN THE FREQUENCY
C       DOMAIN. MULTIPLY THE FOURIER COEFFICIENTS BY THEIR
C       RESPECTIVE ATTENUATIONS FOR DISTANCE OF .01 METERS.
C       THE FILE A CONTAINS THE FOURIER COEFFICIENTS.
C
        DO 50 I=2,64
        F=FLOAT(I-1)*2.E6
        ATTEN=10.**(1.086E-15*F*F/20.)
        A(I)=A(I)/ATTEN
        A(130-I)=A(130-I)/ATTEN
50      CONTINUE
        A(65)=A(65)/7.756
C
C       DONE WITH ATTEN
C
```

```
C       INVERSE FFT
        M(1)=7
        M(2)=0
        M(3)=0
        IFSET=0
        CALL HARM(A,M,INV,S,IFSET,IFERR)
        N=128
        RN=FLOAT(128)
        DO 60 I=1,N
60      A(I)=CONJG(A(I))/RN
        IFSET=1
        CALL HARM(A,M,INV,S,IFSET,IFERR)
        IF (IFERR.NE.0) PRINT*,IFERR
        DO 70 I=1,N
70      A(I)=CONJG(A(I))
C       A CONTAINS THE INVERSE FFT THE SPATIAL DATA
C
        DO 80 I=1,128
        P(I)=REAL(A(I))
80      CONTINUE
C
C       USE THE VARIABLE SPEED EQUATION NOW TO PROPAGATE
C       THE WAVE FOR 1 CM .
C       XP KEEPS TRACK OF THE POSITION OF THE DIFFERENT
C       PRESSURE POINTS ON THE WAVEFORM.
C       THE NEW PRESSURES ARE IN THE P ARRAY.
C
        DO 90 I=1,128

        speed=1.+(5.*p(i)/(2.*998.*1500.*1500))
        speed=speed**(1.+(2./5.))
        speed = speed*1500.
        xp(i) = xp(i) + speed * (6.66667e-6)

c       XP(I)=XP(I)+((1500.+(1.67E-6)*P(I))*(6.66667E-6))
90      CONTINUE
```

```
C
C     INTERPOLATE
C
      DO 100 I=1,126
            XOUT=XP(1)+(((XP(128)-XP(1))/127.)*FLOAT(I))
            NM=1
            DO 15  kext = 1,1000
            if (xout.le.xp(nm)) goto 16
            NM=NM+1
15          continue
16          NM=NM-1
            IF (XOUT.GE.XP(NM).AND.XOUT.LT.XP(NM+1)) THEN
            DO 210 J=1,3
            XIN(J)=XP(NM-2+J)
            YIN(J)=P(NM-2+J)
210         CONTINUE
            ELSE
                  PRINT *,' XOUT OUT OF RANGE',NM
            END IF
            CALL LAGINT(XIN,YIN,3,XOUT,YOUT)
            PINT(I+1)=YOUT
100   CONTINUE
C
C     THE ABOVE TOOK CARE OF GETTING THE PRESSURES ON A
C     UNIFORM GRID.
C
      SPACING=((XP(128)-XP(1))/127.)
      RXP1=XP(1)
      PINT(1)=P(1)
      PINT(128)=P(128)
      DO 220 I=1,128
      P(I)=PINT(I)
      XP(I)=RXP1+(SPACING*FLOAT(I-1))
220   CONTINUE
C
      DO 250  I=1,128
```

```
            PU(I)=P(I)
250         XP1(I)=XP(I)
C
      do 300 i = 1,10
            write(30+(kf*4),*) P(i*13-7)
300   continue
      do 301 i = 1,10
            write(31+(kf*4),*) xp(i*13-7)
301   continue
C
1     CONTINUE
C
c     STOP
      END
```

REFERENCES

R. E. Apfel, Effective nonlinearity parameter for immiscible liquid mixtures, J. Acoust. Soc. Am., vol. 74, pp. 1866-1868, 1983.

R. E. Apfel, Prediction of tissue composition from ultrasonic measurements and mixture rules, J. Acoust. Soc. Am., vol. 79, pp. 148-152, 1986.

D. R. Bacon, Finite amplitude propagation in acoustic beams. Ph.D. dissertation, University of Bath, Bath, UK, 1986.

C. A. Balanis, Antenna Theory - Analysis and Design. Wiley, 1982.

R. Bass, Diffraction effects in the ultrasonic field of a piston source, J. Acoust. Soc. Am., vol. 30, pp. 602-605, 1958.

R. T. Beyer, Parameter of nonlinear in fluids, J. Acoust. Soc. Am., vol. 32, pp. 719-721, 1960.

R. T. Beyer, Nonlinear acoustics. Department of Navy, 1974.

R. T. Beyer and S. V. Letcher, Nonlinear acoustics, in Physical Ultrasonics. New York: Academic Press, 1969, pp. 202-230.

L. Bjorno, Characterization of biological media by means of their nonlinearity, Ultras., vol. 24, pp. 254-259, 1986.

L. Bjorno and P. A. Lewin, Nonlinear focusing effects in ultrasonic imaging, in Proc. IEEE Ultras. Symp., 1982, pp. 659-662.

D. T. Blackstock, Connection between the Fay and Fubini solutions for plane sound wave of finite amplitude, J. Acoust. Soc. Am., vol. 39, pp. 1019-1026, 1966.

D. T. Blackstock, Nonlinear acoustics, in Amer. Inst. Phy. Handbook. New York: McGraw Hill, 1972, Chapter 3.

A. Cai, Diffraction tomography of the acoustic nonlinear parameter. Ph.D. thesis, University of California at Santa Barbara, 1988.

C. A. Cain, Ultrasonic reflection mode imaging of the nonlinear parameter B/A: I. A theoretical basis, J. Acoust. Soc. Am., vol. 80, pp. 28-32, 1986.

W. N. Cobb, Measurement of the acoustic nonlinearity parameter for biological media. Ph.D. dissertation, Yale University, New Haven, CT, 1982.

W. N. Cobb, Finite amplitude method for the determination of the acoustic nonlinearity parameter B/A, J. Acoust. Soc. Am., vol. 73, pp. 1525-1531, 1983.

C. E. Cook and M. Bernfeld, Radar signals: An Introduction to Theory and Applications. New York: Academic, 1967.

A. B. Coppens, R. T. Beyer, M. B. Seiden, J. Donohue, F. Guepin, R. H. Hodson, and C. Townsend, Parameter of nonlinearity in fluids. II, J. Acoust. Soc. Am., vol. 38, pp. 797-804, 1965.

Y. Dong, J. Tong, and Y. Sun, Relations between the acoustic nonlinearity parameter and sound speed and tissue composition, in Proc. IEEE Ultras. Symp., 1987, pp. 931-934.

F. Dunn, W. K. Law, and L. A. Frizzell, Nonlinear ultrasonic wave propagation in biological materials, in Proc. IEEE Ultras. Symp., 1981, pp. 527-532.

R. L. Errabolu, C. M. Sehgal, and J. F. Greenleaf, Dependence of ultrasonic nonlinearity parameter B/A on fat, Ultras. Imag., vol. 9, pp. 180-194, 1987.

E. C. Everbach, Tissue composition determination via measurement of the acoustic nonlinearity parameter. Ph.D. dissertation, Yale University, New Haven, CT, 1989.

X. Gong, R. Feng, C. Zhu, and T. Shi, Ultrasonic investigation of the nonlinearity parameter B/A in biological media, J. Acoust. Soc. Am., vol. 76, pp. 949-950, 1984.

H. S. Heaps, Waveform of finite amplitude derived from equation of hydrodynamics, J. Acoust. Soc. Am., vol. 34, pp. 355-356, 1962.

N. Ichida, T. Sato, H. Miwa, and K. Murakami, Real-time nonlinear parameter tomography using impulsive pumping waves. IEEE Trans. Son. Ultras., vol. SU-31, pp. 635-640, 1984.

F. Ingenito and A. O. Williams, Jr., Calculation of second harmonic generation in a piston beam, J. Acoust. Soc. Am., vol. 49, pp. 319-328, 1971.

L. E. Kinsler, A. R. Frey, A. B. Coppens, and J. V. Sanders, Fundamentals of Acoustics. New York: Wiley, 1982.

W. K. Law, Measurement of the nonlinearity parameter B/A in biological materials using the finite amplitude and thermodynamic method. Ph.D. dissertation, University of Illinois at Urbana-Champaign, 1984.

W. K. Law, L. A. Frizzell, and F. Dunn, Determination of the nonlinearity parameter B/A of biological media, Ultras. in Med. & Bio., vol. 11, pp. 307-318, 1985.

R. J. McGough, Imaging the nonlinearity parameter B/A: simulation and experiment. M.S. thesis, University of Illinois at Urbana-Champaign, 1990.

Y. Nakagawa, W. Hou, A. Cai, G. Wade, M. Yoneyama, and M. Nakagawa, Nonlinear parameter imaging with finite-amplitude sound waves, in Proc. Ultras. Symp., 1986, pp. 901-904.

Y. Nakagawa, M. Nakagawa, M. Yoneyama, and M. Kikuchi, Nonlinear parameter imaging computed tomography by parametric array, in Proc. of the IEEE ultras. symp., 1984, pp. 673-676.

K. L. Narayana and K. M. Swamy, Acoustic nonlinear parameter (B/A) in n-pentane, Acustica, vol. 49, pp. 336-339, 1981.

L. B. Orenstein and D. T. Blackstock, The rise time of N waves produced by sparks. Technical Report ARL-TR-82 51, University of Texas at Austin, 1982

F. M. Pestorius and D. T. Blackstock, Propagation of finite amplitude noise, in IPC Sci. and Tech., Guildford, England, 1974.

D. Rugar, Resolution beyond the diffraction limit in the acoustic microscope: a nonlinear effect, J. Appl. Phys., vol. 56, pp. 1338-1346, 1984.

T. Sato, A. Fukusima, N. Ichida, H. Ishikawa, H. Miwa, Y. Igrarshi, T. Shimura, and K. Murakami,. Nonlinear parameter tomography system using counterpropagating probe and pump waves, Ultras. Imag., vol. 7, pp. 49-59, 1985.

C. M. Sehgal, R. C. Bahn, and J. F. Greenleaf, Measurement of the acoustic nonlinearity parameter B/A in human tissues by a thermodynamic method, J. Acoust. Soc. Am., vol. 76, pp. 1023-1029, 1984.

C. M. Sehgal, G. M. Brown, R. C. Bahn, and J. F. Greenleaf, Measurement and use of acoustic nonlinearity and sound speed to estimate composition of excised livers, Ultras. Med. Biol., vol. 12, pp. 865-874, 1986a.

C. M. Sehgal, B. R. Porter, and J. F. Greenleaf, Ultrasonic nonlinear parameters and sound speed of alcohol-water mixtures, J. Acoust. Soc. Am., vol. 79, pp. 566-570, 1986b.

C. M. Sehgal, B. R. Porter, and J. F. Greenleaf, Relationship between acoustic nonlinearity and the bound and the unbound states of water, in Proc. IEEE Ultras. Symp., 1985, pp. 883-886.

W. A. Swindell, The theoretical study of nonlinear effects with focused ultrasound in tissues: an acoustic Bragg peak, Ultras. Med. Biol., vol. 11, 1985.

J. N. Tjøtta and S. Tjøtta, Nonlinear equations of acoustics, with application to parametric acoustic arrays, J. Acoust. Am., vol. 69, pp. 1664-1652, 1981.

P. J. Westervelt, Parametric acoustic array, J. Acoust. Soc. Am., vol. 35, pp. 535-537, 1963.

K. Yoshizumi, T. Sato, and N. Ichida, A physio-chemical evaluation of nonlinear parameter B/A for media predominantly composed of water, J. Acoust. Soc. Am., vol. 82, pp. 302-305, 1987.

J. Zhang, Influences of biological structural features on the acoustic nonlinearity parameter B/A. Ph.D. dissertation, University of Illinois at Urbana-Champaign, 1990.

Z. Zhu, M. S. Roos, W. L. Cobb, and K. Jensen, Determination of the acoustic nonlinearity parameter B/A from phase measurements, J. Acoust. Soc. Am., vol. 74, pp. 1518-1521, 1983.

VITA

Hooman Houshmand was born in 1960. He received his B.S. and M.S. degrees in electrical engineering from the University of Illinois at Urbana-Champaign. His Ph.D. research has involved the application of signal processing, communication, nonlinear system theory, and optics to nonlinear medical imaging systems. His M.S. research on optical systems included welding systems and devices to measure the step response of the human eye. His future goals are to attempt to bridge the gap between the ideas generated at the university and the manufacturing needs of industry. This, he believes, will improve the welfare of the society by providing a more competitive and challenging work environment.